Department of Physics and Astronomy
University of Heidelberg

Diploma thesis
in Physics

submitted by
Fabian Rühle
born in Herrenberg

2009

Connecting heterotic orbifold models to Calabi-Yau MSSMs in blowup

This diploma thesis has been carried out by Fabian Rühle
at the
Institute for Theoretical Physics
under the supervision of
Priv. Doz. Dr. Stefan Groot Nibbelink

For Anneli, Bastian,
and my parents

Connecting heterotic orbifold models to Calabi-Yau MSSMs in blowup: String theory has received wide attention over the last 25 years as it has promising features which might enable it to unify gravity with the Standard Model gauge interactions. Especially heterotic string theory has proved very fruitful for phenomenological model building. The theory has to be compactified from ten to four spacetime dimensions on either Calabi-Yau manifolds or orbifolds. A blowup mechanism allows to connect the two spaces. The aim of this thesis is to study in detail this connection and its implications for both compactification spaces and their properties with regard to model building. We explore two approaches to building MSSM-like models on Calabi-Yaus and derive necessary conditions which have to be fulfilled in return by the underlying orbifold models. Furthermore, we work out several relations between quantities on the orbifold and the Calabi-Yau side and discuss an ambiguity arising in the blowup procedure from a new point of view. In the course of the thesis, we work out an explicit example for an MSSM-like model on a blown up Calabi-Yau manifold based on a heterotic orbifold model.

Verbindung zwischen heterotischen Orbifaltigkeiten und aufgeblasenen Calabi-Yau MSSMs: Stringtheorie hat in den vergangenen 25 Jahren viel Aufmerksamkeit erregt, da die Theorie in der Lage sein könnte, Gravitation und die Eichwechselwirkungen des Standardmodells zu vereinigen. Vor allem heterotische Stringtheorie hat sich als äußerst vielversprechende Grundlage für phänomenologisch motivierte Modellbildung erwiesen. Die Theorie muss von zehn auf vier Raum-Zeit-Dimensionen mittels Calabi-Yau Mannigfaltigkeiten oder Orbifaltigkeiten kompaktifiziert werden. Ein Aufblasungsmechanismus erlaubt es die beiden Räume zu verbinden. Ziel dieser Diplomarbeit ist es, diesen Zusammenhang im Detail auszuarbeiten und die Implikationen für beide Kompaktifizierungsräume und deren Eigenschaften im Hinblick auf Modellbildung aufzuzeigen. Wir untersuchen zwei Vorgehensweisen um MSSM-artige Modelle auf Calabi-Yaus zu erhalten und leiten notwendige Bedingungen her, welche die zugrundeliegenden Orbifaltigkeiten-Modelle dafür erfüllen müssen. Des Weiteren erarbeiten wir mehrere Zusammenhänge zwischen Orbifaltigkeiten und Calabi-Yau Mannigfaltigkeiten und untersuchen eine bei der Aufblasung auftretende Mehrdeutigkeit von einem neuen Standpunkt aus. Im Verlauf der Diplomarbeit wird ausgehend von einem heterotischen Orbifaltigkeitenmodell ein explizites Beispiel für ein MSSM-artiges Model auf der aufgeblasenen Calabi-Yau Mannigfaltigkeit erarbeitet.

Erklärung

Ich versichere, dass ich diese Arbeit selbständig verfasst habe und keine anderen als die angegebenen Quellen und Hilfsmittel benutzt habe.

Heidelberg, den 2. Dezember 2009 .....

Fabian Rühle

Contents

Chapter 1

. . . . . .

Introduction

Up to now, four fundamental forces have been discovered in our universe: the electro-magnetic force, the weak force, the strong force, and gravity. The history of unification of these forces dates approximately 150 years back. In the middle of the 19^{th} century, J.C. Maxwell consistently unified the electric and the magnetic force to obtain one of the four fundamental forces. One century later, in 1963, S. Glashow discovered that electro-magnetic and weak interactions can be described in one theoretical framework called electro-weak theory. In 1967, S. Weinberg and A. Salam augmented the theory with the Higgs mechanism. For the first three theories, forces between matter particles (fermions) are mediated by gauge bosons. The natural language to describe these gauge interactions is quantum field theory (QFT), or to be more precise Yang-Mills (YM) gauge theory.

The Newtonian theory of gravity dates back to the 17^{th} century. The modern theory of gravity - general relativity - was published by A. Einstein in 1916. It had a tremendous impact on the way we see our universe today. According to Einstein's theory, matter curves spacetime. It is this curvature of spacetime, which attributes to gravitational effects: particles move through spacetime on the shortest trajectory possible, which is a geodesic. In the weak curvature limit, Newtonian gravity is reproduced. Einstein's theory is remarkably successful, as it explains observed phenomena and makes precise predictions, which are confirmed by experiments. In unquantized general relativity there is no force mediating particle - the mediation is in fact caused by properties of spacetime itself.

In the 1970's, the Standard Model of particle physics (SM) was constructed. It describes three fundamental forces excluding gravity and all of the observed matter particles up to date. The matter content of the Standard Model is given by three copies (three generations) of spin 1/2 fermions. Each of these fermions comes with an associated anti-particle. The three forces are mediated by spin 1 gauge bosons. The gauge boson of the electro-magnetic force is the photon and its associated gauge group is an Abelian $U(1)$ group. The three force mediators of the weak force are the $W^{\pm}$ and the Z boson. The weak gauge group is $SU(2)$. Finally, the 8 gluons mediate the strong force, which has an $SU(3)$ gauge group. Note that the matter particles are charged under one or more of the $SU(3) \times SU(2) \times U(1)_Y$ gauge groups. One astonishing fact is that the $SU(2) \times U(1)_Y$ part of the Standard Model is chiral, i.e. different for left-handed and right-handed particles. The particle content of one generation (in our

example the first) fits into the following representations of the SM gauge group

$$\begin{array}{lccccccccc} \text{Multiplet:} & Q_L & + & u_R^c & + & d_R^c & + & L_L & + & e_R^c, \\ \text{Particles:} & (u,d)_L & + & (\overline{u})_R & + & (\overline{d})_R & + & (e^-,\nu_{e^-})_L & + & e_R^+, \\ \text{Representation:} & (\mathbf{3},\mathbf{2})_{1/6} & + & (\overline{\mathbf{3}},\mathbf{1})_{-2/3} & + & (\overline{\mathbf{3}},\mathbf{1})_{1/3} & + & (\mathbf{1},\mathbf{2})_{-1/2} & + & (\mathbf{1},\mathbf{1})_1, \end{array} \tag{1.1}$$

where the two numbers in brackets give the $SU(3) \times SU(2)$ representation and the subscript denotes the hypercharge. As can be seen from the list above, all particles except for the neutrino have a partner with opposite chirality.

At around 240 GeV, the electro-weak symmetry is broken to give the electro-magnetic and weak theory. This symmetry breaking is performed by giving a vacuum expectation value (vev) to the Higgs field. While the electrons, quarks, and weak gauge bosons acquire a mass from the symmetry breaking, the $U(1)_{em}$ gauge boson of electro-magnetism - the photon - remains exactly massless in the theory, which is confirmed to a very high precision in experiments. This gauge boson is a mixture of the hypercharge and another $U(1)$ field, the weak isospin. The fact that it remains massless indicates that the hypercharge is conserved and non-anomalous in the SM.

The Standard Model was tremendously successful and stood up against every test of the last thirty years. With the exception of the Higgs boson, all particles that are predicted by the SM have actually been observed. It is widely expected that the LHC at CERN will discover the Higgs particle. Recently, data from neutrino oscillation experiments indicate that the neutrino does actually have a non-zero mass, which means that there must also be a right-handed neutrino (although this has never been observed). This additional requirement can easily be integrated into the SM by introducing a Dirac mass term into the SM Lagrangian or via the seesaw mechanism. Including the neutrino, the SM has 16 fermionic fields in each generation.

Despite its exceeding success, the SM has severe shortcomings. For example it does not answer the question why the masses and the coupling constants have the values we observe. They are free parameters of the theory which cannot be computed but have to be put in by hand. It neither answers the question why especially the gauge groups we observe arise. Furthermore, there is no explanation for the occurrence of three generations of particles which behave identically except for their masses.

The striving for unification did not end with the SM. The first attempt was to unify all three forces in one big gauge group. These theories go by the name grand unifying theories (GUTs). The GUT gauge group has to be broken to the SM gauge groups at lower energies. One of the first GUT models proposed was the $SU(5)$ GUT of Georgi and Glashow [1]. The 16 SM fermions are accommodated in the $\mathbf{10} + \overline{\mathbf{5}} + \mathbf{1}$ of $SU(5)$ as follows:

$$\begin{array}{rl} \mathbf{10} & \to (\mathbf{3},\mathbf{2})_{1/6} \oplus (\overline{\mathbf{3}},\mathbf{1})_{-2/3} \oplus (\mathbf{1},\mathbf{1})_1 \\ \overline{\mathbf{5}} & \to (\overline{\mathbf{3}},\mathbf{1})_{1/3} \oplus (\mathbf{1},\mathbf{2})_{-1/2} \\ \mathbf{1} & \to (\mathbf{1},\mathbf{1})_0 \end{array} \tag{1.2}$$

It is a non-trivial fact that the anomalies of $\mathbf{10}$ and $\overline{\mathbf{5}}$ cancel exactly.

A further GUT group that can accommodate the SM particles in its representation is $SO(10)$ [2]. Here, one complete generation of fermions fits into the $\mathbf{16}$ of $SO(10)$. The biggest exceptional GUT group that allows for chiral matter is E_6 [3], where the matter

fields are accommodated in the **27**.

The idea of unification is supported by the fact that the coupling constants are not really constant but run when the theories are renormalized. While the electro-magentic coupling increases with energy, the weak and strong couplings decrease such that all are of approximately equal strength at $M_{GUT} \approx 10^{13} - 10^{17}$GeV. A severe problem that occurs is that the Higgs mass receives quadratic loop corrections, which drives its mass to large energies. Unless there is an accidental cancelation of the various contributions, the Higgs mass will generically be pulled towards the GUT or Planck scale. However, in order to cancel the contributions and to keep the Higgs mass at the weak scale, one needs to fine-tune the parameters of the SM to a very high precision in order to induce these cancelation, which is not very satisfactory. The problem of the weak scale being so much lower than the Planck scale is referred to as the hierarchy problem.

A very prominent proposal for solving the hierarchy problem without having to fine-tune the theory too much is supersymmetry (SUSY). This theory postulates that each fermion has a bosonic superpartner, and vice versa, which carry the same quantum numbers and are arranged in multiplets. As bosons and fermions have opposite statistics, their contributions to the Higgs mass cancel automatically, which softens the problem of fine-tuning.

Obviously, SUSY at least doubles the number of particles in a theory. However, we have never observed any superpartner of a SM particle (which could, however, change when the LHC goes online). As we do not observe SUSY below 1 TeV, it needs to be broken below this scale. The SUSY breaking induces a mass term for the superpartners, making them heavier than the current experimental accessible energies. By assuming SUSY to be broken at a scale of 1 - 10TeV, the running of the coupling constants is modified such that they intersect exactly at $M_{GUT} \approx 10^{16}$GeV.

The minimal extension of the SM would be to introduce a superpartner for each SM particle. This model is known as the Minimal Supersymmetric Standard Model (MSSM). It has to be a chiral theory, as the SM is chiral as well. This requires the fermionic charges to form one spinor in four-dimensional Minkowski spacetime, which is known as $\mathcal{N} = 1$ SUSY. Theories with more SUSY generators do not allow for a chiral spectrum. The fermions of the SM receive their mass from two Higgs doublets and their superpartners, the Higgsinos. We need two Higgs and Higgsinos for two reasons: to get a SUSY invariant mass term for the up-type and down-type fermions and to cancel gauge anomalies. The superpartners of the gauge bosons, the gauginos, can be used to break the SUSY of the MSSM at the right scale by giving them a non-vanishing vev [4]. Thus the $\mathcal{N} = 1$ SUSY extension of the SM softens the fine-tuning problem and at the same time leads to gauge coupling unification, which makes it particularly suited for GUT theories.

Consequently following the idea of unification, the next thing to do is to unify the (MS)SM with gravity. One attempt to unify them would be to postulate that gravity is also mediated by a gauge boson, the graviton. However, this approach could encounter problems, as naive power-counting arguments suggest that a quantum field theory of gravity is non-renormalizable because one has to introduce new counter-terms (and consequently new parameters) at every loop order. This eventually leads to an infinite amount of parameters, rendering the theory useless for predictions. So it is desirable to construct a theory in which these divergencies do not appear.

Maybe the most prominent approach to reach unification in a theory which circumvents the power-counting argument of non-renormalizability and still includes the graviton is string theory. String theory starts with the assumption that the elementary particles are not point-

like but in fact extended one-dimensional objects. Since we know that for example the electron has no structure down to 10^{-22}m, these objects must be very small. Different particles emerge from vibrations of these objects called strings. Owing to the smallness of the strings, even the first excited oscillations are so massive that they are inaccessible to current experiments, hence it is enough to look at the massless string spectrum. It is interesting to note that for string theory at its fundamental level the string length is the only free parameter. Additionally, string theory always contains a graviton. Maldacena conjectured [5] that string theory is under certain conditions dual to a gauge theory without gravity, thereby allowing to connect string theory to ordinary gauge theories. Nevertheless, it is yet unknown how to get for example the (MS)SM from string theory. However, as string theory is unlikely to be directly testable due to its high energy scale, it is crucial to check that string theory is consistent with observable phenomena.

Requiring string theory to be renormalizable, supersymmetric and Poincaré invariant, we are left with five different kinds of string theory. *Type I* string theory contains open and closed strings, while all others can be formulated with closed strings only. *Type IIA* has a non-chiral spectrum while the one of *Type IIB* is chiral. The last two theories are $E_8 \times E_8$ and $SO(32)$ *heterotic string theory*. The name stems from the fact that the theory treats left- and right-moving strings differently. Although more recently efforts have been made to get the (MS)SM from Type II string theory using intersecting D-brane stacks [6–9], heterotic string theory has been the most popular string theory for model building in the last years. This thesis will be concerened with heterotic $E_8 \times E_8$ theory and its low-energy limit, ten-dimensional supergravity (SUGRA).

One of the predictions string theory makes is that (under some assumptions) the superstrings live in ten-dimensional spacetime. This follows for example from looking at the central charge. Using BRST quantization, one can show that the total central charge of the fermions cancels only in ten spacetime dimensions. As we perceive only four dimensions, six of them must be hidden. Although other possibilities exist (see e.g. [10]), a very common approach is to compactify these extra dimensions on a scale small enough to be visible only for the strings. Interestingly, this compactification can at the same time break the large gauge groups of heterotic string theory to much smaller ones, like the ones of the MSSM. The small length scale of the string corresponds to a high energy scale and it is reasonable to assume SUSY to be unbroken at this scale, which is desireable to soften the fine-tuning problem. In this way, the compactification space should allow for $\mathcal{N} = 1$ supersymmetry, which is the right setting for the MSSM. This puts severe constraints on the geometry of the compactification spaces. One possible compactification space is called a Calabi-Yau (CY) manifold. These are complex Ricci-flat manifolds. Unfortunately, it is very complicated to give an explicit metric of these spaces, so calculations have to rely on topological invariants and can only be carried out in the low energy approximation, which is ten-dimensional SUGRA. It is therefore crucial to have access to these topological data in order to be able to calculate the gauge groups and the particle spectrum of the theory. Recently, there has been some success in building MSSM-like heterotic string models directly on CY manifolds [11, 12].

Another way of constructing compactification spaces compatible with $\mathcal{N} = 1$ SUSY are orbifolds [13, 14]. Toroidal orbifolds are spaces which are, as the name suggests, compactified on a torus. Additionally, one divides out a discrete symmetry group of the underlying lattice. As the action of the symmetry is not free, this introduces curvature singularities in the formally flat manifold. At first the emergence of singularities in spacetime might seem infeasible. However, with strings being extended objects, they cannot live entirely in these

singularities but can wrap around them (this type of string is called twisted string). Unlike the CY cases, one can use conformal field theory (CFT) on these spaces to perform direct string calculations, as the construction of these spaces is easy and well understood. Orbifolds provide a beautiful mechanism to compactify the space and at the same time break the gauge group. For consistency requirements the symmetry group must act on both the gauge group and the compactification space. By switching on a non-trivial gauge background via the Wilson line mechanism, the gauge group can be further broken down to yield SM or GUT gauge groups [15–19].

More recently, the Mini-Landscape was published, which contains more than 200 MSSM-like orbifold models for the $\mathbb{Z}_{6-II}$ orbifold [20–22]. These models are built on local GUTs, which means that at the fixed points, the spectrum is locally a GUT spectrum. This has the advantage that using the standard hypercharge generator for these GUTs leaves the hypercharge non-anomalous. The spectrum contains further particles which are charged under the SM gauge groups. However, these exotics are vector-like and can be decoupled from the massless spectrum by giving them a mass, yielding a net three generation model. These models contain an anomalous $U(1)$. While the anomaly is canceled by the Green-Schwarz mechanism, it introduces a Fayet-Iliopoulos (FI) term that could spoil D-flatness and consequently supersymmetry. By giving vevs to twisted orbifold states, the exotics can be decoupled and the FI term can be canceled at the same time. As it turns out, giving vevs to twisted states can be described by smoothening out the singularity the corresponding twisted string wraps.

The process of smoothening out the singularities is referred to as blowup procedure [23–28]. The blowup can be performed such that the resulting blowup manifold is a CY manifold [29, 30]. Hence the blowup procedure should give us a way to transfer the orbifold MSSM models to a smooth CY manifold.

It is very useful to understand the connection of these two spaces, as this allows us to use the advantages and to avoid the disadvantages of both approaches. It is therefore one major concern of this thesis to work out relations between the two pictures. This means that we first perform the blowup which makes the transition between the orbifold and the CY and then investigate in detail two orbifold models, the $\mathbb{Z}_{6-II}$ and the $\mathbb{Z}_2 \times \mathbb{Z}_2$ orbifold, when formulated on the resulting CY. Working with the examples helps us to formulate the findings on a more general ground.

The thesis is organized as follows:
In the second chapter, we introduce two compactification spaces, the CY manifold and the orbifold. In the CY case we give the defining properties. We also introduce important topological invariants which can be used to characterize the manifold. Additionally, the notion of divisors as submanifolds of complex codimension one is introduced and it is explained how integrals can be performed using divisors. We make intensive use of this calculation method throughout the thesis. The orbifold section explains in some detail the underlying construction principles, which involve modding out an orbifold point group or space group. The orbifold action has to act on both the space and the gauge group simultaneously. The action on the gauge degrees of freedom is described in terms of the orbifold shift vector and the Wilson lines.

After this, we shortly discuss heterotic string theory and review the conditions that have to be imposed on strings which are modular invariant and obey the orbifold boundary conditions. These conditions strongly constrain the orbifold shift vector and the Wilson lines.

Additional constraints which physical orbifold states have to satisfy are the mass-shell and level-matching conditions. Next, we analyze the bosonic and fermionic string partition function. We introduce local orbifolds, which are defined by giving the physical orbifold states at each fixed point separately rather than giving the (global) orbifold input data, which is commonly done in the literature. The investigation of modular invariance of the partition functions reveals new phases that occur when $E_8 \times E_8$ lattice vectors are added locally to the states at the orbifold fixed points. Orbifold models that are related to each other by a global $E_8 \times E_8$ lattice shift are called brother models in the literature [31]. In this spirit, we propose the name grandchildren models for the localized version of the brother models.

At the end of the chapter, we apply the techniques introduced above to our two example orbifolds, the $\mathbb{Z}_{6-II}$ and the $\mathbb{Z}_2 \times \mathbb{Z}_2$ orbifold. The $\mathbb{Z}_{6-II}$ orbifold is taken from the Mini-Landscape and thus has all the phenomenological properties given above. The $\mathbb{Z}_2 \times \mathbb{Z}_2$ manifold is constructed to give an $SU(5)$ GUT spectrum. The reason for this will become apparent in chapter 6.

The next chapter is devoted to the blowup procedure. We introduce the necessary tools and outline the procedure to perform the blowup. We start with the local resolution of non-compact orbifolds. The resolution process, which corresponds to assigning a topology to the fixed points, involves the introduction of divisors. There is one ordinary divisor for each torus and one exceptional divisor for each twisted orbifold sector. The exceptional divisors are lying inside the orbifold singularity. So-called linear equivalence relations link both divisor types. They can be represented graphically with the help of toric diagrams. The relative divisor position on the CY is determined by the triangulation that is chosen for the diagram. We see that the triangulation is not unique and that different triangulations result in different blowup manifolds. The toric diagrams can equivalently be given in terms of dual graphs. We introduce a further, three-dimensional diagrammatic analog to these graphs, which we propose to call unprojected dual graphs. The two-dimensional dual graphs can be gained from them via a suitable projection. One big advantage of these new graphs is that in their depiction the emergence of different triangulations can be explained in terms of simple parameters in the picture. Additionally, adjusting these continuous parameters allows to switch between different triangulations, which seems to be a discrete change in the toric diagram picture.

The local non-compact discussion is then extended to the compact case, where the different non-local resolutions are glued together. In order to perform the gluing, we introduce another type of divisors, the inherited divisors, which descend directly from the torus. These new divisors modify the previously found linear equivalence relations. As we glue together resolutions of different fixed points, we introduce labels on all divisors in order to be able to distinguish between them.

The intersection numbers, which are a crucial quantity for the rest of the thesis, can be computed with the help of auxiliary polyhedra. After reviewing their construction method and the way they can be used to infer the intersection numbers, we extend the previously introduced unprojected dual graph construction to the compact case. The advantages of this depiction over the auxiliary polyhedra will be discussed in chapter 7.

In the following example sections we apply the methods introduced above to our two example orbifolds. We construct the toric diagrams, the dual graphs, the unprojected dual graphs, and the auxiliary polyhedra, which allow us to read off some of the intersection numbers. Additionally, we work out the linear equivalences from which the rest of the intersection numbers can be computed. The intersection numbers for some triangulations can be found in

Appendix C. We further explain how other topological invariants of the CY, like the Hodge numbers and the Euler number, can be computed and compare the results to the orbifold case. Additionally, we explain how the Chern classes can be expressed in terms of divisors. At the end, we give an estimate on the number of inequivalent triangulations for both blowup models. The numbers turn out to be extremely large.

The fourth chapter is very crucial for this thesis. We investigate conditions that have to be imposed on the gauge flux of the CY manifold in order to define a consistent model. We take the gauge flux of the CY to be Abelian, described by line bundle vectors. Although this simplifies some aspects like stability issues, there are still many requirements that have to be imposed. The most stringent ones come from the Bianchi identities of the three-form field strength H. We first review briefly how to get to these equations. It is then explained how these equations can be calculated explicitly on the blowup manifold using the information obtained from the blowup procedure. For this we argue that the gauge flux can be expanded in exceptional divisors. We also make contact with the orbifold shift vector and Wilson lines by integrating the gauge flux over appropriate curves. This gives an identification of the local orbifold shifts and the line bundle vectors. Having obtained an explicit expression for the Bianchi identities, we need to figure out a way to solve the resulting complicated set of equations. This can be done by rewriting the equations in terms of non-linear Diophantine equations and exploiting recurring patterns to simplify them.

As there generically is an anomalous $U(1)$ on the orbifold, we investigate the Green-Schwarz anomaly cancelation mechanism. This reveals that twisted orbifold states reappear as axions on the CY manifold. These axions can be used to cancel additional anomalous $U(1)$'s on the blowup manifold. Furthermore, the identification reveals an interesting behavior of the volume of the blowup hypersurfaces in the orbifold limit: the limit corresponds to taking the volume to minus infinity. This is astonishing but in agreement with [32]. In addition, the identification of the local orbifold twists and the line bundle vectors allows us to uncover relations between the masses of states on the orbifold and constraints coming from the topology of the blowup manifold.

We conclude this chapter by investigating the $\mathbb{Z}_{6-II}$ and the $\mathbb{Z}_2 \times \mathbb{Z}_2$ orbifold. We explicitly work out the identification between the local orbifold shifts and the line bundle vectors. Subsequently, we calculate the Bianchi identities. It is described in detail how the equations can be simplified and solved. In the analysis of the solution, we compare the bundle vectors to the mass-shell equations. We find that many Bianchi identities reproduce the mass-shell equations for a vanishing oscillator number while (in the $\mathbb{Z}_{6-II}$ case) some Bianchi identities dictate a non-vanishing oscillator number. We further point out that the solution is non-unique and illustrate this point with examples. At the end, we give the identification of the line bundle vectors with the twisted orbifold states.

Having obtained a gauge flux that satisfies all consistency requirements of the CY manifold, we can compute the resulting spectrum and compare it to the orbifold. This is done in the following chapter. At the beginning, we will shortly review some group theoretical properties and index theorems resulting from anomaly cancelation conditions for the gaugino. These techniques are used to compute the massless particle spectrum in blowup. We also discuss possible anomalies that can occur in the spectra.

The analysis is carried out for both example orbifolds at the end of the chapter. We give the number operator which is used to determine the number of generations and use it to compute the spectrum and the anomalies of the underlying model. This reveals that in the $\mathbb{Z}_{6-II}$ case the hypercharge is broken in full blowup. In the $\mathbb{Z}_2 \times \mathbb{Z}_2$ case the hypercharge is

conserved but the particle spectrum is - as in the orbifold case - still that of an $SU(5)$ GUT and not that of the MSSM.

The following chapter deals with a way out of the broken hypercharge problem. It is demonstrated how the anomalous hypercharge arises from the Wilson line that is used to perform the breaking to the $SU(3) \times SU(2)$ part of the SM gauge group. Using very generic arguments, it is shown that all 223 Mini-Landscape models suffer from this problem and are thus unsuited for blowup. It can be seen that the anomalous hypercharge does not arise in GUT theories if its generator is embedded in the usual way in the $SU(5)$, which is the reason why the hypercharge is non-anomalous in the $\mathbb{Z}_2 \times \mathbb{Z}_2$ case. In order to break the GUT group of this orbifold to the SM gauge groups, we divide out a freely acting $\mathbb{Z}_2$ element, which by construction is a remaining symmetry of the model. This approach is unsuited for the $\mathbb{Z}_{6-II}$ case, as no such symmetry exists there. The action of the $\mathbb{Z}_2$ has to be free as we do not want to introduce new singularities in the smooth blowup manifold and as we do not want the Wilson line corresponding to this action to appear in the line bundle identifications.

In a rather technical calculation we again investigate the orbifold string partition function. This allows us to derive new conditions that have to be imposed on the underlying orbifold data. Among already known relations, we uncover a new relation that has to be imposed on the Wilson line of the freely acting $\mathbb{Z}_2$ element. At the end, we check that the $\mathbb{Z}_2 \times \mathbb{Z}_2$ model fulfills these requirements and divide out the freely acting $\mathbb{Z}_2$. We show that the resulting spectrum has a net number of three generations for all SM particles and that the hypercharge is non-anomalous.

The last chapter deals with the issue of preserving SUSY on the orbifold and the blowup manifold. We very briefly introduce the most important supersymmetric quantities. Then we review how D-flat solutions can be found on the orbifold side. This is most conveniently done by arranging fields in so-called holomorphic invariant monomials. This allows to reduce the problem of finding D-flat directions to finding the kernel of a charge matrix. Non-negative integer kernel vectors correspond to the powers of the fields in the monomials, which in turn parameterize the relative size of the vevs of the orbifold fields.

On the blowup side, we argue that D-flatness is connected to a part of the hermitian Yang-Mills equations by looking at the equations of motion for the D-field. By manipulating the integrated version of the hermitian Yang-Mills equations (the so-called Donaldson-Uhlenbeck-Yau equations) we rewrite the equation in terms of the volume of exceptional divisors. Comparing the resulting equation to the previous discussion allows us to argue that the relative volume of the divisors corresponds to the relative size of the vevs of the orbifold states. Subsequently, we consider the changes in the presence of anomalous $U(1)$'s. In this case, we need to take (one-)loop corrections to the Donaldson-Uhlenbeck-Yau conditions into account. On the orbifold side, the vevs of the fields have to be chosen such that they cancel the FI term.

After that, we point out that finding F-flat directions on the orbifold side is rather complicated. It can be performed by analyzing the superpotential. However, as the exact form of the superpotential is unknown, the analysis has to be performed in general at each order of the superpotential. On the blowup side, we can again establish a connection between the F-flatness constraints and the hermitian Yang-Mills equations, which force the gauge flux to be holomorphic by using the equations of motion for the F-field. As we expand the gauge flux in divisors, which are $(1,1)$-forms, F-flatness is intrinsically satisfied in our construction.

To conclude, we apply our discussion to the $\mathbb{Z}_2 \times \mathbb{Z}_2$ orbifold example. We calculate the one-loop corrected Donaldson-Uhlenbeck-Yau equations and investigate the volume of the

divisors. We find that for the gauge flux derived from the Bianchi identities, the volumes of all exceptional divisors can be chosen positive, indicating that all singularities can be blown up. Finding this last consistency check fulfilled, we conclude that we have found a supersymmetry conserving gauge flux in the example sections which produces a net number of three Standard Model generations on the blowup Calabi-Yau manifold. We then illustrate qualitatively a connection between the Kähler moduli on the one hand and the parameters characterizing the unprojected dual graphs on the other. Qualitatively, the two quantities seem to agree, which is checked by analyzing the dependence of the volume of all occurring curves on these parameters in both pictures.

At the end of the thesis we give a discussion of the various results and an outlook on possible further research directions. The appendix contains a list of the most frequently used symbols and give more details on certain topics.

Chapter 2

. . . . . .

Compactification spaces

As was already mentioned in chapter 1, we need to compactify ten-dimensional string theory to four dimensions on either a Calabi-Yau manifold or an orbifold. Chirality of the MSSM necessitates having left $\mathcal{N} = 1$ SUSY in four dimensions after compactification. This constrains the compactification space in the case of a vanishing three-form field strength to being Ricci flat, Kähler, and of $SU(3)$ holonomy. In the first section we briefly review how this condition is satisfied when using Calabi-Yau manifolds. The second chapter deals with orbifolds as compactification spaces. We will see that there are only a few $\mathcal{N} = 1$ SUSY orbifolds possible. Furthermore, the orbifold construction gives rise to new boundary conditions, which in turn impose constraints on the partition function and with it on the orbifold action.

2.1 Compactification on Calabi-Yau manifolds

This section outlines the conditions that have to be imposed on a manifold in order to preserve $\mathcal{N} = 1$ SUSY upon compactification from ten to four dimensions. The outline given here follows [30, 33]. Let us factorize our ten-dimensional target space as $\mathcal{M}_{10} = \mathcal{M}_{1,3} \times K$, where $\mathcal{M}_{1,3}$ is the four-dimensional Minkowski space (indexed in small Greek letters) and K is some six-dimensional space (indexed in lower case Latin letters).

The ten-dimensional $\mathcal{N} = 1$ supergravity multiplet contains a metric g, the gravitino ψ, the dilatino χ, and the dilaton Φ. The gaugino λ and the two-form field $\mathfrak{F}$ are from the super Yang-Mills multiplet. H is the three-form field strength associated to the two-form field B, and ω is the spin connection. Under the assumption that $H = 0$, the dilatino variations imply that the dilaton is constant, $\partial_m \Phi = 0$. We already assumed a constant dilaton to derive the requirement of a ten-dimensional spacetime. When splitting the ten-dimensional manifold into a four- and a six-dimensional part, the **16** of $SO(9, 1)$ decomposes as

$$\mathbf{16} \to (\mathbf{2}, \mathbf{4}) + (\overline{\mathbf{2}}, \overline{\mathbf{4}}). \tag{2.1}$$

This means that a Majorana-Weyl **16** SUSY parameter can be written as

$$\epsilon \to \epsilon_{\alpha\beta} + \epsilon^*_{\alpha\beta}, \tag{2.2}$$

where the indices (α, β) transform in the $(\mathbf{2}, \mathbf{4})$. If any SUSY is unbroken, we can apply $SO(3,1)$ rotations to bring this to the form

$$\epsilon_{\alpha\beta} = u_\alpha \zeta_\beta \tag{2.3}$$

for an arbitrary Weyl spinor u. Each internal spinor ζ for which the variations vanish gives a copy of the four-dimensional SUSY algebra. From the vanishing of the gravitino variation, we find that ζ must be covariantly constant:

$$\nabla_m \zeta = 0. \tag{2.4}$$

As it turns out, this is a very strong condition. For example it implies that $0 = [\nabla_m, \nabla_n]\zeta = \frac{1}{4} R_{mnpq} \Gamma^{pq} \zeta$. From this condition it follows that the internal space K must be Ricci flat, $R_{mn} = 0$. By investigating the complex structure it can be seen that K is a Kähler manifold. Additionally, one finds that K must have $SU(3)$ holonomy. This follows because a covariantly constant spinor must return to itself upon parallel transport along closed loops. So we are looking for the stabilizer subgroup of the general holonomy group $SO(6)$ of a six-dimensional manifold. As a Lie algebra, $SO(6) \cong SU(4)$ with the positive- and negative-chirality spinors living in the fundamental $\mathbf{4}$ and $\overline{\mathbf{4}}$ of $SU(4)$ respectively. The subgroup that acts trivially on an element of the $\mathbf{4}$ is $SU(3)$. Thus K must have $SU(3)$ holonomy.
The gaugino variation vanishes if $\mathcal{F}_{mn}\Gamma^{mn}$ is also an $SU(3)$ rotation. Written in terms of the complex indices transforming under $SU(3)$, this means that

$$\mathcal{F}_{ij} = \mathcal{F}_{\bar{i}\bar{j}} = 0, \quad G^{i\bar{j}} \mathcal{F}_{i\bar{j}} = 0. \tag{2.5}$$

A general compact manifold does of course not allow for a Ricci flat Kähler metric of $SU(3)$ holonomy, and there are very few examples with an explicit metric. It can be shown that for a Kähler manifold, only the mixed components $\mathcal{R}_{i\bar{j}}$ of the Ricci tensor are non-zero. One defines the first Chern class $c_1 := (2\pi)^{-1} \mathcal{R}_{i\bar{j}} dz^i dz^{\bar{j}}$. Obviously this is zero for a Ricci flat manifold. It was conjectured by Calabi and proved by Yau that any Kähler manifold with vanishing first Chern class always admits a Kähler metric of $SU(3)$ holonomy. In their honor, Kähler manifolds with vanishing first Chern class are called Calabi-Yau manifolds.
The discussion in the case of a non-vanishing H is much more involved [34] and there is not much literature in this case. One important difference that occurs is that the compactification space is not Kähler anymore, i.e. the Kähler form J is not closed. However, the form ω defined by $\omega := e^{-2\phi} J \wedge J$ is closed. The H-field is related to the derivatives of the Kähler form by $H = i(\overline{\partial} - \partial)J$. In the case of the six-dimensional background fluxes being T^2 fibers over a K3 Calabi-Yau twofold, there is a theorem which guarantees the existence of a solution for the differential equation of the dilaton. Apart from this case, we are not aware of a theorem which guarantees that the occurring differential equations have a solution.

It turns out that Calabi-Yau manifolds impose several constraints on the possible dimensions of the Dolbeault cohomology classes. The dimension of the cohomology classes, the Hodge numbers $h^{p,q}$, are conventionally written as the Hodge diamond, which must be of the

form

$$\begin{array}{ccccc} & & h^{3,3} & & \\ & h^{3,2} & & h^{2,3} & \\ h^{3,1} & & h^{2,2} & & h^{1,3} \\ h^{3,0} & & h^{2,1} & & h^{1,2} & & h^{0,3} \\ h^{2,0} & & h^{1,1} & & h^{0,2} \\ & h^{1,0} & & h^{0,1} & \\ & & h^{0,0} & & \end{array} = \begin{array}{ccccc} & & 1 & & \\ & 0 & & 0 & \\ 0 & & h^{1,1} & & 0 \\ 1 & & h^{2,1} & & h^{2,1} & & 1. \\ 0 & & h^{1,1} & & 0 \\ & 0 & & 0 & \\ & & 1 & & \end{array} \tag{2.6}$$

This means that the Hodge numbers of a CY manifold are completely fixed by $h^{1,1}$, which gives the number of Kähler moduli and $h^{2,1}$, which gives the number of complex structure moduli. Using the relation between the Betti numbers and the Hodge numbers, the Euler number of the manifold is found to be

$$\chi = 2(h^{1,1} - h^{2,1}). \tag{2.7}$$

The submanifolds of the CY with complex codimension one (i.e. complex dimension two) are called divisors. We can associate a line bundle to each divisor S whose first Chern class gives the Poincaré dual of the cycle. This will be a $(1,1)$-form for holomorphic line bundles. Thus $h^{1,1}$ in (2.6) gives the number of independent divisors on the CY manifold. By an abuse of notation, we will refer to both the cycle and the $(1,1)$-form as S, as it should be clear from the context which object is meant. From the divisors we can calculate the intersection numbers, which are a very important topological quantity of the CY manifold and will play a major role throughout the thesis. They are defined as

$$\mathrm{Int}(S_i S_j S_k) = \int_X S_i \wedge S_j \wedge S_k = \int_{S_i S_j S_k} \mathbb{1}. \tag{2.8}$$

As long as at least one divisor is a compact hypersurface, the intersection numbers count how often the hypersurfaces intersect. However, using (2.8) we can also compute self-intersections, i.e. intersections which involve the same divisor more than once. It turns out that albeit having the same Hodge diamond, two CY can still have different intersection numbers.

Another quantity that is given in terms of divisors is the Kähler $(1,1)$-form J. It can be expanded in divisors as

$$J := \sum_i k_i S_i, \tag{2.9}$$

where the coefficients k_i are called Kähler moduli. The Kähler form can be used to calculate the volumes of cycles $\mathcal{C}$, divisors S, and the whole manifold X via

$$\mathrm{vol}(\mathcal{C}) := \int_{\mathcal{C}} J, \qquad \mathrm{vol}(S) := \frac{1}{2!}\int_S J \wedge J, \qquad \mathrm{vol}(X) := \frac{1}{3!}\int_X J \wedge J \wedge J. \tag{2.10}$$

These integrals, as well as many other integrals like the ones appearing in the Bianchi identities and the Donaldson-Uhlenbeck-Yau equations, can be computed via (2.8) by summing

up intersection numbers. That way the intersection numbers provide access to computations on the CY manifold. In chapter 3, we will work out in some detail how to obtain them. But before discussing this procedure, we want to discuss orbifolds as compactification spaces.

2.2 Orbifolds

In this section we will look in some detail at another way of compactifying our theory, namely toroidal orbifolds [13, 14]. These are flat spaces except for fixed points, where conical curvature singularities occur. Toroidal orbifolds can be either constructed by modding out a lattice and a point group, or by modding out a space group, which is subsequently discussed. After that we introduce the notion of locally defined orbifolds and examine their transformation properties under a change in the underlying orbifold data. At the end of the chapter, we illustrate two examples for orbifolds, the $\mathbb{Z}_{6-II}$ and the $\mathbb{Z}_2 \times \mathbb{Z}_2$ orbifold.

2.2.1 Construction methods

In the point group construction approach, we generate a six-dimensional torus T^6 by choosing a six-dimensional lattice spanned by basis vectors e_i

$$\Gamma_T = \{n_i e_i,\ n_i \in \mathbb{Z}\}. \tag{2.11}$$

We choose this lattice to be equal to the root lattice of some semi-simple Lie algebra. One can introduce an equivalence relation on $\mathbb{R}^6$ by taking the quotient space

$$T^6 \equiv \mathbb{R}^6/\Gamma_T. \tag{2.12}$$

The construction is schematically illustrated in two dimensions in figure 2.1. Conventionally, the two lattice vectors are 1 and τ, where τ is called the modular parameter. Its direction parameterizes the "shearing" of the torus. In the models we investigate the six-dimensional torus factorizes, $T^6 = T^2 \otimes T^2 \otimes T^2$. In order to get from the torus to the orbifold $\mathbb{O}$, we divide out a symmetry group of the underlying lattice, the so-called point group P: $\mathbb{O} = T^6/P$. In this thesis, we will exclusively deal with the Abelian $\mathbb{Z}_N$ or $\mathbb{Z}_M \times \mathbb{Z}_N$ point groups, so $\mathbb{O} = T^6/\mathbb{Z}_N$ or $\mathbb{O} = T^6/(\mathbb{Z}_M \times \mathbb{Z}_N)$. The point group must act crystallographically, i.e. it must be an automorphism of the underlying lattice. The action of the $\mathbb{Z}_N$ twist can be written in terms of complex coordinates $z_j = \frac{1}{\sqrt{2}}\left(x^{2j-1} + ix^{2j}\right),\ j \in \{1,2,3\}$ as

$$\theta : (z^1, z^2, z^3) \mapsto (e^{2\pi i\varphi^1}\ z^1, e^{2\pi i\varphi^2}\ z^2, e^{2\pi i\varphi^3}\ z^3). \tag{2.13}$$

The action of $\mathbb{Z}_M \times \mathbb{Z}_N$ orbifolds is given in terms of two twists

$$\begin{aligned} \theta_1^M :&\quad (z^1, z^2, z^3) \mapsto (e^{2\pi i\varphi_1^1}\ z^1, e^{2\pi i\varphi_1^2}\ z^2, e^{2\pi i\varphi_1^3}\ z^3), \\ \theta_2^N :&\quad (z^1, z^2, z^3) \mapsto (e^{2\pi i\varphi_2^1}\ z^1, e^{2\pi i\varphi_2^2}\ z^2, e^{2\pi i\varphi_2^3}\ z^3). \end{aligned} \tag{2.14}$$

As the underlying symmetry is of order N, the orbifold twist vector φ must fulfill

$$\theta^N = 1 \qquad \Rightarrow \qquad N\varphi^i \equiv 0 \bmod 1. \tag{2.15}$$

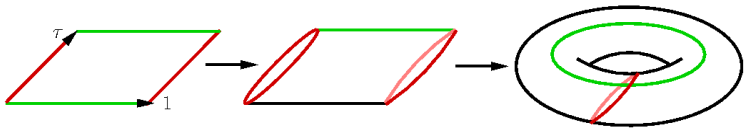

Figure 2.1: Construction of a torus: First put a lattice on $\mathbb{R}^2$. By identifying the green lines, we get a cylinder. Subsequently, we identify the red lines to get a torus.

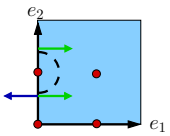

Figure 2.2: The dashed line is a closed loop on the $\mathbb{Z}_2$ orbifold, as the endpoints are identified by a $\mathbb{Z}_2$ twist. Upon parallel transport around this closed loop, the green vector does not return to itself but is twisted by 180° (blue vector). The red dots are fixed points.

Preserving $\mathcal{N} = 1$ SUSY in four dimensions requires that the $\mathbb{Z}_N$ twist, which corresponds to the holonomy group, is contained in the $SU(3)$ subgroup of $SO(6)$, cf. section 2.1. This is the so-called Calabi-Yau condition, which can be written as

$$\sum_{i=1}^{3} \varphi^i \equiv 0 \bmod 1. \tag{2.16}$$

So although the torus is flat, the quotient can have a non-trivial holonomy as illustrated in figure 2.2.

The automorphisms of $SO(6)$ are of order 2 to $10, 12, 14, 15, 18, 20, 24,$ or 30. Imposing additionally (2.16), we find that the only possibilities for the point group are $\mathbb{Z}_N$ with $N = 3, 4, 6, 7, 8, 12$ or $\mathbb{Z}_N \times \mathbb{Z}_M$ with M being a multiple of N and $N = 2, 3, 4, 6$. This thesis deals with both kinds of orbifolds, namely the $\mathbb{Z}_{6-II}$ and the $\mathbb{Z}_2 \times \mathbb{Z}_2$ orbifold.

Orbifolds can also be constructed by starting with a group of translations followed by rotations, the so-called space group $\mathbb{S}$: $\mathbb{O} = \mathbb{R}^6/\mathbb{S}$. Let the lattice translations be denoted by l and the rotations by θ^k, $k \in \{1, 2, \ldots, N-1\}$. The action of the space group elements (θ^k, l) lead to an equivalence relation on $\mathbb{R}^6$:

$$z \sim (\theta^k, l)z := \theta^k z + l. \tag{2.17}$$

The composition of two elements of $\mathbb{S}$ is simply $(\theta^{k_1}, l_1) \circ (\theta^{k_2}, l_2) = (\theta^{k_1+k_2}, \theta^{k_1} l_1 + l_2)$. Compared to the first approach, the torus shifts l define the lattice (2.11) and the rotations θ represent the point group P. The orbifold construction is schematically depicted in figure 2.3.

The space group does not act freely but has fixed points f which are invariant under the action of a non-trivial space group element (θ^k, l):

$$f = (\theta^k, l)f = \theta^k f + l = \theta^k f + n_i e_i, \quad n_i \in \mathbb{Z}. \tag{2.18}$$

If a twist θ^k acts trivially on one complex coordinate, $\theta^k z_i = z_i$, one obtains a two-dimensional fixed subspace. On the covering space, such a space looks just like a fixed torus (although the orbifold itself does not necessarily have the geometry of a torus). Hence such subspaces are called fixed tori or fixed (complex) lines.

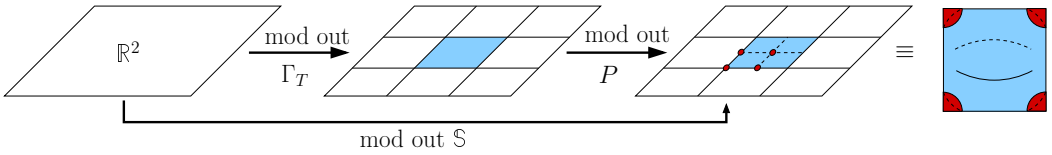

Figure 2.3: An orbifold is constructed by first modding out a torus lattice. Subsequently, we mod out a discrete symmetry group of the lattice. This "folds" the fundamental domain along the broken line and one obtains a "pillow" (in the $\mathbb{Z}_2$ case). The procedure introduces fixed points (red). Equivalently, we can mod out the space group $\mathbb{S}$ from $\mathbb{R}^2$.

2.2.2 Orbifold conditions

Next we review some technical details about heterotic strings on orbifolds. In heterotic string theory, we treat left-movers and right-movers differently. The left-movers are (in the bosonized version) bosonic strings in 26 dimensions, the right-movers are ten-dimensional bosonic and fermionic strings linked by supersymmetry. In order to have the same dimensionality for left- and right-movers, 16 dimensions of the left-movers are compactified on a 16-torus. Consistency requirements force the lattice of the 16-torus to be even and self-dual. The only 16-dimensional weight lattices fulfilling these requirements are $E_8 \times E_8$ and $SO(32)$. This thesis deals exclusively with heterotic $E_8 \times E_8$ string theory. After quantization, a string state can be given as $|q\rangle_R \otimes \tilde{\alpha} |p\rangle_L$ where q is the $SO(8)$ weight lattice momentum of the right-movers describing the space-time properties of the string and p is the $E_8 \times E_8$ root lattice momentum of the 16 gauge degrees of freedom of the left-movers. Furthermore, $\tilde{\alpha}$ describes possible oscillator excitations. The root lattice Λ_{E_8} can be defined as

$$\Lambda_{E_8} \equiv \Lambda_V \oplus \Lambda_S \equiv \left\{\underline{\pm 1, \pm 1, 0^6}\right\} \oplus \left\{\left\{\underline{\pm \frac{1}{2}^8}\right\} \middle| \#(-) \equiv 0 \bmod 2\right\}, \tag{2.19}$$

where the underline indicates permutation of the entries and the superscript denotes repetition of the entry as often as indicated. E_8 can be thought of as a spinor bundle over $SO(16)$. Owing to the self-duality of E_8, the momentum lies in the same lattice as the coordinates themselves.

The orbifold construction additionally imposes new constraints on the boundary conditions of the strings. A space group element $g = (\theta^k, n_i e_i)$ of $\mathbb{S}$ has to fulfill:

$$\begin{aligned} Z(\tau, \sigma + 2\pi) &\stackrel{!}{=} gZ(\tau, \sigma) = \theta^k Z(\tau, \sigma) + n_i e_i, \;\; k \in \{0, 1, \ldots, N-1\}, \;\; n_i \in \mathbb{Z}, \\ \psi(\tau, \sigma + 2\pi) &\stackrel{!}{=} \pm \theta^k \psi, \end{aligned} \tag{2.20}$$

where Z and ψ are the complex three-dimensional bosonic and fermionic coordinates, which provide a map from the two-dimensional worldsheet (τ, σ) to the ten-dimensional target space. If $g = \mathbb{1}$, the boundary condition is that of an ordinary closed string on the torus. These strings are referred to as untwisted strings. They can move freely around the orbifold. For non-trivial g, the string is closed on the orbifold but not on the torus. These strings are located around a fixed point f and are called twisted strings (see figure 2.4).

Modular invariance of the partition function requires that the geometrical action of the

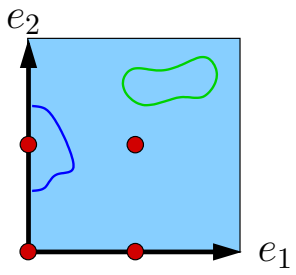

Figure 2.4: Schematic drawing of twisted (blue) and untwisted (green) strings on a $\mathbb{Z}_2$ orbifold. The red dots are fixed points.

space group $\mathbb{S}$ be extended from the six-dimensional compactification space to the gauge degrees of freedom ($E_8 \times E_8$ in our case) of the left-moving sector. This means we are also orbifolding the 16-torus. Requiring that the action is an automorphism of $E_8 \times E_8$, this orbifolding can be described by a shift and hence does not have any fixed points. The shift embedding of the space group is given by

$$g = (\theta^k, n_i e_i) \hookrightarrow (\mathbb{1}, V_g) \qquad V_g = kV_{sh} + \sum_{i=1}^{6} n_i W_i. \tag{2.21}$$

This means that a rotation by θ^k and a translation by $n_i e_i$ in the six-dimensional compactification space is accompanied by a shift V_g in the 16 gauge degrees of freedom. V_{sh} is called the orbifold shift vector and W_i are up to six Wilson lines. They are constrained to lie on the root lattice as follows:

$$NV_{sh} \in \Lambda_{E_8 \times E_8} \quad \text{and} \quad N_i W_i \in \Lambda_{E_8 \times E_8}. \tag{2.22}$$

Wilson lines can be thought of as being non-trivial – i.e. non-contractible – loops of the torus, or equivalently, as being constant gauge background fields with vanishing field strength. In the above equation N is the order of the orbifold action and N_i the order of the Wilson line, which is determined by the order of the twist in the direction of the Wilson line. Modular invariance of one loop amplitudes imposes yet additional requirements on the orbifold shift vector and on the Wilson lines [31]:

$$\begin{array}{ll} N(V_{sh}^2 - \varphi^2) & \equiv 0 \bmod 2, \\ N_i(W_i \cdot V_{Sh}) & \equiv 0 \bmod 2, \\ N_i W_i^2 & \equiv 0 \bmod 2, \\ \gcd[N_i, N_j](W_i \cdot W_j) & \equiv 0 \bmod 2, \ (i \neq j). \end{array} \tag{2.23}$$

Here, $\gcd[x, y]$ denotes the greatest common divisor[1] of x and y.

In general, physical states have to satisfy the mass-shell condition for left-movers (2.24a)

[1] In the case of the $\mathbb{Z}_2 \times \mathbb{Z}_2$ orbifold on an $SO(4)$ lattice, the constraint can be relaxed to $\gcd[N_i, N_j] \to 4$.

and right-movers (2.24b)

$$\frac{M_L^2}{8} = \frac{(p+V_g)^2}{2} + \tilde{N} + \delta c - 1 \tag{2.24a}$$

$$\frac{M_R^2}{8} = \frac{(q+\varphi_g)^2}{2} + \delta c - \frac{1}{2} \tag{2.24b}$$

$$M_L^2 = M_R^2. \tag{2.24c}$$

The constraint (2.24c) is the so-called level-matching condition. The vector V_g denotes the local shifts (2.21) corresponding to the spacegroup element $g = (\theta^k, n_i e_i)$. Analogously, $\varphi_g = k\varphi$ is called the local twist. The numbers δc contribute to the zero point energy and are given by

$$\delta c = \frac{1}{2}\sum_{i=1}^{3} \omega_i(1-\omega_i), \quad \text{where} \quad \omega_i = (\varphi_g)_i \bmod 1 \quad \text{such that} \quad 0 \leq \omega_i < 1. \tag{2.25}$$

An important quantity of twisted strings is the shifted momentum $p_{sh} := p + V_g$. It allows to determine the charge of the twisted states under gauge transformations.

2.2.3 Orbifold partition functions and local orbifold models

Taking into account the discussion of the previous subsection, it is sufficient to specify an orbifold model by giving its orbifold shift vector V_{sh} and Wilson lines W_i, which describe the orbifold action in the gauge degrees of freedom. Interestingly, the theory is not invariant under the addition of $E_8 \times E_8$ lattice vectors to the shift vectors and Wilson lines [31]. Adding lattice vectors ΔV_{sh} and ΔW_i to the shift vector and to the Wilson lines will in general induce a relative phase in the twisted sector and thus lead to inequivalent models. Models with different spectra whose input data differs only by lattice vectors are called brother models. It was shown that they are related to each other via non-trivial discrete torsion.

One could even go one step further and look at the change of the partition function when adding lattice vectors to the local orbifold shifts V_g. So in contrast to specifying the orbifold by giving the orbifold shift vector and Wilson lines, we will look at orbifolds that are defined by their local orbifold shifts V_g. We will refer to these models as locally defined (compact) orbifolds. The phase factor arising from adding $E_8 \times E_8$ lattice vectors to V_g can be derived from the string partition function, which is most conveniently given in terms of θ-functions and the Dedekind η-functions, cf. appendix B. We give the complete partition function Z as a product of the bosonic part Z_B and the fermionic part Z_F:

$$Z = \sum_{g,\overline{g}} \frac{1}{N_g} Z_B\begin{bmatrix} g \\ \overline{g} \end{bmatrix} Z_F\begin{bmatrix} V_g \\ V_{\overline{g}} \end{bmatrix}. \tag{2.26}$$

The N_g denote the order of the orbifold action in the g-sector. The dependence on (z,τ) will not be written explicitly most of the times in order to avoid cluttering up the notation. The fermionic part is subdivided into the partition function of the left-movers Z_λ and right-

movers Z_ψ,

$$Z_F = e^{-2\pi i \frac{1}{2} V_g \cdot (V_{\overline{g}} - e_{16})} Z^*_\psi \begin{bmatrix} \varphi_g \\ \varphi_{\overline{g}} \end{bmatrix} \prod_{a=1}^{2} Z_{\lambda_a} \begin{bmatrix} V_g \\ V_{\overline{g}} \end{bmatrix}, \tag{2.27}$$

where we defined $e_k \equiv (1, 1, \ldots, 1)$ to be a vector having k times the entry 1 and the index a to label the first and the second E_8. We introduced the partition functions

$$Z_{\lambda_a} \begin{bmatrix} V_g^{(a)} \\ V_{\overline{g}}^{(a)} \end{bmatrix} := \frac{1}{2} \sum_{s_a, \overline{s_a}} e^{-2\pi i \frac{\overline{s_a}}{2} e_8 \cdot V_g^{(a)}} \theta \begin{bmatrix} \frac{1-s_a}{2} e_8 - V_g^{(a)} \\ \frac{1-\overline{s_a}}{2} e_8 - V_{\overline{g}}^{(a)} \end{bmatrix} \cdot \eta^{-8} \tag{2.28a}$$

$$Z_\psi \begin{bmatrix} \varphi_g \\ \varphi_{\overline{g}} \end{bmatrix} := \frac{1}{2} \sum_{s} e^{-\pi i s \overline{s}} \theta \begin{bmatrix} \frac{1-s}{2} e_4 - \varphi_g \\ \frac{1-\overline{s}}{2} e_4 - \varphi_{\overline{g}} \end{bmatrix} \cdot \eta^{-4}, \tag{2.28b}$$

where $s, \bar{s}$ label the spin structure. Let us now investigate how the partition function changes under $V_g \to V_g' = V_g + \Delta V_g$ with $\Delta V_g \in \Lambda_{E_8 \times E_8}$. For this we first work out the transformation of Z_{λ_a}. It is convenient to calculate the transformation property for the vectorial and the spinorial weights of E_8 separately, cf. (2.19). Note that with the help of e_8, the spinorial part can be written as $V_S = \frac{1}{2} e_8 \oplus \Lambda_V$. Let us start with the case $\Delta V_g \in \Lambda_V$:

$$\begin{aligned} Z_{\lambda_a} \begin{bmatrix} V_g + \Delta V_g \\ V_{\overline{g}} \end{bmatrix} &= \tfrac{1}{2} \sum_{s_a, \overline{s_a}} e^{-2\pi i \frac{\overline{s_a}}{2} e_8 \cdot (V_g + \Delta V_g)} \theta \begin{bmatrix} \frac{1-s_a}{2} e_8 - (V_g + \Delta V_g) \\ \frac{1-\overline{s_a}}{2} e_8 - V_{\overline{g}} \end{bmatrix} \\ &= \tfrac{1}{2} \sum_{s_a, \overline{s_a}} e^{-2\pi i \frac{\overline{s_a}}{2} e_8 \cdot \Delta V_g} e^{-2\pi i \frac{\overline{s_a}}{2} e_8 \cdot V_g} \theta \begin{bmatrix} \frac{1-s_a}{2} e_8 - V_g \\ \frac{1-\overline{s_a}}{2} e_8 - V_{\overline{g}} \end{bmatrix} = Z_{\lambda_a} \begin{bmatrix} V_g \\ V_{\overline{g}} \end{bmatrix}, \end{aligned} \tag{2.29a}$$

$$\begin{aligned} Z_{\lambda_a} \begin{bmatrix} V_g \\ V_{\overline{g}} + \Delta V_{\overline{g}} \end{bmatrix} &= \tfrac{1}{2} \sum_{s_a, \overline{s_a}} e^{-2\pi i \frac{\overline{s_a}}{2} e_8 \cdot V_g} \theta \begin{bmatrix} \frac{1-s_a}{2} e_8 - V_g \\ \frac{1-\overline{s_a}}{2} e_8 - (V_{\overline{g}} + \Delta V_{\overline{g}}) \end{bmatrix} = \tfrac{1}{2} \sum_{s_a, \overline{s_a}} e^{-2\pi i \frac{\overline{s_a}}{2} e_8 \cdot V_g} \\ &\cdot e^{-2\pi i (\frac{1-s_a}{2} e_8 - V_g) \Delta V_{\overline{g}}} \theta \begin{bmatrix} \frac{1-s_a}{2} e_8 - V_g \\ \frac{1-\overline{s_a}}{2} e_8 - V_{\overline{g}} \end{bmatrix} = e^{2\pi i V_g \Delta V_{\overline{g}}} Z_{\lambda_a} \begin{bmatrix} V_g \\ V_{\overline{g}} \end{bmatrix}, \end{aligned} \tag{2.29b}$$

where we used $e_8 \cdot \Delta V_g \in 2\mathbb{Z}$ and (B.4a) for (2.29a) and (B.4b) for (2.29b).
Having worked out the relations above, it is now sufficient to look at $\Delta V_g = \frac{1}{2} e_8$ for the case $\Delta V_g \in \Lambda_S = \frac{1}{2} e_8 \oplus \Lambda_V$:

$$Z_{\lambda_a} \begin{bmatrix} V_g + \frac{1}{2} e_8 \\ V_{\overline{g}} \end{bmatrix} = \frac{1}{2} \sum_{s_a, \overline{s_a}} e^{-2\pi i \frac{\overline{s_a}}{2} e_8 \cdot (V_g + \frac{1}{2} e_8)} \theta \begin{bmatrix} \frac{1-s_a}{2} e_8 - (V_g + \frac{1}{2} e_8) \\ \frac{1-\overline{s_a}}{2} e_8 - V_{\overline{g}} \end{bmatrix} = Z_{\lambda_a} \begin{bmatrix} V_g \\ V_{\overline{g}} \end{bmatrix}, \tag{2.30a}$$

$$\begin{aligned} Z_{\lambda_a} \begin{bmatrix} V_g \\ V_{\overline{g}} + \frac{1}{2} e_8 \end{bmatrix} &= \tfrac{1}{2} \sum_{s_a, \overline{s_a}} e^{-2\pi i \frac{\overline{s_a}}{2} e_8 \cdot V_g} \sum_{n \in \mathbb{Z}^8} e^{-2\pi i \left(\frac{1-\overline{s_a}}{2} e_8 - V_{\overline{g}} - \frac{1}{2} e_8 \right) \cdot (n - V_g)} e^{2\pi i \tau \frac{1}{2} (n - V_g)^2} \\ &= \tfrac{1}{2} \sum_{s_a, \overline{s_a}} e^{-2\pi i \frac{\overline{s_a} - 1}{2} e_8 \cdot V_g} \theta \begin{bmatrix} \frac{1-s_a}{2} e_8 - V_g \\ \frac{1-\overline{s_a}}{2} e_8 - V_{\overline{g}} \end{bmatrix} = e^{2\pi i \frac{1}{2} e_8 \cdot V_g} Z_{\lambda_a} \begin{bmatrix} V_g \\ V_{\overline{g}} \end{bmatrix}, \end{aligned} \tag{2.30b}$$

where we used $e_8^2 = 8$ and $s_a \to s_a - 1$ for (2.30a), and (B.1) as well as $\overline{s_a} \to \overline{s_a} - 1$ for (2.30b). Substituting (2.29) and (2.30) into (2.27) yields for the phase change:

$$\begin{aligned} Z_F\begin{bmatrix} V_g + \Delta V_g \\ V_{\overline{g}} + \Delta V_{\overline{g}} \end{bmatrix} &= e^{-2\pi i \frac{1}{2}(V_g+\Delta V_g)(V_{\overline{g}}+\Delta V_{\overline{g}}-e_{16})+2\pi i V_g(V_{\overline{g}}-e_{16})} e^{2\pi i \Delta V_{\overline{g}}\cdot V_g} Z_F\begin{bmatrix} V_g \\ V_{\overline{g}} \end{bmatrix} \\ &= e^{-2\pi i \frac{1}{2}(V_g\cdot\Delta V_{\overline{g}}+\Delta V_g\cdot V_{\overline{g}}+\Delta V_g\Delta V_{\overline{g}})} e^{2\pi i \Delta V_{\overline{g}} V_g} Z_F\begin{bmatrix} V_g \\ V_{\overline{g}} \end{bmatrix} \\ &= e^{-2\pi i \frac{1}{2}(V_g\cdot\Delta V_{\overline{g}}-\Delta V_g\cdot V_{\overline{g}}+\Delta V_g\Delta V_{\overline{g}})} Z_F\begin{bmatrix} V_g \\ V_{\overline{g}} \end{bmatrix}. \end{aligned} \tag{2.31}$$

We find that two models with local shifts V_g and $V_g' = V_g + \Delta V_g$ with $\Delta V_g \in \Lambda_{E_8\times E_8}$ are equivalent if for all sectors $\overline{g} \neq g$:

$$\frac{1}{2}(V_g \cdot \Delta V_{\overline{g}} - \Delta V_g \cdot V_{\overline{g}} + \Delta V_g \Delta V_{\overline{g}}) \equiv 0 \bmod 1. \tag{2.32}$$

The above equation can be considered a local version of the brother model conditions. We propose to call models that are connected to each other via (2.32) grandchildren models.

2.3 Example: The $\mathbb{Z}_{6-II}$ orbifold

In order to get an MSSM-like model in blowup we resort to a project in which many of these models have been constructed for the $\mathbb{Z}_{6-II}$ orbifold. They are summarized in the Mini-Landscape [20–22, 35, 36]. Altogether, there are 223 models that have an MSSM-like structure with the Standard Model gauge group and three numbers of generations after decoupling vector-like exotics. We want to discuss a well-studied model called the Benchmark model 2.

The $\mathbb{Z}_{6-II}$ orbifold is obtained by taking the root lattice of $G_2 \times SU(3) \times SO(4)$ as Γ_T. The root vectors are given in table 2.1. As the lattice factorizes into 3 two-dimensional parts, the six torus also factorizes and can thus be depicted by three parallelograms spanned by the simple roots. The orbifold twist vector (2.13) is given by

$$\varphi = \frac{1}{6}(1, 2, -3). \tag{2.33}$$

A single twist acts as a counterclockwise rotation of 60° and 120° on the first and second torus and as a (clockwise) rotation of 180° on the third.

For later reference we want to compute the values of δc for this model. Using equation (2.25), we find for the five sectors:

$$\theta^1: \quad 1\varphi \equiv \tfrac{1}{6}(1,2,3) \Rightarrow \delta c^1 = \frac{11}{36} \tag{2.34a}$$

$$\theta^2: \quad 2\varphi \equiv \tfrac{1}{3}(1,2,0) \Rightarrow \delta c^2 = \frac{2}{9} \tag{2.34b}$$

$$\theta^3: \quad 3\varphi \equiv \tfrac{1}{2}(1,0,1) \Rightarrow \delta c^3 = \frac{1}{4} \tag{2.34c}$$

$$\theta^4: \quad 4\varphi \equiv \tfrac{1}{3}(2,1,0) \Rightarrow \delta c^4 = \frac{2}{9} \tag{2.34d}$$

$$\theta^5: \quad 5\varphi \equiv \tfrac{1}{6}(5,4,3) \Rightarrow \delta c^5 = \frac{11}{36} \tag{2.34e}$$

torus	basis vectors on $\mathbb{R}^2$	$\mathbb{C}$	$\mathbb{R}^2$	$\mathbb{C}$
T_1^2 on G_2	$e_1 = \begin{pmatrix} 1 \\ 0 \end{pmatrix}$,	1	$e_2 = \begin{pmatrix} -\frac{1}{2} \\ \frac{1}{2\sqrt{3}} \end{pmatrix}$,	$\frac{1}{\sqrt{3}}\, e^{5\pi i/6}$
T_2^2 on SU(3)	$e_3 = \begin{pmatrix} 1 \\ 0 \end{pmatrix}$,	1	$e_4 = \begin{pmatrix} -\frac{1}{2} \\ \frac{\sqrt{3}}{2} \end{pmatrix}$,	$e^{2\pi i/3}$
T_3^2 on SO(4)	$e_5 = \begin{pmatrix} 1 \\ 0 \end{pmatrix}$,	1	$e_6 = \begin{pmatrix} 0 \\ 1 \end{pmatrix}$,	i

Table 2.1: The basis vectors of the root lattice $G_2 \times SU(3) \times SO(4)$ in real and complex notation.

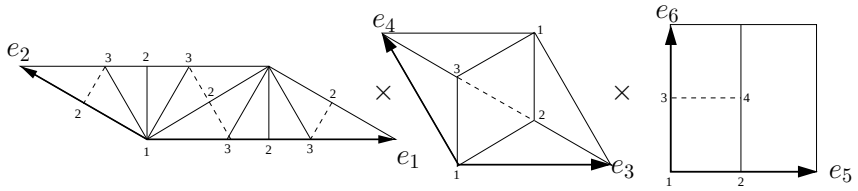

Figure 2.5: The general fixed point structure of the $\mathbb{Z}_{6-II}$ orbifold. For each complex plane, equal numbers denote singularities that are mapped to the same point on the orbifold. Lines symmetric to the broken lines are identified.

The geometry of the $\mathbb{Z}_{6-II}$ orbifold has been discussed in various places [21,23,24,28,35,37] and is only summarized briefly here. The general structure of the singularities that appears after modding out the $\mathbb{Z}_{6-II}$ action is shown in figure 2.5. The numbers denote the locations of the orbifold singularities. Singularities in the covering space (i.e. the torus) that are identified on the orbifold are labeled by the same number.

In order to obtain the detailed fixed point structure we look at every θ^k-sector separately. For the twist θ (and its inverse θ^5) one obtains the full order of the group $\mathbb{Z}_6$. The fixed points are shown in figure 2.6. They are labeled by α in the first torus, by β in the second and by γ in the third torus. The lattice shifts needed to bring the points back after a rotation are given in the table of figure 2.6. Since $\alpha = 1$ in the first and fifth sector, the fixed points are determined by β and γ.

Next we consider the fixed points in the θ^2- and θ^4-sector with twists 2φ and 4φ respectively. The order of these twists is 3 and they act trivially on the third torus. Thus, concentrating solely on the θ^2- and θ^4-sector, the compactification can be described as a $T^4/\mathbb{Z}_3$ orbifold resulting in a six-dimensional theory. The fixed lines of the $T^4/\mathbb{Z}_3$ orbifold are shown in figure 2.7. By comparing this with figure 2.5 we see that the points $\alpha = 3$ and $\alpha = 5$ correspond to the same point on the orbifold, as they are mapped onto each other by further twists. Hence, there are six independent fixed lines, labeled by $\alpha = 1, 3$ and $\beta = 1, 2, 3$. The corresponding lattice shifts are given in the table of figure 2.7.

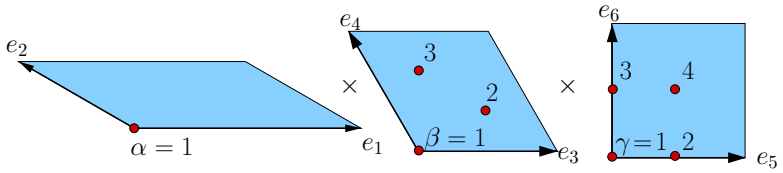

torus shifts $l_{\beta\gamma}$ in the θ-sector				
β \ γ	1	2	3	4
1	0	e_5	e_6	$e_5 + e_6$
2	e_3	$e_3 + e_5$	$e_3 + e_6$	$e_3 + e_5 + e_6$
3	$e_3 + e_4$	$e_3 + e_4 + e_5$	$e_3 + e_4 + e_6$	$e_3 + e_4 + e_5 + e_6$
torus shifts $l_{\beta\gamma}$ in the θ^5-sector				
β \ γ	1	2	3	4
1	0	e_5	e_6	$e_5 + e_6$
2	$e_3 + e_4$	$e_3 + e_4 + e_5$	$e_3 + e_4 + e_6$	$e_3 + e_4 + e_5 + e_6$
3	e_4	$e_4 + e_5$	$e_4 + e_6$	$e_4 + e_5 + e_6$

Figure 2.6: Upper figure: the fixed points in the θ- and θ^5-sector. They are labeled by $\alpha = 1$, $\beta = 1, 2, 3$ and $\gamma = 1, \ldots, 4$.
Lower table: the corresponding torus shifts $l_{\beta\gamma}$, see equation (2.18). For example, the space group element associated to the fixed point $\beta = 2$ and $\gamma = 1$ in the θ-sector reads $(\theta, l_{21}) = (\theta, e_3)$.

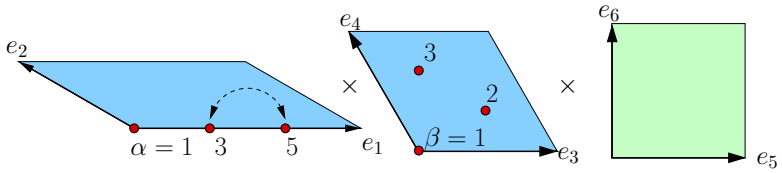

torus shifts $l_{\alpha\beta}$ in the θ^2-sector			
α \ β	1	2	3
1	0	$e_3 + e_4$	e_4
3	$-e_2$	$-e_2 + e_3 + e_4$	$-e_2 + e_4$
5	$-2e_2$	$-2e_2 + e_3 + e_4$	$-2e_2 + e_4$
torus shifts $l_{\alpha\beta}$ in the θ^4-sector			
α \ β	1	2	3
1	0	e_3	$e_3 + e_4$
3	$e_1 + e_2$	$e_1 + e_2 + e_3$	$e_1 + e_2 + e_3 + e_4$
5	$2e_1 + 2e_2$	$2e_1 + 2e_2 + e_3$	$2e_1 + 2e_2 + e_3 + e_4$

Figure 2.7: Upper figure: the fixed lines in the θ^2- and θ^4-sector. They are labeled by $\alpha = 1, 3, 5$ and $\beta = 1, 2, 3$, where the points $\alpha = 3$ and $\alpha = 5$ are identified on the orbifold (cf. figure 2.5).
Lower table: the corresponding torus shifts $l_{\alpha\beta}$.

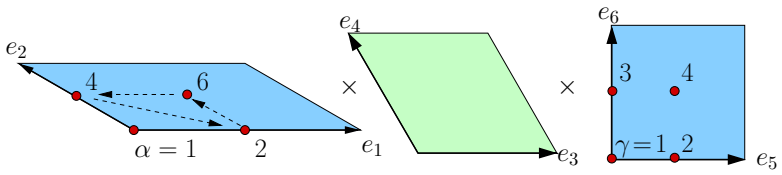

torus shifts $l_{\alpha\gamma}$ in the θ^3-sector				
α \ γ	1	2	3	4
1	0	e_5	e_6	$e_5 + e_6$
2	e_1	$e_1 + e_5$	$e_1 + e_6$	$e_1 + e_5 + e_6$
4	e_2	$e_2 + e_5$	$e_2 + e_6$	$e_2 + e_5 + e_6$
6	$e_1 + e_2$	$e_1 + e_2 + e_5$	$e_1 + e_2 + e_6$	$e_1 + e_2 + e_5 + e_6$

Figure 2.8: Upper figure: the fixed lines in the θ^3-sector. They are labeled by $\alpha = 1, 2, 4, 6$ and $\gamma = 1, \ldots, 4$, where the points $\alpha = 2$, $\alpha = 4$ and $\alpha = 6$ are identified on the orbifold (cf. figure 2.5).
Lower table: the corresponding torus shifts $l_{\alpha\gamma}$.

At last we examine the θ^3-sector. Here, the twist 3φ leaves the second torus invariant and acts with order two. In this case one obtains $T^4/\mathbb{Z}_2$ fixed lines, depicted in figure 2.8. Again one notes by comparing with figure 2.5 that the points $\alpha = 2$, 4 and 6 are mapped onto each other by further twists and correspond to one point on the orbifold. Hence, there are eight independent fixed lines, labeled by $\alpha = 1, 2$ and $\gamma = 1, \ldots, 4$. The lattice shifts for this sector are given in the table of figure 2.8.

Next, let us give the orbifold shift vector and Wilson lines. The geometry of the orbifold restricts the Wilson lines that can be used. The most general case is no Wilson line in the first torus, the same Wilson line W_3 in both directions e_3 and e_4 of the second torus and two Wilson lines W_2 and W_2' in the third torus. For the Benchmark model 2, the Wilson line W_2' is trivial and the rest reads:

$$V_{sh} = \left(\frac{1}{3}, -\frac{1}{2}, -\frac{1}{2}, \ 0^2, \ 0^3\right)\left(\ 0, -\frac{2}{3}, \ 0^2, \ 0^3, 1\right), \tag{2.35a}$$

$$W_2 = \left(\frac{1}{4}, -\frac{1}{4}, -\frac{1}{4}, -\frac{1}{4}^2, \frac{1}{4}^3\right)\left(-\frac{3}{2}, \ \frac{1}{2}, \ 0^2, \ 0^3, 0\right), \tag{2.35b}$$

$$W_3 = \left(-\frac{1}{2}, -\frac{1}{2}, \ \frac{1}{6}, \ \frac{1}{6}^2, \frac{1}{6}^3\right)\left(\ \frac{4}{3}, \ 0, -\frac{1}{3}^2, 0^3, 0\right). \tag{2.35c}$$

We added lattice vectors to the model data of [20] in order to make it easier to see the breaking of the gauge groups. However, the lattice vectors have been added such that the spectrum does not change, i.e. such that we do not get a brother model. The gauge group of the model is given by the root vectors that have an integral inner product with the orbifold shift vector and Wilson lines, thus

$$G = [SU(3) \times SU(2) \times U(1)^5] \times [SO(8) \times SU(2) \times U(1)^3]. \tag{2.36}$$

The spectrum of the orbifold is summarized in table 2.2. The SM part of the orbifold

#	irrep.	label	#	irrep.	label
3	$(\mathbf{3},\mathbf{2};\mathbf{1},\mathbf{1})_{1/6}$	q_i	3	$\left(\overline{\mathbf{3}},\mathbf{1};\mathbf{1},\mathbf{1}\right)_{-2/3}$	$\overline{u}_i$
7	$\left(\overline{\mathbf{3}},\mathbf{1};\mathbf{1},\mathbf{1}\right)_{1/3}$	$\overline{d}_i$	4	$(\mathbf{3},\mathbf{1};\mathbf{1},\mathbf{1})_{-1/3}$	d_i
8	$(\mathbf{1},\mathbf{2};\mathbf{1},\mathbf{1})_{-1/2}$	ℓ_i	5	$(\mathbf{1},\mathbf{2};\mathbf{1},\mathbf{1})_{1/2}$	$\overline{\ell}_i$
3	$(\mathbf{1},\mathbf{1};\mathbf{1},\mathbf{1})_{1}$	$\overline{e}_i$			
47	$(\mathbf{1},\mathbf{1};\mathbf{1},\mathbf{1})_{0}$	s_i^0	26	$(\mathbf{1},\mathbf{1};\mathbf{1},\mathbf{2})_{0}$	h_i
20	$(\mathbf{1},\mathbf{1};\mathbf{1},\mathbf{1})_{1/2}$	s_i^+	20	$(\mathbf{1},\mathbf{1};\mathbf{1},\mathbf{1})_{-1/2}$	s_i^-
2	$(\mathbf{1},\mathbf{1};\mathbf{1},\mathbf{2})_{1/2}$	x_i^+	2	$(\mathbf{1},\mathbf{1};\mathbf{1},\mathbf{2})_{-1/2}$	x_i^-
4	$\left(\overline{\mathbf{3}},\mathbf{1};\mathbf{1},\mathbf{1}\right)_{-1/6}$	$\overline{\varphi}_i$	4	$(\mathbf{3},\mathbf{1};\mathbf{1},\mathbf{1})_{1/6}$	φ_i
2	$(\mathbf{1},\mathbf{2};\mathbf{1},\mathbf{2})_{0}$	y_i	9	$(\mathbf{1},\mathbf{1};\mathbf{8},\mathbf{1})_{0}$	w_i
4	$(\mathbf{1},\mathbf{2};\mathbf{1},\mathbf{1})_{0}$	m_i			

Table 2.2: The massless spectrum of the benchmark model 2 contains three generations of quarks and leptons plus vector-like exotics. The representations (irrep.) with respect to $[SU(3)\times SU(2)]\times[SO(8)\times SU(2)]$ are given in brackets and the hypercharge is given as a subscript.

spectrum (upper part of the table) has 3 left-handed quark doublets, right-handed up quarks, and right-handed leptons. There are 4 right-handed down quark generations and 7 anti-down quark generations, which leaves a net number of 3 down quarks by decoupling four pairs. In a similar manner, there remain a net number of $8-5=3$ left-handed lepton doublets. Altogether, we have three net generations for all Standard model particles plus vector-like exotics, which can be decoupled, and states that are charged under the hidden sector gauge groups or singlets.

2.4 Example: The $\mathbb{Z}_2\times\mathbb{Z}_2$ orbifold

Our second example is a $\mathbb{Z}_2\times\mathbb{Z}_2$ orbifold. In contrast to the $\mathbb{Z}_{6-II}$ example above, the orbifold model under consideration does not have an MSSM spectrum but rather an $SU(5)$ GUT spectrum. The reason for considering a GUT orbifold rather than an MSSM orbifold is be explained in section 5.2. As is discussed in chapter 6, it is possible to break the GUT group to the SM gauge group by using a freely acting $\mathbb{Z}_2$ element, henceforth referred to as $\mathbb{Z}_{2,\text{free}}$. Note that, as the action of the $\mathbb{Z}_{2,\text{free}}$ is free, it does not introduce new fixed points. Instead, existing fixed points are mapped onto each other. Therefore, the discussion of the fixed point structure below is complete.

For the $\mathbb{Z}_2\times\mathbb{Z}_2$ orbifold, one takes the root lattice of $SO(4)\times SO(4)\times SO(4)$. The root vectors are

$$e_{2j-1}=\begin{pmatrix}1\\0\end{pmatrix},\ e_{2j}=\begin{pmatrix}0\\1\end{pmatrix},\quad \text{for } j\in\{1,2,3\}. \tag{2.37}$$

In complex notation, the directions are simply 1 and i.

Again the lattice factorizes and thus we can depict T^6 as $T^2\otimes T^2\otimes T^2$. The orbifold twist

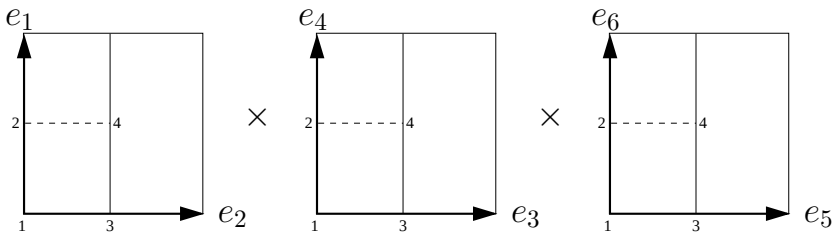

Figure 2.9: The general fixed point structure of the $\mathbb{Z}_2 \times \mathbb{Z}_2$ orbifold. Lines symmetric to the broken lines are identified.

vectors (2.14) are

$$\varphi_1 = \left(0, \frac{1}{2}, -\frac{1}{2}\right), \quad \varphi_2 = \left(-\frac{1}{2}, 0, \frac{1}{2}\right), \quad \varphi_3 = \left(-\frac{1}{2}, \frac{1}{2}, 0\right), \tag{2.38}$$

where φ_3 describes the combined action $\theta_3 \equiv \theta_1\theta_2$ of both $\mathbb{Z}_2$. The convention is chosen such that θ_i leaves the i^{th} torus invariant. Calculating the value of δc as given by (2.25), we find for all three twists θ_i:

$$\theta_1, \theta_2, \theta_1\theta_2: \quad \delta c = \frac{1}{4}. \tag{2.39}$$

In figure 2.9, we give the fixed point structure of the $\mathbb{Z}_2 \times \mathbb{Z}_2$ orbifold on the covering space. The numbers again denote the locations of the orbifold singularities.

Let us now look at the action of θ_1, θ_2 and θ_3 separately. We label fixed points in the first torus by α, in the second by β and in the third by γ. In each torus we have four fixed points, so $\alpha, \beta, \gamma \in \{1, 2, 3, 4\}$. Hence, the 16 fixed lines under θ_1 can be labeled by the indices (β, γ), the 16 fixed lines under θ_2 by (α, γ), and the 16 fixed lines under θ_3 by (α, β). Fixed lines are of complex codimension two. At the intersection of two fixed lines, we have a fixed point labeled by all three indices (α, β, γ), which is of complex codimension three. So altogether there are 64 fixed points. For the three sectors, the fixed lines and their associated lattice shifts are given in figures 2.10 to 2.12.

Now we can look at the orbifold shift vectors V^1_{sh} and V^2_{sh} associated with the twists θ_1 and θ_2 respectively. Additionally, the three tori allow for six independent Wilson lines W_i in the direction of e_i. However, in the model under investigation[2], the Wilson line W_1 is not switched on, so the model data read:

$$V^1_{sh} = \left(\frac{1}{4}, -\frac{1}{4}, -\frac{1}{4}, \frac{1}{4}, -\frac{3}{4}, -\frac{3}{4}, \frac{1}{4}, \frac{1}{4}\right) \left(1, 0, 0, 0, 0, 0, 0, 0\right), \tag{2.40a}$$

$$V^2_{sh} = \left(\frac{3}{4}, \frac{1}{4}, -\frac{1}{4}, \frac{1}{4}, \frac{1}{4}, -\frac{3}{4}, \frac{1}{4}, \frac{1}{4}\right) \left(1, 0, 0, 0, 0, 0, 0, 0\right), \tag{2.40b}$$

$$W_2 = W_4 = W_6 = \left(-\frac{5}{4}, \frac{3}{4}, -\frac{3}{4}, \frac{9}{4}, -\frac{7}{4}, -\frac{3}{4}, \frac{5}{4}, -\frac{3}{4}\right) \left(-\frac{1}{4}, \frac{11}{4}, \frac{3}{4}, -\frac{3}{4}, -\frac{7}{4}, -\frac{3}{4}, \frac{5}{4}, \frac{3}{4}\right), \tag{2.40c}$$

$$W_3 = \left(-1, -1, 0, -2, 0, -2, 2, -3\right) \left(-\frac{7}{4}, -\frac{1}{4}, \frac{3}{4}, -\frac{1}{4}, -\frac{5}{4}, \frac{1}{4}, \frac{1}{4}, \frac{5}{4}\right), \tag{2.40d}$$

$$W_5 = \left(\frac{1}{4}, \frac{9}{4}, -\frac{13}{4}, \frac{11}{4}, \frac{3}{4}, \frac{11}{4}, -\frac{1}{4}, -\frac{1}{4}\right) \left(\frac{3}{4}, \frac{1}{4}, -\frac{11}{4}, -\frac{3}{4}, -\frac{3}{4}, -\frac{1}{4}, -\frac{5}{4}, \frac{3}{4}\right). \tag{2.40e}$$

[2]We are grateful that P.K.S. Vaudrevange and M. Ratz constructed this model for us.

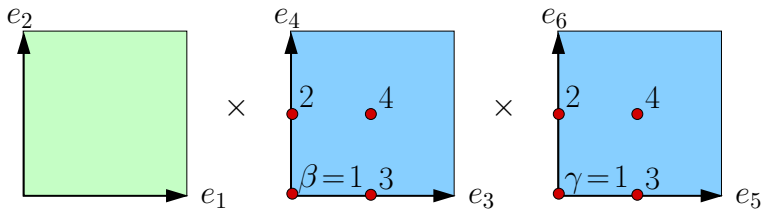

torus shifts $l_{\beta\gamma}$ in the θ_1-sector				
β \ γ	1	2	3	4
1	0	e_6	e_5	e_5+e_6
2	e_4	e_4+e_6	e_4+e_5	$e_4+e_5+e_6$
3	e_3	e_3+e_6	e_3+e_5	$e_3+e_5+e_6$
4	e_3+e_4	$e_3+e_4+e_6$	$e_3+e_4+e_5$	$e_3+e_4+e_5+e_6$

Figure 2.10: Upper figure: the fixed points in the θ_1-sector. They are labeled by $\beta,\gamma=1,2,3,4$. Lower table: the corresponding torus shifts $l_{\beta\gamma}$, see equation (2.18). For example, the space group element associated to the fixed point $\beta=2$ and $\gamma=1$ in the θ-sector reads $(\theta,l_{21})=(\theta_1,e_4)$.

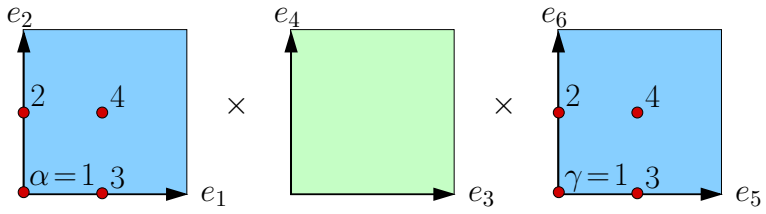

torus shifts $l_{\alpha\gamma}$ in the θ_2-sector				
α \ γ	1	2	3	4
1	0	e_6	e_5	e_5+e_6
2	e_2	e_2+e_6	e_2+e_5	$e_2+e_5+e_6$
3	e_1	e_1+e_6	e_1+e_5	$e_1+e_5+e_6$
4	e_1+e_2	$e_1+e_2+e_6$	$e_1+e_2+e_5$	$e_1+e_2+e_5+e_6$

Figure 2.11: Upper figure: the fixed points in the θ_2-sector. They are labeled by $\alpha,\gamma=1,2,3,4$. Lower table: the corresponding torus shifts $l_{\alpha\gamma}$.

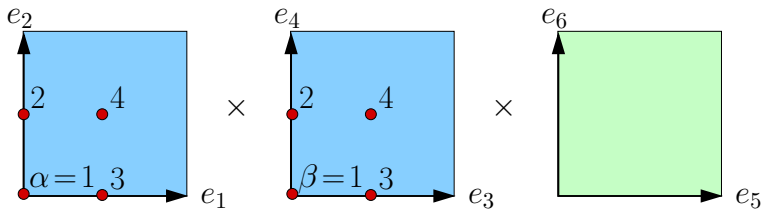

torus shifts $l_{\alpha\beta}$ in the $\theta_1\theta_2$-sector				
α \ β	1	2	3	4
1	0	e_4	e_3	e_3+e_4
2	e_2	e_2+e_4	e_2+e_3	$e_2+e_3+e_4$
3	e_1	e_1+e_4	e_1+e_3	$e_1+e_3+e_4$
4	e_1+e_2	$e_1+e_2+e_4$	$e_1+e_2+e_3$	$e_1+e_2+e_3+e_4$

Figure 2.12: Upper figure: the fixed points in the θ_3-sector. They are labeled by $\alpha,\beta=1,2,3,4$. Lower table: the corresponding torus shifts $l_{\alpha\beta}$.

#	irrep.	label	#	irrep.	label
15	$(\overline{\mathbf{5}};\mathbf{1},\mathbf{1})$	$\overline{D}$	9	$(\mathbf{5};\mathbf{1},\mathbf{1})$	D
6	$(\mathbf{10};\mathbf{1},\mathbf{1})$	Q			
12	$(\mathbf{1};\mathbf{4},\mathbf{1})$	T^1	12	$(\mathbf{1};\overline{\mathbf{4}},\mathbf{1})$	$\overline{T^1}$
12	$(\mathbf{1};\mathbf{1},\mathbf{4})$	T^2	12	$(\mathbf{1};\mathbf{1},\overline{\mathbf{4}})$	$\overline{T^2}$
2	$(\mathbf{1};\overline{\mathbf{6}},\mathbf{1})$	$\overline{V^1}$	2	$(\mathbf{1};\mathbf{1},\overline{\mathbf{6}})$	$\overline{V^2}$
56	$(\mathbf{1};\mathbf{1},\mathbf{1})$	S			

Table 2.3: The massless GUT spectrum of the $\mathbb{Z}_2 \times \mathbb{Z}_2$ can accommodate six net generations of quarks and leptons. The representations (irrep.) with respect to $[SU(5)] \times [SU(4) \times SU(4)]$ are given in brackets.

The gauge group of the model is

$$G = [SU(5) \times U(1)^3] \times [SU(4) \times SU(4) \times U(1)^2]. \tag{2.41}$$

Note that in this model, three Wilson lines are chosen to be equal, $W_2 = W_4 = W_6 \equiv W$. This is not a restriction imposed by the lattice but one that was chosen deliberately. The reason for this is that - in the end - we want to mod out the $\mathbb{Z}_{2,\text{free}}$ translation in the i-directions of the three tori simultaneously. Thus the Wilson lines in these directions have to be chosen equal in order to be compatible with this. We will further discuss the freely acting $\mathbb{Z}_{2,\text{free}}$ element in chapter 6.

Finally, let us look at the spectrum of the model, which is summarized in table 2.3. The GUT part of the spectrum is given in the upper part of the table. It has six **10**-plets. For the $\overline{\mathbf{5}}$-plets, we find a net number of $15 - 9 = 6$. Hence it can accommodate six SM generations after decoupling vector-like states (cf. listing (1.2)). The remaining states are charged under the hidden gauge group or are singlets. Having discussed the orbifold models and their fixed point structure, we now introduce a method to smoothen the curvature singularities occurring at the fixed points.

Chapter 3

. . . . . .

Blowing up heterotic orbifolds

In the previous chapter we introduced Calabi-Yau spaces and orbifolds as possible compactification spaces for (heterotic) string theory. We saw that the latter are flat except for curvature singularities occurring at the fixed points of the orbifold action. The so-called blowup procedure flattens out these singularities. Blowing up the fixed points thus allows us to make the transition from a singular orbifold space to a smooth Calabi-Yau manifold. The idea is schematically illustrated in figure 3.1. We start with a singular orbifold space. The singularities are cut out and smooth hypersurfaces are glued into the orbifold instead, yielding a smooth manifold.

The details of the procedure have already been worked out in [23–28, 37], so we only briefly summarize the necessary steps without giving many details and restrict the discussion to the cases needed in this thesis. The essential tool for the blowup is toric geometry. Basic mathematical tools are provided in [38, 39]. For a more mathematical approach to toric varieties see [40].

The first section in the chapter explains how to resolve local fixed points of non-compact orbifolds. This leads to the introduction of divisors and to toric diagrams together with the concept of triangulation. In the second section, we learn how to combine the local information we gained at each fixed point to obtain a resolved compact orbifold using linear equivalence relations. We introduce the construction of unprojected dual graphs, which help to better understand the triangulation ambiguity. Having gained the topological data of the underlying space from this procedure, we can use the information to calculate many topological quantities. The most important ones will be the intersection numbers. The last two sections are devoted to applying the blowup methods to the $\mathbb{Z}_{6-II}$ and the $\mathbb{Z}_2 \times \mathbb{Z}_2$ orbifold.

3.1 Local resolution of non-compact orbifolds

In order to perform the blowup of fixed points, we start by looking at each fixed point separately, i.e. we take the flat space $\mathbb{C}^d$ and divide out the $\mathbb{Z}_N$ orbifold group:

$$\theta : (z_1, z_2, \ldots, z_d) \mapsto (e^{2\pi i\varphi^1}\ z_1, e^{2\pi i\varphi^2}\ z_2, \ldots, e^{2\pi i\varphi^d}\ z_d). \tag{3.1}$$

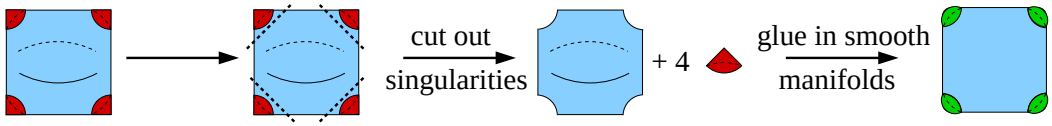

Figure 3.1: Outline of the blowup procedure. The orbifold singularities (red) are cut out and replaced by smooth manifolds (green).

As a next step we form θ-invariant monomials $u_j = z_1^{(v_1)_j} \cdot \ldots \cdot z_d^{(v_d)_j}$, $j \in \{1, 2, \ldots, d\}$ from these coordinates. In order to be invariant under θ, the vectors v_i have to satisfy

$$v_1\varphi_1 + v_2\varphi_2 + \ldots + v_d\varphi_d \equiv 0 \text{ mod } 1. \tag{3.2}$$

The toric diagram of the orbifold is defined by connecting all the points given by the v_i. As we also know from the Calabi-Yau condition (2.16), $\varphi_1 + \varphi_2 + \ldots + \varphi_d \equiv 0$ mod 1. This can be automatically fulfilled if we set $(v_i)_d = 1$ in (3.2). This means that all v_i and thus the toric diagram itself will lie in one plane. In order to simplify the visualization, the toric diagrams are conventionally drawn in two dimensions. Every vector v_i is associated with a codimension one hypersurface D_i obtained by setting $z_i = 0$. These hypersurfaces are called ordinary divisors.

The dual graph of a toric diagram is obtained by taking the lines perpendicular to the boundary lines of the toric diagram. These lines have to meet in one point, which corresponds to the area of the toric diagram. The points of the toric diagram (the divisors) are turned into areas, while lines stay lines. Unbounded areas mean that the corresponding divisor is non-compact, while compact divisors will be represented by bounded areas. The lines represent the intersection curve of the two corresponding divisors.

It is noteworthy that for $d = 3$, the dual toric diagrams can be neatly visualized by the following procedure, henceforth called the unprojected dual graph procedure. In $d = 3$, there will be three ordinary divisors D_i, corresponding to the 3 three-dimensional vectors v_i. Thus the toric diagram itself lives in three dimensions. It only happens to lie in a plane due to the CY condition. So the lines of the dual graphs actually correspond to planes in three dimensions. This means that the dual graph is the projection of a three-dimensional object to a subspace of $\mathbb{R}^3$. The three-dimensional picture can be reconstructed by drawing planes orthogonal to the vectors in the toric diagram. In order to allow for a much easier construction, we rotate and rescale the toric diagram such that D_1, D_2, and D_3 correspond to the three coordinate planes[1]. They then intersect at the coordinate axes. By projecting the three-dimensional graph to two dimensions from a suitable viewpoint, one gets back the dual toric diagram, hence the name unprojected dual graph. The areas of the dual toric diagram arise from the three planes, the lines of the diagram will be given by the intersection of two planes and the points come from the intersection of all three planes (i.e. the origin in our case). In the simple case at hand this method seems to be introducing more complication rather than help. The use of this construction will become apparent later, when we introduce more divisors and look at the relative positions of them on the CY manifold.

The toric diagrams allow us to read off equivalence relations in terms of cohomology for

[1]This procedure might actually require an anisotropic rescaling which changes the intersection angles of the planes. The qualitative results are, however, unaffected by this.

the divisors D_i. One can show that

$$\sum_{i=1}^{d}(v_i)_j D_j \ \sim\ 0 \quad \text{with } j \in \{1,2,\ldots,d\}. \tag{3.3}$$

By Poincaré duality, we can translate this into an equivalence in terms of homology for the cycles D_i. Upon integration over a closed cycle, the equivalence becomes an equality.

In order to resolve and blow up the fixed points of the orbifold, we need to introduce another class of divisors called the exceptional divisors E_k. In the case of $d = 2$, we introduce one exceptional divisor for every non-trivial twist $\theta^k \neq \mathbb{1}$. In the case of $d = 3$, an exceptional divisor is placed at each point (given by a vector w_k) in the toric diagram that satisfies

$$k\sum_{i=1}^{3}\varphi_i = 1 \ \text{ and } \ 0 \leq k\varphi_i < 1 \quad \Rightarrow \quad w_k = k(\varphi_1 v_1 + \varphi_2 v_2 + \varphi_3 v_3). \tag{3.4}$$

This restriction ensures that the resolved space stays a Calabi-Yau manifold.

The exceptional divisors can be included in the invariant monomials u_j by assigning a new coordinate y_k to each of them. The equivalence relations then read:

$$u_j = \prod_{i,k} z_i^{(v_i)_j} y_k^{(w_k)_j} \ \Rightarrow\ 0 \sim \sum_i (v_i)_j D_i + \sum_k (w_k)_j E_k. \tag{3.5}$$

It is convenient to rewrite these relations such that they contain only one D_i per equivalence relation.

As mentioned above, we use toric diagrams to infer the intersection numbers of the divisors. However, in order to obtain the intersection numbers we have to give the relative position of all the divisors on the CY. This is achieved by triangulating the toric diagram, which is done by introducing lines between all divisors such that no lines cross each other and that no additional line that does not cross another line can be added. In general, this procedure is ambiguous, i.e. there are several distinct ways of drawing these lines. Having chosen a triangulation, the intersection of distinct divisors can be directly read off from the toric diagram. The intersection of divisors which are directly connected by a line is 1, while the intersection of divisors which are not connected by lines or whose lines are interrupted by other divisors is 0.

The dual graphs can be derived from the toric diagram using the perpendicular lines construction given above. Another way to get the dual graph is to make again use of the unprojected dual graph procedure. We add planes that correspond to the exceptional divisors E_k which satisfy the equation

$$E_k: \ \varphi_1 x + \varphi_2 y + \varphi_3 z = t_k, \ t_k \in \mathbb{R}^+. \tag{3.6}$$

A priori, the t_k are arbitrary parameters of the planes. Via a suitable projection to two dimensions, we get the dual graph of the toric diagram involving the exceptional divisors. The advantage of the three-dimensional picture is the following: as stated above, there are in general several possible triangulations for the same toric diagram. These triangulations are crucial for the relative position of the divisors and consequently for the intersection numbers. It turns out that changing the relative value of the t_k takes you from the dual graph of one

triangulation to the dual graph of another triangulation, which is not that easy to see in two dimensions.

All intersection numbers (including the self-intersections) can be gained from the intersection numbers of three distinct divisors by multiplying and combining the equivalence relations (3.5). We want to emphasize that the intersection numbers depend on the chosen triangulation, as the lines that connect divisors (and thus determine the value of the intersection number) differ between different triangulations.

3.2 Resolution of compact orbifolds

Next, we want to discuss how to resolve compact orbifolds. This is done by gluing together the resolutions of the non-compact case discussed above in an appropriate way. To account for the fact that we are now dealing with a compact space (i.e. a torus) instead of the whole complex plane, we have to introduce yet another class of divisors, called the inherited divisors. The name comes from the fact that these divisors descend from the torus to the orbifold. A basis of $(1,1)$-forms on the torus is given by $dz_i \wedge d\overline{z}_{\overline{j}}$. These forms transform under an orbifold twist as $e^{2\pi i(\varphi_i - \varphi_j)}$. As $\varphi_i \neq \varphi_j$ for the orbifolds we are considering in this thesis, the only possibility to get an invariant form under the orbifold action is to choose $i = j$ so that the basis is given by $dz_i \wedge d\overline{z}_{\overline{i}}$. We can again switch to cycles using Poincaré duality.

In order to distinguish the different fixed points of the orbifold, we introduce additional labels on the divisors. For the inherited divisors R_i, the label i which identifies the torus from which it descends is enough to completely specify the divisor. The ordinary divisors account for the fixed points in each torus T^2 separately. In the convention introduced in section 2.2, the fixed points in the three tori are labeled by α, β, and γ respectively. Hence the ordinary divisors carry a torus label $i \in \{1,2,3\}$ and a fixed point label $\delta \in \{\alpha, \beta, \gamma\}$. So the ordinary divisors will be labeled by $D_{1,\alpha}$, $D_{2,\beta}$, and $D_{3,\gamma}$. Lastly, the exceptional divisors are introduced at each fixed point of T^6. As the different twisted sectors θ^k have a different fixed point structure, it is convenient to label the exceptional divisors by an index k giving the order of the twist and all three indices $(\alpha\beta\gamma)$ specifying the fixed point location on T^6, so $E_r = E_{k,\alpha\beta\gamma}$ with the multi-index $r = (k, \alpha\beta\gamma)$.

Note that not every twisted sector θ^k necessarily fulfills (3.4), hence the label k need not run over all values $1, 2, \ldots, N-1$. Also, there might be fixed lines in some sectors. In this case, there are no fixed points in the fixed torus and the corresponding Greek index is missing on these exceptional divisors. Also note that (in the $\mathbb{Z}_{6-II}$ case) there are cases in which different fixed points on the torus are identified under the orbifold action. In this case, one has to construct an invariant combination of them by summing all exceptional divisiors belonging to the fixed points that are mapped onto each other.

One can derive a relation between the inherited and the local divisors, namely $R_i \sim n_i D_{i,\delta}$, where n_i is the order of the (sub-)group of the orbifold action acting in the i^{th} coordinate plane (which is associated with the divisor D_i). Upon introducing the exceptional divisor, the linear equivalences are modified to

$$R_i \sim n_i D_{i,\delta} + \sum_r c_r E_r, \tag{3.7}$$

where the right hand side agrees with the right hand side of (3.5). We get an equivalence relation like (3.7) for every ordinary divisor. This means every ordinary divisor can be

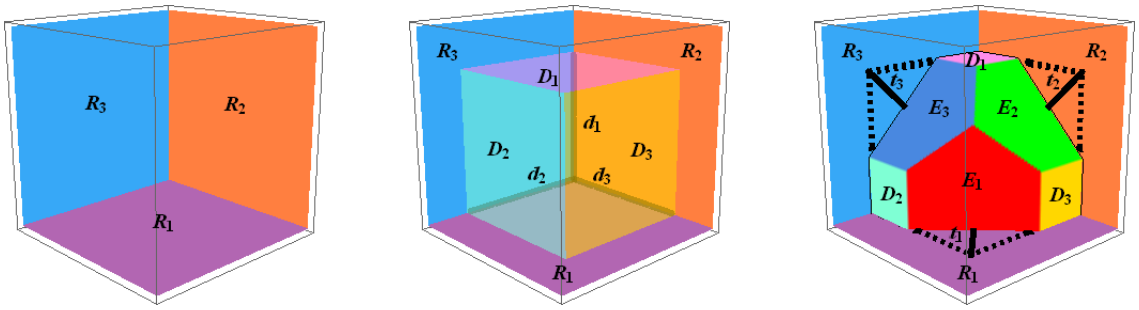

(a) Identify coordinate planes with R_i.

(b) Place D_i at a distance d_i.

(c) Cut out E_k at a distance t_k from the edges.

Figure 3.2: Schematic construction of the unprojected dual graphs for the auxiliary polyhedron of the $\mathbb{Z}_2 \times \mathbb{Z}_2$ orbifold. The coordinate planes are identified with the divisors R_i. The divisors D_i correspond to planes placed at a distance d_i, while the E_k are placed at distance t_k from the edges. The planes are cut at their intersection lines.

expressed through a linear combination of inherited and exceptional divisors. In this way the R_i and E_r provide a basis of $(1,1)$-forms on the resolved manifold. Note that (3.7) relates the globally defined inherited divisors to several local equivalence relations, so it is clearly the outcome of a gluing procedure. The linear equivalences are triangulation-independent, as the local linear equivalences were.

As in the non-compact case, we proceed with calculating the intersection numbers for all divisors. In the non-compact case these numbers could be read off from the toric diagram and the rest could be computed using linear equivalence relations. In the compact case the toric diagram is augmented with the inherited divisors yielding the so-called auxiliary polyhedron. It has to be constructed for all r fixed points in the following manner: start by introducing the lattice $N \cong \mathbb{Z}^3$ with a basis $f_i = m_i e_i$, where the e_i are the canonical basis vectors and the m_i are chosen such that $m_1 m_2 m_3 = n_1 n_2 n_3 / N$. As before, N is the order of the orbifold group and the n_i are the order of the subgroup in the i^{th} coordinate plane. We then rotate and rescale the toric diagram such that the D_i correspond to the vectors $v_{i+3} = n_i f_i,\ i \in \{1,2,3\}$. This will give one face of the auxiliary polyhedron. Then we add vertices $v_i = -f_i,\ i \in \{1,2,3\}$ for the inherited divisors R_i. We next build simplices by connecting all points to the origin such that the triangulation of the toric diagram is preserved (this is called the star triangulation of the auxiliary polyhedron).

In those sectors, where the action is not the full orbifold group but a subgroup thereof, we proceed similarly. The toric diagram will look the same apart from the absence of the corresponding E_r. A subtlety arises if several distinct fixed points are mapped onto each other. As explained above, in this case one has to build an invariant object by taking the sum of these divisors. The corresponding position vector v_{i+3} has to be divided by the number of fixed points mapped onto each other.

It is also possible to draw the equivalent of a dual graph of the auxiliary polyhedra using the unprojected dual graph procedure. The construction menthod is schematically given in figure 3.2. We associate the three coordinate planes with the three inherited divisors R_i (figure 3.2a). The ordinary divisors D_i, which are by construction of the auxiliary polyhedra opposite to the R_i, are represented by planes placed at distances $d_i \in \mathbb{R}$ from the coordinate planes (figure 3.2b). This results in a cuboid. The planes corresponding to the exceptional

divisors are placed at

$$E_k : \ \varphi_1 x + \varphi_2 y + \varphi_3 z = \varphi_1 d_1 + \varphi_2 d_2 + \varphi_3 d_3 - t_k, \ t_k \in \mathbb{R}^+. \tag{3.8}$$

They thus eat away parts of the cuboid (figure 3.2c.). All planes are cut off at the lines where they intersect. The resulting object is compact, as the auxiliary polyhedra are compact. Again one can change from one triangulation to another by adjusting the distance parameters d_i and t_k.

The intersection numbers involving three distinct divisors can now be read off in a manner similar to the toric diagram case. The only non-zero intersection numbers are those for which the involved divisors and the origin span a simplex in the auxiliary polyhedron. Simplices that are interrupted by any other points as well as intersections between different auxiliary polyhedra are zero. The non-zero intersections for the three distinct divisors S_1, S_2 and S_3 are given by

$$\mathrm{Int}(S_1 S_2 S_3) = C \cdot |\det[\{v(S_1), v(S_2), v(S_3)\}]|^{-1}, \tag{3.9}$$

where the normalization constant C has to be chosen such that the R-independent intersection numbers agree with the non-compact case. All other intersection numbers can again be calculated from those of three distinct divisors by using the linear equivalences (3.7).

3.3 Example: Blowup of the $\mathbb{Z}_{6-II}$ orbifold

We want to use the above technique to calculate the intersection numbers of the $\mathbb{Z}_{6-II}$ orbifold. As explained above, we start with the local non-compact case and then glue together the pieces. We will construct the toric diagrams, the dual graphs, the auxiliary polyhedra, and the unprojected dual graphs. Additionally, we will give the linear equivalence relations. At the end we look at topological invariants of the blowup manifold X.

3.3.1 Local resolution

We start with calculating the vectors entering the invariant monomials u_j. The $\mathbb{Z}_{6-II}$ orbifold acts with its full $\mathbb{Z}_6$ twist only in the θ- and θ^5-sector (cf. section 2.3). The θ^2- and θ^4 sector have fixed lines and correspond locally to a $\mathbb{C}^2/\mathbb{Z}_3$ action. The θ^3-sector also has fixed lines and corresponds locally to $\mathbb{C}^2/\mathbb{Z}_2$.
Let us start with the case $\mathbb{C}^3/\mathbb{Z}_{6-II}$. With the twist vector (2.33), equation (3.2) reads

$$\frac{1}{6}v_1 + \frac{2}{6}v_2 - \frac{3}{6}v_3 \equiv 0 \bmod 1 \rightarrow v_1 = \begin{pmatrix} -2 \\ -1 \\ 1 \end{pmatrix}, \ v_2 = \begin{pmatrix} 1 \\ -1 \\ 1 \end{pmatrix}, \ v_3 = \begin{pmatrix} 0 \\ 1 \\ 1 \end{pmatrix}. \tag{3.10}$$

Of course the solution presented here is not unique. Note that all vectors have a 1 in the last component, which ensures that the CY condition is fulfilled.

It is now easy to draw the toric diagrams. As all divisors lie in one plane, we give the diagram in figure 3.3a in two dimensions for the sake of clarity. Note that the toric diagrams in figure 3.3b and 3.3c appear as edges in the toric diagram in figure 3.3a. In order to calculate the position of the exceptional divisors, we have to check which of the $k \cdot \varphi$ fulfill the restriction in (3.4) and thus introduce exceptional divisors. From the list given in (2.34),

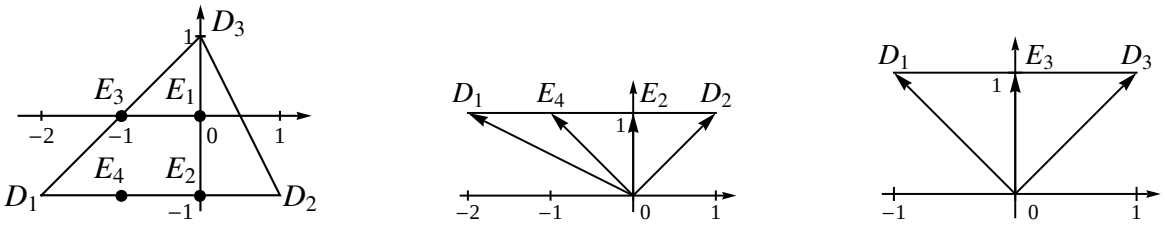

(a) Toric diagram of $\mathbb{C}^3/\mathbb{Z}_{6-II}$.

(b) Toric diagram of $\mathbb{C}^2/\mathbb{Z}_3$.

(c) Toric diagram of $\mathbb{C}^2/\mathbb{Z}_2$.

Figure 3.3: The toric diagrams for $\mathbb{C}^3/\mathbb{Z}_{6-II}$, $\mathbb{C}^3/\mathbb{Z}_3$, and $\mathbb{C}^2/\mathbb{Z}_2$. We needed to add four, two, and one exceptional divisor respectively.

we see that only the θ^5 sector does not fulfill the condition. Substituting (3.10) into (3.4), we find for the positions w_i:

$$w_1 = \begin{pmatrix} 0 \\ 0 \\ 1 \end{pmatrix}, \; w_2 = \begin{pmatrix} 0 \\ -1 \\ 1 \end{pmatrix}, \; w_3 = \begin{pmatrix} -1 \\ 0 \\ 1 \end{pmatrix}, \; w_4 = \begin{pmatrix} -1 \\ -1 \\ 1 \end{pmatrix}. \tag{3.11}$$

In the cases of $\mathbb{C}^2/\mathbb{Z}_N$, we simply introduce one exceptional divisor for each non-trivial twist. In the $\mathbb{Z}_{6-II}$ case, there are five possible ways of triangulating the toric diagram given in figure 3.3a. The resulting toric diagrams, their dual graphs and their unprojected dual graphs are given in figure 3.4. It is especially nice to see how the compactness of E_1 arises.

As explained in (3.5), the linear equivalences can be read off from (3.10) and (3.11). They have been combined such that each linear equivalence contains one ordinary divisor only:

$$\begin{aligned} \mathbb{C}^2/\mathbb{Z}_2: &\quad 2D_1 + E_3 \sim 0, \\ &\quad 2D_2 + E_3 \sim 0, \\ \mathbb{C}^2/\mathbb{Z}_3: &\quad 3D_1 + E_2 + 2E_4 \sim 0, \\ &\quad 3D_2 + 2E_2 + E_4 \sim 0 \end{aligned} \qquad \begin{aligned} \mathbb{C}^3/\mathbb{Z}_{6-II}: &\quad 6D_1 + E_1 + 2E_2 + 3E_3 + 4E_4 \sim 0, \\ &\quad 3D_2 + E_1 + 2E_2 + E_4 \sim 0, \\ &\quad 2D_3 + E_1 + E_3 \sim 0 \end{aligned} \tag{3.12}$$

3.3.2 Gluing procedure

With the results from the previous subsection at hand, we can now start gluing together the different patches. There are six fixed points in the first torus, three in the second and four in the third. Hence the ordinary divisors will be labeled by $D_{1,\alpha}$, $D_{2,\beta}$, and $D_{3,\gamma}$, whereas the exceptional divisors carry labels $E_{1,1\beta\gamma}$, $E_{2,\alpha\beta}$, $E_{3,\alpha\gamma}$, and $E_{4,\alpha\beta}$ with $\alpha \in \{1, 2, \ldots, 6\}$, $\beta \in \{1, 2, 3\}$, $\gamma \in \{1, 2, 3, 4\}$.

As can be seen from figures 2.6 to 2.8, in the first torus in the θ^2, θ^3, and θ^4 sector, there are fixed points on the cover that are mapped onto each other on the orbifold. As explained above, we need to form invariant combinations of the involved divisors in this case, by summing all divisors associated with the respective fixed points. The divisors that are concerned are D_1, as this lives in the first torus, and E_2, E_3, and E_4, as these correspond to the θ^2, θ^3, and θ^4 sector respectively. The invariant combinations are given by

$$\begin{aligned} &\widetilde{D}_{1,2} := D_{1,2} + D_{1,4} + D_{1,6}, \;\; \widetilde{D}_{1,3} := D_{1,3} + D_{1,5}, \\ &\widetilde{E}_{2,3\beta} := E_{2,3\beta} + E_{2,5\beta}, \;\; \widetilde{E}_{3,2\gamma} := E_{3,2\gamma} + E_{3,4\gamma} + E_{3,6\gamma}, \;\; \widetilde{E}_{4,3\beta} := E_{4,3\beta} + E_{4,5\beta}. \end{aligned} \tag{3.13}$$

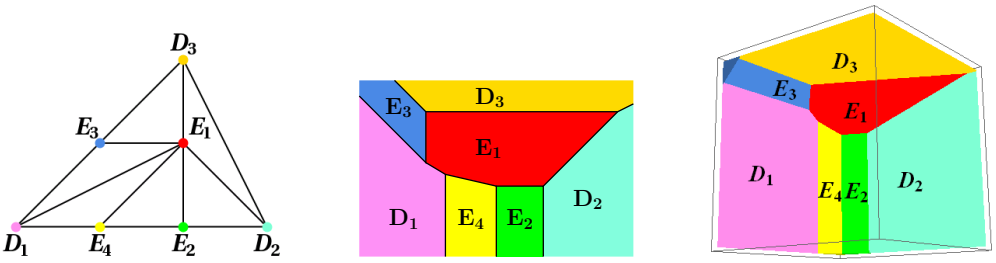

(a) Diagrams for triangulation (i) with $(t_1 : t_2 : t_3 : t_4) \approx (1 : 0.5 : 0.4 : 0.5)$.

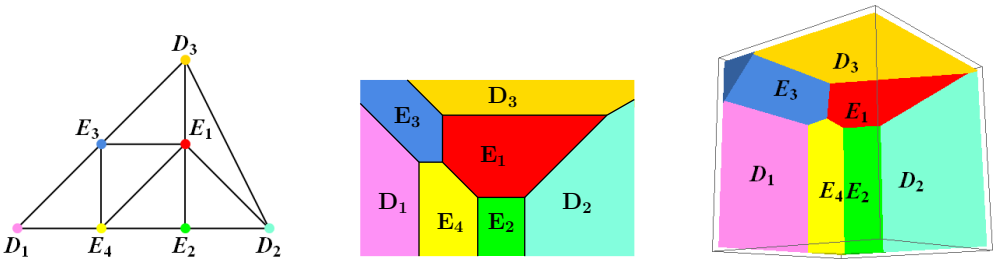

(b) Diagrams for triangulation (ii) with $(t_1 : t_2 : t_3 : t_4) \approx (1 : 0.7 : 0.7 : 0.7)$.

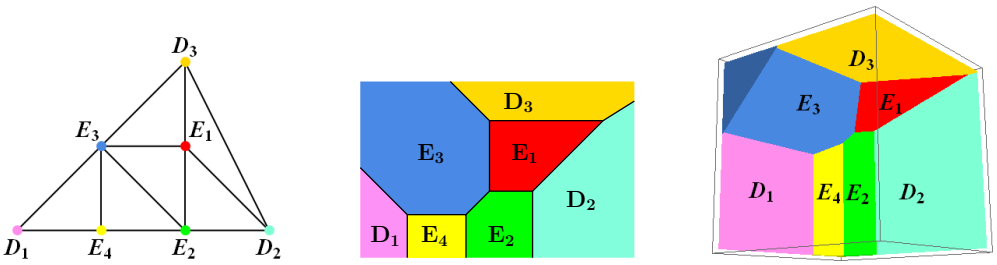

(c) Diagrams for triangulation (iii) with $(t_1 : t_2 : t_3 : t_4) \approx (0.8 : 0.4 : 1 : 0.5)$.

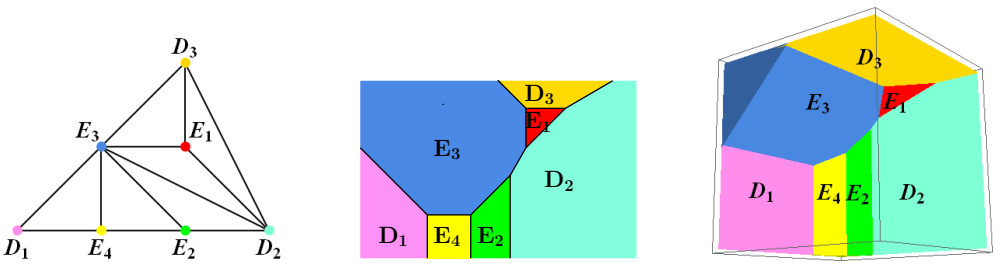

(d) Diagrams for triangulation (iv) with $(t_1 : t_2 : t_3 : t_4) \approx (0.5 : 0.4 : 1 : 0.4)$.

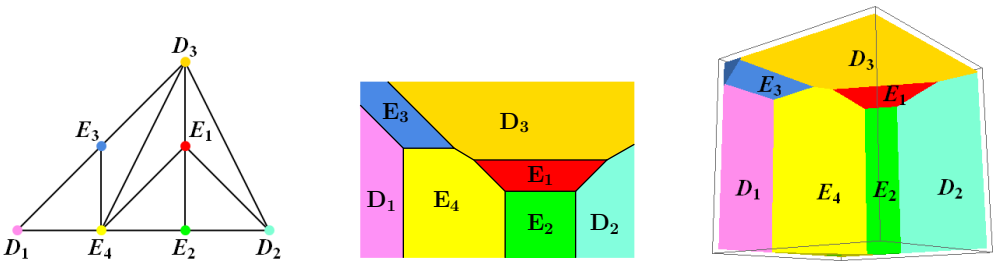

(e) Diagrams for triangulation (v) with $(t_1 : t_2 : t_3 : t_4) \approx (0.6 : 0.7 : 0.3 : 1)$.

Figure 3.4: The toric diagrams, their dual graphs and the unprojected dual graphs for the five triangulation possibilities of the $\mathbb{C}^3/\mathbb{Z}_{6-II}$ fixed points. For each unprojected dual graph the values of the t_i are given. The graph has been rotated back to match the orientation of the other graphs.

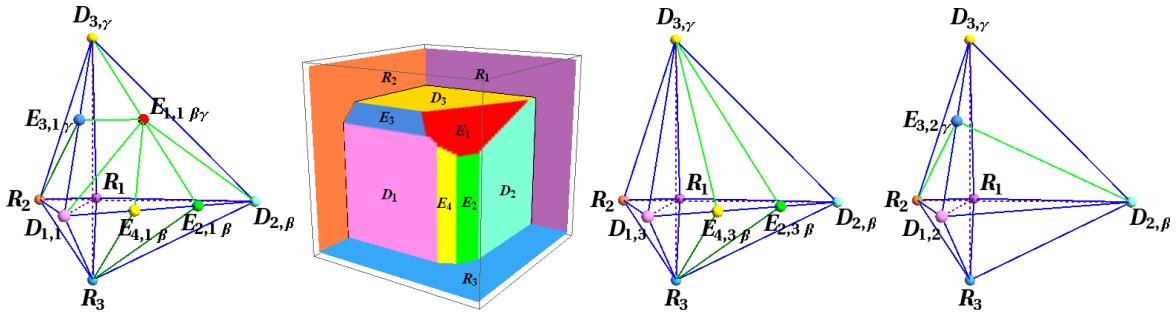

(a) The polyhedron for $\mathbb{C}^3/\mathbb{Z}_{6-II}$ ($\alpha = 1$) with triangulation (i). Each of the twelve possible polyhedra can have a different triangulation.

(b) The unprojected dual graph of $\mathbb{C}^3/\mathbb{Z}_{6-II}$ with triangulation (i).

(c) The polyhedron for $\mathbb{C}^2/\mathbb{Z}_3$ ($\alpha = 3$). There is only one possible triangulation for these polyhedra.

(d) The polyhedron for $\mathbb{C}^2/\mathbb{Z}_2$ ($\alpha = 2$). There is only one possible triangulation for these polyhedra.

Figure 3.5: The auxiliary polyhedra for $T^6/\mathbb{Z}_{6-II}$ and the corresponding unprojected dual graph.

As we will only work with the invariant combinations defined above, we will henceforth drop the tilde on the divisors in order to keep the notation simple. This means that α will effectively run from 1 to 3 from now on. Counting the number of divisors, we find $\#(D_{1,\alpha})+\#(D_{2,\beta})+\#(D_{3,\gamma}) = 3+3+4 = 10$ ordinary divisors and $\#(E_{1,1\beta\gamma})+\#(E_{2,\alpha\beta})+\#(E_{3,\alpha\gamma})+\#(E_{4,\alpha\beta}) = 3\cdot 4+2\cdot 3+2\cdot 4+2\cdot 3 = 32$ exceptional divisors.

From these invariant objects, we can deduce the linear equivalences in the compact case with the help of (3.12) as explained in section 3.2:

$$\begin{aligned}
R_1 &\sim 6D_{1,1} + \sum_{\beta=1}^{3}\sum_{\gamma=1}^{4} E_{1,1\beta\gamma} + \sum_{\beta=1}^{3}(2E_{2,1\beta}+4E_{4,1\beta}) + 3\sum_{\gamma=1}^{4} E_{3,1\gamma},\\
R_1 &\sim 2D_{1,2} + \sum_{\gamma=1}^{4} E_{3,2\gamma},\\
R_1 &\sim 3D_{1,3} + \sum_{\beta=1}^{3}(E_{2,3\beta}+2E_{4,3\beta}),\\
R_2 &\sim 3D_{2,\beta} + \sum_{\gamma=1}^{4} E_{1,1\beta\gamma} + \sum_{\alpha=1,3}(2E_{2,\alpha\beta}+E_{4,\alpha\beta}) \quad \text{for } \beta\in\{1,2,3\},\\
R_3 &\sim 2D_{3,\gamma} + \sum_{\beta=1}^{3} E_{1,1\beta\gamma} + \sum_{\alpha=1,2} E_{3,\alpha\gamma} \qquad\qquad \text{for } \gamma\in\{1,2,3,4\}.
\end{aligned} \tag{3.14}$$

Next we construct the auxiliary polyhedra for the three different types of fixed points. They are given in figure 3.5 (with triangulation (i) in the $\mathbb{C}^3/\mathbb{Z}_{6-II}$ case). The lines connecting the simplices with the origin are not drawn. The triangulation-dependent face is the upper front one. One can recognize the toric diagram given in figure 3.4a on this face. By reading off the intersection numbers between three distinct divisors and cleverly combining the equivalence relations (3.14), all intersection numbers can be computed.

3.3.3 Properties of the blowup manifold

Now that we have the topological information of the blowup manifold at our disposal, we want to compute topological invariants. The first quantities we want to compute are the Hodge numbers. As explained before, we can take the R_i and E_r as a basis for the $(1,1)$-forms, so $h^{1,1} = 3 + 32 = 35$, where the R_i and E_r correspond to the untwisted and the twisted sector respectively. By defining the $(1,0)$-forms $\omega_i := dz_i,\ i \in \{1,2,3\}$, we can build the invariant $(3,0)$ volume form $\omega_1 \wedge \omega_2 \wedge \omega_3$, so $h^{3,0} = 1$. Additionally, we can form the invariant $(1,1)$-forms $\omega_i \wedge \overline{\omega}_{\bar{i}}$, but these are equivalent to the R_i. As the ω_i alone are not invariant, $h^{1,0} = 0$. However, the combination $\omega_1 \wedge \omega_2 \wedge \overline{\omega}_{\bar{3}}$ yields an invariant $(2,1)$-form. One can build 10 further $(2,1)$-forms by wedging ω_2 with E_2, E_4 and by wedging ω_3 with E_3, so $h^{2,1} = 11$. Additionally, there is the trivial element of $H^{0,0}$. These are all invariant forms that can be built on the manifold. Using the symmetry of the Hodge numbers and Poincaré duality, we find for the Hodge diamond:

$$\begin{array}{ccccccc} & & h^{3,3} & & & & \\ & h^{3,2} & & h^{2,3} & & & \\ h^{3,1} & & h^{2,2} & & h^{1,3} & & \\ h^{3,0} & & h^{2,1} & & h^{1,2} & & h^{0,3} \\ h^{2,0} & & h^{1,1} & & h^{0,2} & & \\ & h^{1,0} & & h^{0,1} & & & \\ & & h^{0,0} & & & & \end{array} = \begin{array}{ccccccc} & & 1 & & & & \\ & 0 & & 0 & & & \\ 0 & & 3+32 & & 0 & & \\ 1 & & 1+10 & & 1+10 & & 1 \\ 0 & & 3+32 & & 0 & & \\ & 0 & & 0 & & & \\ & & 1 & & & & \end{array} \tag{3.15}$$

Note that it has the Calabi-Yau structure (2.6) and agrees with [23], which is a good cross-check that the resolution procedure is correct.

Another topological quantity that follows from the Hodge diamond is the Euler number (2.7). With the numbers given above, we find

$$\chi(X) = 2(1 + 35 - (1 + 11)) = 48 \tag{3.16}$$

in agreement with [41] in the orbifold case.

The next topological quantities we can compute are the Chern classes. By expressing the total Chern class $c(X)$ through divisors [28, 40]

$$c(X) = \prod_{i=1}^{10} \prod_{r=1}^{32} (1 + D_i)(1 + E_r)(1 - R_1)(1 - R_2)(1 - R_3)^2 \tag{3.17}$$

we can compute the three Chern classes by expanding (3.17)

$$c_1(X) = \sum_{i=1}^{10} D_i + \sum_{r=1}^{32} E_r - R_1 - R_2 - 2R_3, \tag{3.18a}$$

$$c_2(X) = \frac{1}{2!} \sum_{\text{all divisors}} (c_1(X) - S_i) S_i, \tag{3.18b}$$

$$c_3(X) = \frac{1}{3!} \sum_{\text{all divisors}} (c_1(X) - S_i - S_j) S_i S_j. \tag{3.18c}$$

Substituting the linear equivalences (3.14) into (3.18a), we find $c_1(X) = 0$, as it has to be for a Calabi-Yau manifold. The third Chern class is the top Chern class of a complex three-dimensional manifold and is thus equal to the Euler number. Substituting the triple intersection numbers into (3.18c), we find $c_3(X) = 48$, in agreement with (3.16). This is remarkable, as the expression (3.18c) is in principle triangulation-dependent. Nevertheless, we obtained the same result for all triangulations we tested.

To conclude the section we want to briefly comment on the number of different CYs resulting from the triangulation ambiguity. Two CYs are considered different if their intersection numbers differ. At most, there can be $5^{12} \approx 2.44 \cdot 10^8$ different models. However, some of these models are equivalent, i.e. they differ only in the labeling of their fixed points. This relabeling freedom occurs in sectors with fixed lines. In these cases, there remains a sum over the unfixed index in the linear equivalences used to calculate the intersection numbers. In this sum, the ordering of the fixed points is irrelevant. Fixed lines occur in the second and third torus, hence the affected indices are β and γ. To visualize the different possibilities we assign a triangulation $\tau_{\beta,\gamma} \in \{1, 2, \ldots, 5\}$ to each fixed point and arrange them in a 3×4 matrix M where β labels the rows and γ the columns:

$$M = \begin{pmatrix} \tau_{1,1} & \tau_{1,2} & \tau_{1,3} & \tau_{1,4} \\ \tau_{2,1} & \tau_{2,2} & \tau_{2,3} & \tau_{2,4} \\ \tau_{3,1} & \tau_{3,2} & \tau_{3,3} & \tau_{3,4} \end{pmatrix}. \tag{3.19}$$

Two matrices are equivalent if they can be transformed into each other by exchanging whole rows and whole columns. As a lower bound estimate, we introduce a single column index which runs from 1 to 5^3, symmetrize this in the four γ indices and divide the result by the permutation symmetry of the columns, which is 3!. This is a lower bound as the permutation symmetry actually is smaller than 3!: it considers the number of permutations even if two $\tau_{\beta,\gamma}$ are equal and thus permuting them does not change the matrix. The resulting number of inequivalent models is

$$N^1_{\text{triang}} = \frac{1}{3!} \begin{pmatrix} 5^3 + 4 - 1 \\ 4 \end{pmatrix} \approx 1.78 \cdot 10^6. \tag{3.20}$$

Another possibility would have been to take one row as an index running from 1 to 5^4 and symmetrize over the columns. This gives

$$N^2_{\text{triang}} = \frac{1}{4!} \begin{pmatrix} 5^4 + 3 - 1 \\ 3 \end{pmatrix} \approx 1.70 \cdot 10^6. \tag{3.21}$$

As explained above, the estimates are lower bounds. Thus the better bound comes from N^1_{triang}. In a computer search that constructed all models and checked them for equivalency, we found that there are 1.797.090 different blowup possibilities, which is close to the lower bound estimates. In this sense, scanning one orbifold model is equivalent to checking almost two million CY models.

3.4 Example: Blowup of the $\mathbb{Z}_2 \times \mathbb{Z}_2$ orbifold

This example deals with the $\mathbb{Z}_2 \times \mathbb{Z}_2$ orbifold. Due to its higher symmetry, the discussion is not so involved as the one of the $\mathbb{Z}_{6-II}$ orbifold in the last section. We start with computing

the vectors of the ordinary and exceptional divisors. After that, we give the toric diagrams and the linear equivalences. At the end, we compute topological invariants.

3.4.1 Local resolution

As a first step, we compute the vectors entering the invariant monomial u_j. The $\mathbb{Z}_2 \times \mathbb{Z}_2$ orbifold has fixed lines in each sector θ_1, θ_2, and θ_3, (cf. section 2.4). From the twist vectors (2.38), we find for (3.2)

$$\left.\begin{array}{l} \frac{1}{2}(v_2+v_3) \equiv 0 \bmod 1 \\ \frac{1}{2}(v_1+v_3) \equiv 0 \bmod 1 \\ \frac{1}{2}(v_1+v_2) \equiv 0 \bmod 1 \end{array}\right\} \rightarrow v_1 = \begin{pmatrix} 2 \\ 0 \\ 1 \end{pmatrix}, \; v_2 = \begin{pmatrix} 0 \\ 0 \\ 1 \end{pmatrix}, \; v_3 = \begin{pmatrix} 0 \\ 2 \\ 1 \end{pmatrix}, \tag{3.22}$$

where the solution is again not unique and chosen such that the CY condition is fulfilled.

As all θ_i fulfill (3.4), we get exceptional divisors from all sectors. Their positions w_i are calculated according to (3.4) using (3.22):

$$w_1 = \begin{pmatrix} 0 \\ 1 \\ 1 \end{pmatrix}, \; w_2 = \begin{pmatrix} 1 \\ 0 \\ 1 \end{pmatrix}, \; w_3 = \begin{pmatrix} 1 \\ 1 \\ 1 \end{pmatrix}. \tag{3.23}$$

There are four different triangulation possibilities. The corresponding toric diagrams, the dual graphs and the unprojected dual graphs are given in figure 3.6.

The linear equivalences (3.5) are computed using (3.22) and (3.23):

$$0 \sim 2D_1 + E_2 + E_3, \quad 0 \sim 2D_2 + E_1 + E_3, \quad 0 \sim 2D_3 + E_1 + E_2, \tag{3.24}$$

where the equivalences have again been combined such that they contain only one ordinary divisor.

3.4.2 Gluing procedure

To get the compact resolution from gluing together the local resolution of the fixed points, we again introduce labels on the divisors. The ordinary divisors are labeled by $D_{1,\alpha}$, $D_{2,\beta}$, and $D_{3,\gamma}$. The exceptional divisors carry labels $E_{1,\beta\gamma}$, $E_{2,\alpha\gamma}$, and $E_{3,\alpha\beta}$ with $\alpha, \beta, \gamma \in \{1,2,3,4\}$. So altogether we have $4+4+4 = 12$ ordinary and $16+16+16 = 48$ exceptional divisors.

Using (3.24), we find for the linear equivalences in the compact case:

$$\begin{aligned} R_1 &\sim 2D_{1,\alpha} + \sum_{\gamma=1}^{4} E_{2,\alpha\gamma} + \sum_{\beta=1}^{4} E_{3,\alpha\beta}, \quad \alpha \in \{1,2,3,4\}, \\ R_2 &\sim 2D_{2,\beta} + \sum_{\gamma=1}^{4} E_{1,\beta\gamma} + \sum_{\alpha=1}^{4} E_{3,\alpha\beta}, \quad \beta \in \{1,2,3,4\}, \\ R_3 &\sim 2D_{3,\gamma} + \sum_{\beta=1}^{4} E_{1,\beta\gamma} + \sum_{\alpha=1}^{4} E_{2,\alpha\gamma}, \quad \gamma \in \{1,2,3,4\}. \end{aligned} \tag{3.25}$$

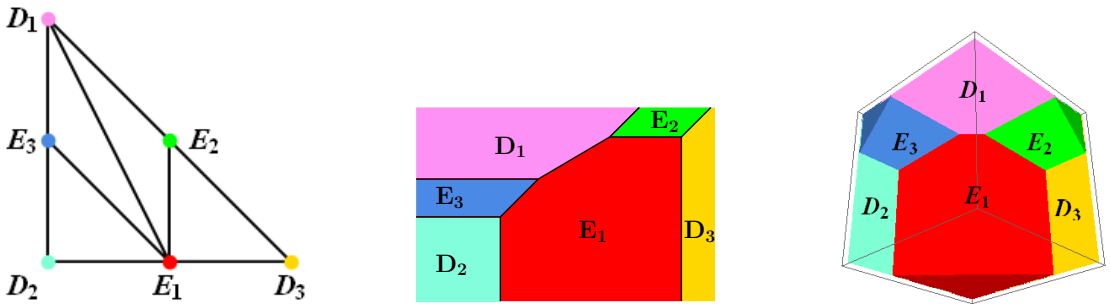

(a) Diagrams for triangulation (i) with $(t_1 : t_2 : t_3) \approx (1 : 0.4 : 0.4)$.

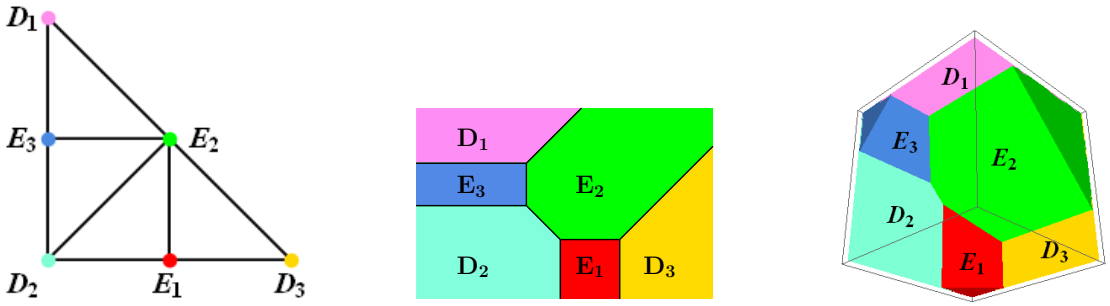

(b) Diagrams for triangulation (ii) with $(t_1 : t_2 : t_3) \approx (0.4 : 1 : 0.4)$.

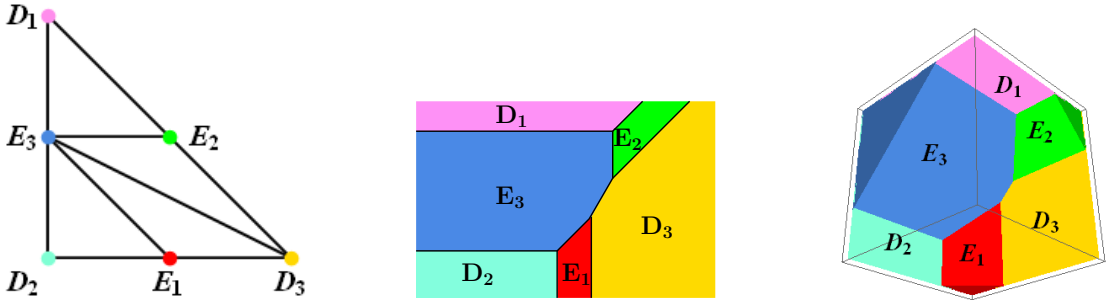

(c) Diagrams for triangulation (iii) with $(t_1 : t_2 : t_3) \approx (0.4 : 0.4 : 1)$.

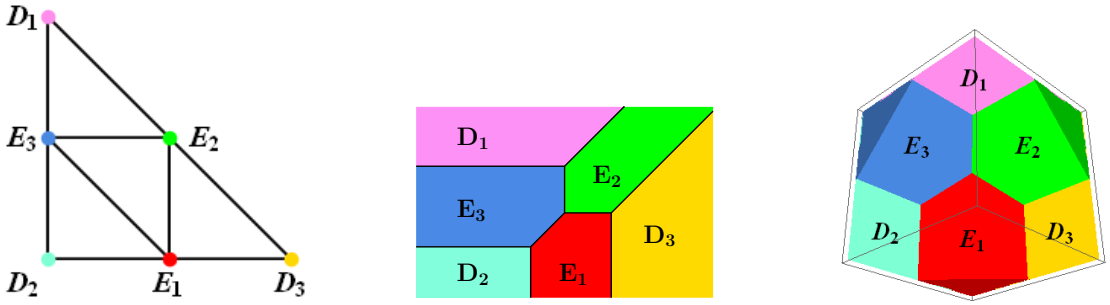

(d) Diagrams for triangulation (iv) with $(t_1 : t_2 : t_3) \approx (1 : 1 : 1)$.

Figure 3.6: The toric diagrams, their dual graphs and the unprojected dual graphs for the four triangulation possibilities of the $\mathbb{C}^3/\mathbb{Z}_2 \times \mathbb{Z}_2$ fixed points. The unprojected dual graphs have been rotated in order to match the orientation of the other diagrams.

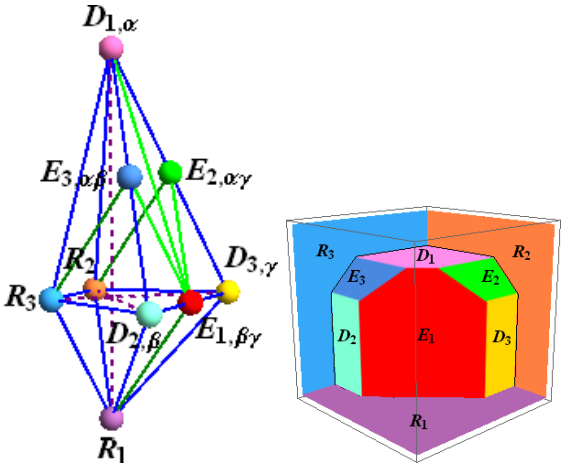

(a) The polyhedron and unprojected dual graph for $\mathbb{C}^3/\mathbb{Z}_2 \times \mathbb{Z}_2$ with triangulation (i).

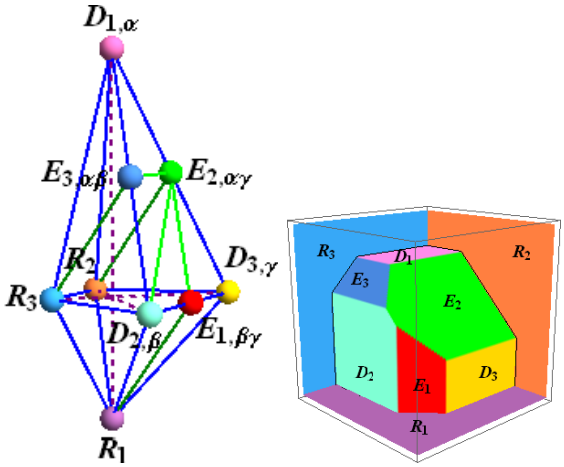

(b) The polyhedron and unprojected dual graph for $\mathbb{C}^3/\mathbb{Z}_2 \times \mathbb{Z}_2$ with triangulation (ii).

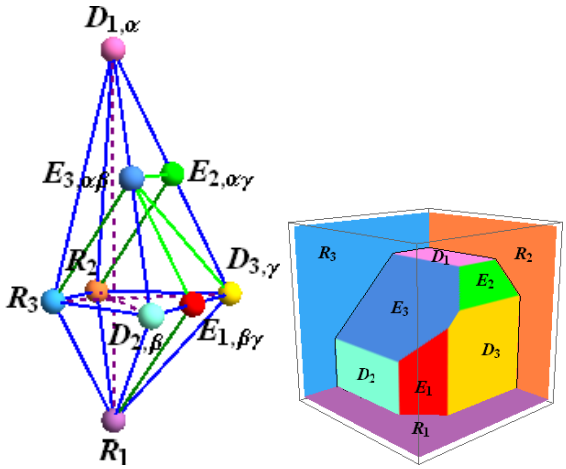

(c) The polyhedron and unprojected dual graph for $\mathbb{C}^3/\mathbb{Z}_2 \times \mathbb{Z}_2$ with triangulation (iii).

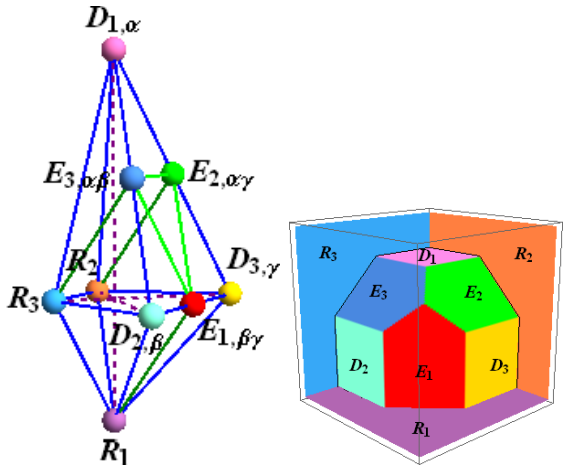

(d) The polyhedron and unprojected dual graph for $\mathbb{C}^3/\mathbb{Z}_2 \times \mathbb{Z}_2$ with triangulation (iv).

Figure 3.7: The auxiliary polyhedra for $T^6/\mathbb{Z}_2 \times \mathbb{Z}_2$ with all possible triangulations.

In order to get the intersection numbers, we need to construct the auxiliary polyhedra for this orbifold, which are given in figure 3.7. The lines connecting the simplices with the origin are again omitted and the triangulation-dependent face is also the upper front one. Having both the auxiliary polyhedron and the compact linear equivalences, we can compute all intersection numbers.

3.4.3 Properties of the blowup manifold

Next, we want to compute the topological invariants for the $\mathbb{Z}_2 \times \mathbb{Z}_2$ manifold. We start with the Hodge numbers. Taking the R_i and E_r as a basis for $H^{1,1}$, we find $h^{1,1} = 3 + 48 = 51$. We define again the $(1,0)$-forms ω_1, ω_2, ω_3 as in the $\mathbb{Z}_{6-II}$ case. As they are not invariant by themselves, $h^{1,0} = 0$. We can build the invariant $(3,0)$ volume form $\omega_1 \wedge \omega_2 \wedge \omega_3$ from these. Invariant $(2,1)$-forms are $\overline{\omega}_{\overline{1}} \wedge \omega_2 \wedge \omega_3$, $\omega_1 \wedge \overline{\omega}_{\overline{2}} \wedge \omega_3$, and $\omega_1 \wedge \omega_2 \wedge \overline{\omega}_{\overline{3}}$, so $h^{2,1} = 3$. There

are no further contributions from the twisted sector since we only have fixed lines with fixed points on them [23]. As there are no further invariant forms, we find for the Hodge diamond by using the symmetry of the Hodge numbers and Poincaré duality:

$$\begin{array}{ccccccc} & & h^{3,3} & & & & \\ & h^{3,2} & & h^{2,3} & & & \\ h^{3,1} & & h^{2,2} & & h^{1,3} & & \\ h^{3,0} & & h^{2,1} & & h^{1,2} & & h^{0,3} \\ & h^{2,0} & & h^{1,1} & & h^{0,2} & \\ & & h^{1,0} & & h^{0,1} & & \\ & & & h^{0,0} & & & \end{array} = \begin{array}{ccccccc} & & 1 & & & & \\ & 0 & & 0 & & & \\ 0 & & 3+48 & & 0 & & \\ 1 & & 3 & & 3 & & 1, \\ 0 & & 3+48 & & 0 & & \\ & 0 & & 0 & & & \\ & & 1 & & & & \end{array} \tag{3.26}$$

which again has the Calabi-Yau structure (2.6) and agrees with [23].
The next topological quantity we compute is the Euler number (2.7), which is found to be

$$\chi(X) = 2(1 + 51 - (1 + 3)) = 96. \tag{3.27}$$

After dividing out the $\mathbb{Z}_{2,\text{free}}$ element, the number of fixed points is halved. So there will be only 24 exceptional divisors. This changes the Hodge numbers $h^{1,1} = h^{2,2} = 3 + 24 = 27$ in (3.26), and we find for the Euler number

$$\chi(X/\mathbb{Z}_{2,\text{free}}) = 2(1 + 27 - (1 + 3)) = 48, \tag{3.28}$$

which is in agreement with [42]. By comparing the fixed point structure and the topological invariants, we can infer that the $C^3/[(\mathbb{Z}_2 \times \mathbb{Z}_2) \times \mathbb{Z}_{2,\text{free}}]$ orbifold can be equivalently defined as a $\mathbb{Z}_2 \times \mathbb{Z}_2$ orbifold on the non-factorizable $SO(12)$ lattice [43].

Next, we again turn to the Chern classes. For computing them, we express the total Chern class $c(X)$ through divisors

$$c(X) = \prod_{i=1}^{12} \prod_{r=1}^{48} (1 + D_i)(1 + E_r)(1 - R_1)^2(1 - R_2)^2(1 - R_3)^2. \tag{3.29}$$

Expanding (3.29) yields

$$c_1(X) = \sum_{i=1}^{12} D_i + \sum_{r=1}^{48} E_r - 2\sum_{i=1}^{3} R_i \tag{3.30a}$$

$$c_2(X) = \frac{1}{2!} \sum_{\text{all divisors}} (c_1(X) - S_i)S_i \tag{3.30b}$$

$$c_3(X) = \frac{1}{3!} \sum_{\text{all divisors}} (c_1(X) - S_i - S_j)S_iS_j \tag{3.30c}$$

Using (3.30a) and the linear equivalences (3.25), we find for our blowup manifold the Calabi-Yau condition $c_1(X) = 0$. Furthermore, we find $c_3(X) = 96$ by substituting the triple intersection numbers into (3.30c), which agrees with (3.27) for all triangulation possibilities we checked.

We also want to estimate the number of different blowups in the $\mathbb{Z}_2 \times \mathbb{Z}_2$ case. The discussion is analogous to the $\mathbb{Z}_{6-II}$ case. The upper bound in this case is $4^{64} \approx 3.40 \cdot 10^{38}$.

We have fixed lines in each torus, hence we need to symmetrize in all three indices α, β, γ. We again assign a triangulation $\tau_{\alpha,\beta,\gamma} \in \{1,2,3,4\}$ to each fixed point and arrange them in a $4\times4\times4$ tensor. This tensor can be visualized as a cube with α labeling the length (rows), β the width (columns), and γ the depth (stacks). Two such cubes are equivalent if they can be transformed into each other by exchanging whole rows, whole columns, or whole stacks. In this case we estimate the total number by introducing a row index which runs from 1 to 4^4, symmetrize this in the four β indices and divide out the permutation symmetry 4!. The resulting double-index, which corresponds to the front face of the cube is symmetrized in a second step over its four γ indices and divided by the γ symmetry factor of 4!. This results in

$$N_{\text{triang}} = \frac{1}{4!}\left(\begin{array}{c} \frac{1}{4!}\left(\begin{array}{c} 4^4+4-1 \\ 4 \end{array}\right)+4-1 \\ 4 \end{array}\right) \approx 5.89\cdot10^{24} \tag{3.31}$$

inequivalent models. Of course this estimate is much cruder than in the $\mathbb{Z}_{6-II}$ case. Due to the huge number we could not use the approach we followed in the $\mathbb{Z}_{6-II}$ case to get the exact number of different triangulations, where we explicitly constructed all 5^{12} possibilities and eliminated those that are equivalent. For the 4^{64} models at hand, this would take $\mathcal{O}(10^{30})$ times longer.

Chapter 4

. . . . . .

The Bianchi identities

The previous chapter showed how to resolve singular orbifold spaces. The topological data gained from the blowup procedure can be used to pass from the singular orbifold space to a smooth six-dimensional Calabi-Yau manifold. This manifold is used to compactify the ten-dimensional $E_8 \times E_8$ heterotic supergravity theory to four dimensions. In this chapter the Bianchi identities for the three-form field strength H of the supergravity multiplet two-form field B will be discussed. They are the central consistency requirements that have to be imposed on the theory. In the first section, we give an outline of how to derive the Bianchi identity equations for H. Then it is discussed how these equations can be formulated when using Abelian gauge fluxes. We will see how we can use the blowup procedure given in chapter 3 to explicitly calculate the equations via Poincaré duality. Subsequently, we have to think about a way to solve these complicated and stringent equations. The possibility of identifying twisted orbifold states with line bundle vectors comes to our rescue. This identification has some astonishing consequences, which are investigated subsequently. At the end we will describe explicitly how to solve the Bianchi identities for the $\mathbb{Z}_{6-II}$ and the $\mathbb{Z}_2 \times \mathbb{Z}_2$ orbifold with one particular choice of triangulations at the fixed points.

4.1 Derivation of the BI equations

This section shortly outlines how to derive the Bianchi identities. The description follows [44, 45]. We want to investigate $\mathcal{N} = 1$ supergravity in ten dimensions coupled to ten-dimensional $\mathcal{N} = 1$ super Yang-Mills theory. The super Yang-Mills theory alone is constructed such that it is invariant under *global* supersymmetry transformations. When introducing supergravity, the combined system has to be invariant under *local* supersymmetry transformations. This already uniquely determines the coupling of the super Yang-Mills multiplet to the supergravity multiplet. It can be shown that the field strength of the two-form field B must be generalized from $H = dB$ to

$$H = dB - \frac{\alpha'}{4}\omega_{3,YM}, \tag{4.1}$$

where $\omega_{3,YM}$ is the so-called Yang-Mills Chern-Simons three-form

$$\omega_{3,YM} = \mathrm{Tr}\left(\mathcal{A}\wedge\mathcal{F} - \frac{1}{3}\mathcal{A}\wedge\mathcal{A}\wedge\mathcal{A}\right). \tag{4.2}$$

Here, $\mathcal{F} = d\mathcal{A} + \mathcal{A}\wedge\mathcal{A}$ is the field strength two-form and $\mathcal{A}$ the gauge fields. In the following we use the abbreviation $\Omega\wedge\Omega \equiv \Omega^2$ for some form Ω and do not write the wedge product explicitly. In order to have an anomaly free theory, the Lorentz transformation for B must be changed. With this change, the combination (4.1) stays gauge invariant but is not Lorentz invariant anymore. In order to restore Lorentz invariance, one introduces another Chern-Simons term, the Lorentz Chern-Simons three-form $\omega_{3,L}$:

$$\omega_{3,L} = \mathrm{Tr}\left(\omega\mathcal{R} - \frac{1}{3}\omega^3\right). \tag{4.3}$$

Here, $\mathcal{R}$ is the Riemann curvature tensor and ω the spin connection. The three-form field strength H is then given by

$$H = dB - \frac{\alpha'}{4}(\omega_{3,YM} - \omega_{3,L}). \tag{4.4}$$

Taking the exterior derivative, one obtains the Bianchi identities

$$dH = \frac{\alpha'}{4}(-d\omega_{3,YM} + d\omega_{3,L}) = \frac{\alpha'}{4}\left(-\mathrm{TR}(\mathcal{F}^2) + \mathrm{TR}(\mathcal{R}^2)\right). \tag{4.5}$$

The trace TR is normalized as the trace in the fundamental representation of $SO(N)$. As $\mathcal{F}$ is taken to be Abelian in this thesis, there is a relation among the traces TR in the fundamental of $SO(N)$, tr in the fundamental of $SU(N)$, and Tr in the adjoint of E_8 [28]:

$$\mathrm{Tr}\mathcal{F}^2 = 30\mathrm{TR}\mathcal{F}^2 = 60\mathrm{tr}\mathcal{F}^2. \tag{4.6}$$

For gauge field strengths in E_8, only Tr is defined and the equation above is taken to be a definition. As the left hand side of (4.5) is exact, it vanishes by virtue of Stokes' theorem when integrating over any compact space $\mathcal{C}$:

$$0 = \int_{\mathcal{C}} dH = \int_{\mathcal{C}} -\mathrm{TR}(\mathcal{F}^2) + \mathrm{TR}(\mathcal{R}^2). \tag{4.7}$$

This assumes that H is globally defined, which it must be as it appears for example in the energy.

The Bianchi identities seem to be very hard to satisfy. Let us look at the case $H = 0$. In this case the Bianchi identities read $\mathrm{TR}(\mathcal{F}^2) = \mathrm{TR}(\mathcal{R}^2)$. As stated in section 2.1, the internal manifold is of $SU(3)$ holonomy, i.e. its spin connection is $SU(3)$-valued. If now the ten-dimensional gauge group was also $SU(3)$, we could set the gauge fields $\mathcal{A}$ equal to the spin connection ω. This would then mean that the Riemann curvature tensor $\mathcal{R}$ equals the Yang-Mills field strength $\mathcal{F}$ and the Bianchi identities were satisfied automatically. This procedure is called embedding the spin connection in the gauge group. Now, $SU(3)\times E_6$ is a maximal subgroup of E_8. Thus by embedding the $SU(3)$ holonomy group in the first E_8, say, we are left with the gauge group $E_6\times E_8$. This is of course particularly nice, since E_6 is a GUT group (cf. chapter 1).

However, if one does not choose the standard embedding, the Bianchi identities are highly non-trivial. In this case one does not obtain $E_6 \times E_8$, but some other gauge group determined by the orbifold shift vector and the Wilson lines which describe the action in the gauge degrees of freedom (see section 2.2.2). Although the standard embedding satisfies stringent equations automatically and we get the GUT group E_6 for free, there are also drawbacks to this procedure. The main disadvantage is that generically there is a huge number of generations ($N_f \gg 3$) in the spectrum, which is not desirable from a phenomenological point of view. Note that if one does not choose the standard embedding, H will generically be non-zero. As mentioned in section 2.1, this case is not investigated very well. Nevertheless, many heterotic model building techniques rely on non-standard embeddings and do not comment on this issue any further. Although it is definitely worthwile to study the consistency requirements arising from a non-vanishing H, we also will not discuss this issue further and deal with finding a solution to the Bianchi identities in the case of non-standard embeddings in the remainder of this chapter. As in the integrated version of the Bianchi identities (4.7) (henceforth simply referred to as the Bianchi identities for the sake of brevity) the right hand side is zero independent from the value of H, there are, however, no corrections to (4.7) and other integrated equations discussed subsequently.

4.2 Bianchi identities for Abelian gauge fluxes

In general it is a difficult task to construct stable vector bundles on Calabi-Yau manifolds. For this reason this work only deals with Abelian gauge bundles which are intrinsically μ-stable [46, 47]. But still, there are many consistency requirements for the Abelian gauge background. Firstly, the gauge flux needs to be properly quantized, i.e. it has to be equal to an $E_8 \times E_8$ lattice vector when integrated over any compact curve. Secondly, in order to make contact to the heterotic orbifold, we will need to see how to identify the orbifold gauge vectors and Wilson lines with the gauge flux. Thirdly, the gauge background has to be chosen such that the Bianchi identities and, for a supersymmetric solution, also the hermitian Yang-Mills equations are fulfilled.

As we are considering Abelian gauge backgrounds, we can choose a Cartan basis in the $E_8 \times E_8$ gauge group with generators $H_I, I = 1, 2, \ldots, 16$ in which we then expand the two-form field strength $\mathcal{F}$. As can be seen from the first part of the hermitian Yang-Mills equations (2.5), the gauge flux needs to be a $(1,1)$-form. Hence we can expand it in divisors. A priori we should take all divisors, but as we discussed in section 3.2, it is sufficient to consider the inherited and exceptional divisors only. However, when going to the blowdown limit one should recover the results from the orbifold theory. There we allowed for gauge shifts and Wilson lines that correspond to non-trivial boundary conditions around the orbifold fixed points, but not for magnetized tori. Hence the field strength on the orbifold must be non-trivial only at the singularities. For this reason we expand $\mathcal{F}$ in exceptional divisors only,

$$\frac{\mathcal{F}}{2\pi} = E_r V_r^I H_I, \tag{4.8}$$

as those are lying inside the singularities in the orbifold limit. The vectors V_r (one vector per exceptional divisor) encode how the gauge flux is embedded into the $E_8 \times E_8$ gauge group.

Next, we investigate the relation between $\mathcal{F}$ and the orbifold shift vector and the Wilson

lines. In order to identify the heterotic orbifold data with the characterization of the bundle, one considers all the fixed points and fixed lines with their associated gauge shifts individually. As explained in [27,28], the identification between the local gauge shift and the local Abelian bundle flux is obtained on the resolution by integrating over an appropriately chosen non-compact curve represented by ordinary divisors,

$$V_g \equiv \int_{\mathcal{C}} \frac{\mathcal{F}}{2\pi}\bigg|_r = V_r, \tag{4.9}$$

where the vertical bar means restriction to the local fixed point or fixed line (labeled by r) that is being investigated, i.e. all other exceptional divisors in $\mathcal{F}$ are not considered. The local orbifold shift vector V_g is characterized by its space group element $g = (\theta, l)$. The equivalence sign is used to express that the bundle vectors V_r are only determined up to lattice vectors, as the orbifold shift vectors and Wilson lines entering V_g are themselves only determined up to $E_8 \times E_8$ lattice vectors[1]. By virtue of equation (4.9) we can match the local orbifold gauge shifts - i.e. the orbifold shift vector and Wilson lines - with the line bundle vectors of the blowup.

4.3 Computing the Bianchi identities from toric geometry

As explained before, the Bianchi identities are very stringent consistency requirements that have to be fulfilled by the gauge fluxes. Our first task is to compute the integral in the Bianchi identity equations (4.7). To do so, we exploit a relation between the second Chern class c_2 of the resolved manifold X and the Riemann curvature tensor $\mathcal{R}$,

$$c_2(X) = -\mathrm{tr}\frac{\mathcal{R}^2}{8\pi^2}. \tag{4.10}$$

In chapter 3, we saw in equations (3.18b) and (3.30b) how to express $c_2(X)$ in terms of a product of divisors. Using the expansion of the gauge flux in $(1,1)$-forms (4.8), and the relation (4.10), the Bianchi identities can be rewritten in terms of divisors as

$$\int_{\mathcal{C}} \left(\sum_r E_r V_r\right)^2 - \sum_{\text{all divisors}} S_i^2 = 0. \tag{4.11}$$

These equations can be calculated using (2.8). By providing the intersection numbers, toric geometry allows us to access the computation of integrals in blowup. The compact cycles of our resolved manifold are the inherited and exceptional divisors, i.e. $\mathcal{C} = R, E$ in (4.11). This means that calculating the integrals for the Bianchi identities boils down to summing up integers, as explained in section 2.1. The Bianchi identities have to hold when integrating over any compact cycle, i.e. for any divisor. This gives a whole set of non-trivial equations the gauge flux has to satisfy (as many as there are R's and E's).

Having computed the Bianchi identities, we face a serious problem: how do we solve such a huge set of equations? A good starting point is the identification of orbifold shift vectors and Wilson lines with the line bundle vectors, given by equation (4.9). However, as explained above, this identification is only valid up to $E_8 \times E_8$ lattice vectors. So from each

[1] Here one has to be careful with the issue of brother or grandchild models, cf. section 2.2.3.

of the (infinite-dimensional) equivalence classes of V_r defined as the local orbifold shift plus lattice vectors (4.9), we have to choose one vector such that the gauge background given by the combination of all bundle vectors fulfills all Bianchi identities simultaneously. By taking $8+8=16$ root vectors from the first and second E_8, we can express the line bundle vectors as

$$V_r \equiv V_g = c_0^r V_{sh} + \sum_{\text{all WL}} c_i^r W_i + \sum_{i=1}^{16} a_i^r \lambda_i, \tag{4.12}$$

where the c_i are (known) coefficients appearing in the expression for the local orbifold gauge shift derived from (4.9) and the last sum is an arbitrary linear combination of $E_8 \times E_8$ root vectors. Inserting this into (4.11), we have rephrased the Bianchi identities as equations in the (integer) linear combination coefficients a_i^r. Note that for each Bianchi identity, we get 16 of these coefficients and there are as many Bianchi identities as there are divisors. So we are left with a big system of generically highly coupled nonlinear Diophantine equations[2]. This type of equation is notoriously difficult to solve. So in order to solve it, it is convenient to make simplifying assumptions. These assumptions depend on the model under investigation and are described in the example sections at the end of this chapter for the $\mathbb{Z}_{6-II}$ and the $\mathbb{Z}_2 \times \mathbb{Z}_2$ orbifold respectively. Additionally, there is a very useful relation between the orbifold states and the line bundle vectors, which is explored in the next section.

4.4 Relation between the orbifold and the Calabi-Yau

Being confronted with the complicated set of Bianchi identities, it is advisable to see if one can make contact to other theories. Our goal is rather ambitious: we do not only want some gauge background on the blowup manifold that satisfies all Bianchi identities simultaneously, but we also want the solution to have the particle content of the MSSM, i.e. three generations of quarks and leptons. Note however, since the method we are using to break the $E_8 \times E_8$ to the Standard Model gauge group does not reduce the rank of the group, there will be additional $U(1)$'s under which the matter content of the theory is charged. However, these $U(1)$'s will generically be anomalous. As the anomalies are canceled by the Green-Schwarz mechanism, the $U(1)$'s can aquire a mass. This means that the theory is anomaly free but the $U(1)$ symmetry is broken. Another way of reducing the rank of the gauge group is to embed the orbifold space group $\mathbb{S}$ into the gauge group in a non-Abelian way [48], but this is beyond the scope of this thesis. Also there should be no (or at least very massive) color triplets which mediate fast proton decay, and the hidden sector gauge group should not be too small in order to allow for gaugino condensation.

While satisfying the Bianchi identities on all compact divisors is sufficient for the spectrum to be free of non-Abelian anomalies [49], Abelian and mixed anomalies do in general arise for Abelian gauge backgrounds. These anomalies can be canceled via the Green-Schwarz mechanism. The mechanism in ten dimensions heavily relies on the fact that the anomaly polynomial twelve-form I_{12} factorizes into a four-form and an eight-form, $I_{12} = X_4 X_8$. The relevant graphs in ten, six, and four dimensions are shown in figure 4.1, see also section 5.1. We can write the three-form field strength H as

$$H_3 = dB_2 + \frac{\alpha'}{4} X_3, \qquad dX_3 = X_4 = \text{tr} R^2 - \text{tr} F^2. \tag{4.13}$$

[2]These are polynomial equations with fewer equations than unknowns to be solved over the integer domain.

(a) Ten-dimensional anomaly graphs.

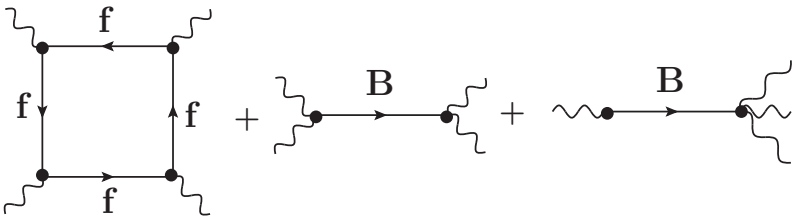

(b) Six-dimensional anomaly graphs.

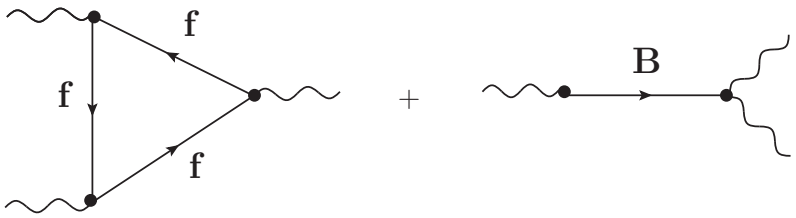

(c) Four-dimensional anomaly graphs.

Figure 4.1: Relevant anomaly graphs in ten, six, and four dimensions. In the loop, the gravitinos, gauginos, and dilatinos are running. The legs are either gravitons or gauge fields. The graphs involving the B field are used to cancel the anomalies.

Here, R and F are the four-dimensional curvature and field strength. Upon compactification to four dimensions, we can expand the two-form field B in harmonic $(1,1)$-forms, i.e. in the divisors R and E:

$$B_2 = b_2 + 2\pi\alpha'(\alpha_i R_i + \beta_r E_r). \tag{4.14}$$

Here b_2 is the two-form in four dimensions and the α_i and β_i are scalars. By also expanding the Kähler $(1,1)$-form J in the divisor basis, we can write

$$J = a_i R_i - b_r E_r \tag{4.15}$$

with a_i and b_i the Kähler moduli, cf. equation (2.9). The sign has been chosen for later convenience (cf. chapter 7).

The normalization in (4.14) was chosen such that under Abelian gauge transformations $\delta A^I = d\lambda^I$, with gauge parameter λ^I. The β_r transform as axions and the α_i transform trivially [28],

$$\delta\beta_r = V_r^I \lambda^I, \qquad \delta\alpha_i = 0. \tag{4.16}$$

Since compactification on a Calabi-Yau preserves supersymmetry (cf. section 2.1), all states fall in supersymmetric multiplets. The scalars α_i and axions β_r form the scalar components of the chiral multiplets T_i and U_r. These components are defined by the expansion of the dimensionless complexified Kähler form

$$i\left(\frac{B_2 - b_2}{2\pi\alpha'} + iJ\right) = T_i|\, R_r + U_r|\, E_r. \tag{4.17}$$

Their lowest components, as can be seen by substituting (4.14) and (4.15) into (4.17), are given by

$$T_i| = -a_i + i\alpha_i, \qquad U_r| = b_r + i\beta_r, \tag{4.18}$$

where the vertical bar indicates that all Grassmann coordinates $\theta, \overline{\theta}$ have been set to zero. The states β_r are located at the exceptional divisors E_r. The same is true for the twisted states from the orbifold (see section 2.2.2). Consider now the superfield redefinition

$$\Psi_r = M_s e^{2\pi U_r} = M_s e^{2\pi(b_r + i\beta_r)}, \qquad \delta\Psi_r = e^{2\pi i V_r^I \lambda^I}\Psi_r, \tag{4.19}$$

where we used the lowest component of U_r (4.18) and (4.16). We see that Ψ_r transforms linearly under gauge transformations. This shows that Ψ_r is a definite state from the orbifold perspective. The identification of the Abelian bundle vectors V_r with the orbifold gauge shift and Wilson lines, as given in (4.9), is the same as the local orbifold shift V_g, up to possible lattice vectors. As the twisted states are identified by their shifted momenta $p_{sh} = p + V_g$, where V_g is the local orbifold shift and p is an $E_8 \times E_8$ lattice vector (cf. section 2.2.2), this implies that each bundle vector V_r defines a shifted momentum and therefore each superfield corresponds to a definite twisted state. This bridges a gap between the line bundle vectors on the one side and the twisted orbifold states on the other.

This has some remarkable consequences. From the orbifold perspective, the blowdown corresponds to having a vanishing vev for the twisted state Ψ_r. According to (4.19) this limit is obtained by letting the Kähler modulus $b_r \to -\infty$. So the areas of certain curves become negative. This is astonishing but consistent with [32]. There it was argued that the volumes of exceptional divisors defined by the "algebraic" measure tends to $-\infty$ in the blowdown limit. We see that the expectation value of the twisted states precisely correspond to this measure. It is possible to define another measure, the "σ-model" measure, where the blowdown limit corresponds to actually taking the volume of the exceptional divisors to zero. However, the explicit construction is very involved and will not be pursued further here.

Another consequence of the correspondence between the local orbifold shifts and the line bundle vectors is that the mass-shell conditions of physical states, which is quadratic in the shifted momenta (see equation (2.24a)) translates into an equation for the absolute value squared of the bundle vectors. In the blowup picture, the absolute value squared of the vectors is constrained by the instanton number obtained from integrating $\mathrm{tr}\mathcal{R}^2$ in (4.7).

We will also see that the ratio of the vevs which is needed to cancel the D-term of the twisted fields on the orbifold side is correlated to the ratio of volumes of exceptional divisors which is needed in order to satisfy the tree level hermitian Yang-Mills equation. But this discussion will be postponed until we discuss the hermitian Yang-Mills equation and the one loop corrected Donaldson-Uhlenbeck-Yau equations in section 7.2. With all these tools at hand we now give two examples of how to solve the Bianchi identities.

4.5 Example: Solving the Bianchi identities for the $\mathbb{Z}_{6-II}$ orbifold

This section is dedicated to applying our earlier findings to the $\mathbb{Z}_{6-II}$ orbifold. We start with computing the relations (4.9). For the $\mathbb{Z}_{6-II}$ singularities $(1, 1\beta\gamma)$, the curve over which we integrate can only be $D_{2,\beta}D_{3,\gamma}$, as this curve is not interrupted by exceptional divisors in the projected toric diagram. The identification therefore reads

$$V_{(\theta,l_{1\beta\gamma})} \equiv \int_{D_{2,\beta}D_{3,\gamma}} \frac{\mathcal{F}}{2\pi}\bigg|_{1\beta\gamma} = V_{1,1\beta\gamma}. \tag{4.20}$$

Written out in terms of the orbifold shift and Wilson lines, one obtains:

$$\begin{array}{ll} V_{1,111} \equiv V_{sh} & , \quad V_{1,112} \equiv V_{sh} + W_2, \\ V_{1,113} \equiv V_{sh} + W_2' & , \quad V_{1,114} \equiv V_{sh} + W_2 + W_2', \\ V_{1,121} \equiv V_{sh} + W_3 & , \quad V_{1,122} \equiv V_{sh} + W_2 + W_3, \\ V_{1,123} \equiv V_{sh} + W_2' + W_3 & , \quad V_{1,124} \equiv V_{sh} + W_2 + W_2' + W_3, \\ V_{1,131} \equiv V_{sh} + 2W_3 & , \quad V_{1,132} \equiv V_{sh} + W_2 + 2W_3, \\ V_{1,133} \equiv V_{sh} + W_2' + 2W_3 & , \quad V_{1,134} \equiv V_{sh} + W_2 + W_2' + 2W_3. \end{array} \tag{4.21}$$

The identifications above will be worked out in two examples. At all fixed points $(1,1\beta\gamma)$, the orbifold twist is simply described by V_{sh}. For the fixed point $(1, 111)$ no torus shift $l_{\alpha\beta\gamma}$ is needed to bring the image under θ back to its original position in the fundamental domain, so $V_{1,111} \equiv V_{sh}$ (compare table 2.6). At the fixed point $(1, 122)$, we need a torus shift in the e_3 and one in the e_5 direction to bring the image back to its original position. In these directions the Wilson lines W_3 and W_2 are switched on. Hence $V_{1,122} \equiv V_{sh} + W_3 + W_2$. The other line bundle vectors can be worked out similarly. Note that the integrals in (4.20) are triangulation-independent, as the triangle $D_2D_3E_1$ is present in all five possible triangulations.

The $\mathbb{Z}_3$ singularities (the θ^2 - and θ^4 - sector) have one fixed torus, i.e. they are of complex codimension two. This means that the matching has to be performed in two complex dimensions, so

$$V_{(\theta^2,l_{\alpha\beta})} \equiv \int_{D_{2,\beta}} \frac{\mathcal{F}}{2\pi}\bigg|_{\alpha\beta} = V_{2,\alpha\beta}, \qquad V_{(\theta^4,l_{\alpha\beta})} \equiv \int_{D_{1,\alpha}} \frac{\mathcal{F}}{2\pi}\bigg|_{\alpha\beta} = -V_{2,\alpha\beta}. \tag{4.22}$$

Note that since the orbifold action in the second twisted sector is opposite to the action in the fourth, the identification on the orbifold requires that $V_{(\theta^2,l_{\alpha\beta})} \equiv -V_{(\theta^4,l_{\alpha\beta})}$. Hence the same relation holds for the line bundle vectors $V_{2,\alpha\beta}$ and $V_{4,\alpha\beta}$:

$$\begin{array}{ll} V_{2,11} \equiv V_{2,31} \equiv 2V_{sh} & , \quad V_{4,11} \equiv V_{4,31} \equiv -2V_{sh}, \\ V_{2,12} \equiv V_{2,32} \equiv 2V_{sh} + 2W_3 & , \quad V_{4,12} \equiv V_{4,32} \equiv -2V_{sh} - 2W_3, \\ V_{2,13} \equiv V_{2,33} \equiv 2V_{sh} + W_3 & , \quad V_{4,13} \equiv V_{4,33} \equiv -2V_{sh} - W_3. \end{array} \tag{4.23}$$

These relations can again be easily worked out analogously to the case described above with the help of table 2.7 and noting that $3W_3 \equiv 0$, as given in (2.22).

Finally, we find for the bundle vectors $V_{3,\alpha\gamma}$:

$$V_{(\theta^3,l_{\alpha\gamma})} \equiv \int_{D_{3,\gamma}} \frac{\mathcal{F}}{2\pi}\bigg|_{\alpha\gamma} = V_{3,\alpha\gamma}, \tag{4.24}$$

which can be written with the help of table 2.8 as

$$\begin{aligned} V_{3,11} &\equiv V_{3,21} \equiv 3V_{sh} \quad , \quad V_{3,12} \equiv V_{3,22} \equiv 3V_{sh} + W_2, \\ V_{3,13} &\equiv V_{3,23} \equiv 3V_{sh} + W_2' \, , \quad V_{3,14} \equiv V_{3,24} \equiv 3V_{sh} + W_2 + W_2'. \end{aligned} \tag{4.25}$$

The fact that there are line bundle vectors in all but the first sector that are degenerate (i.e. the line bundle vectors at different fixed points have the same identification with orbifold shifts and Wilson lines) can be traced back to the fact that these fixed points differ only by torus shifts along directions in which no Wilson line is switched on. Generically, only the torus of the G_2 lattice does not allow for a Wilson line, hence all bundle vectors that carry an index in this torus will be degenerate.

The next step is to calculate the integrals over the divisors in the Bianchi identities (4.7). The first three Bianchi identities are obtained by integrating over the inherited divisors R_i. These integrals are triangulation-independent, as they are outside the face of the auxiliary polyhedron where the triangulation ambiguity arises. However, the integrals over the 32 exceptional divisors do depend on the chosen triangulation in a complicated manner. The 12 integrals over $E_{1,1\beta\gamma}$ depend only on the local resolution of the fixed point $(1, 1\beta\gamma)$. In contrast, the remaining 20 integrals over the divisors $E_{2,\alpha\beta}$, $E_{4,\alpha\beta}$, and $E_{3,\alpha\gamma}$ depend on a combination of triangulations at the $\mathbb{Z}_{6-II}$ fixed points. This is due to the fact that integrating over $E_{2,\alpha\beta}$ and $E_{4,\alpha\beta}$ leaves γ unspecified, while integrating over $E_{3,\alpha\gamma}$ leaves β unspecified. As a consequence, a sum over divisors that carry this unspecified index remains in the expansion of the gauge flux and the second Chern class. In order to perform explicit calculations, we need to make a choice with regard to the triangulation that is employed at the fixed points. As no particular triangulation seems preferable over the others, this example deals with one of the most symmetric choices, that is triangulation (i) at all 12 $\mathbb{C}^3/\mathbb{Z}_{6-II}$ fixed points. As we choose the same triangulation at all fixed points, the complication pointed out above does not arise.

Carrying out the integration, we get the following set of non-trivial Bianchi identities:

$$\sum_\gamma V_{3,1\gamma}^2 + 3\sum_\gamma V_{3,2\gamma}^2 = 24, \tag{4.26a}$$

$$\sum_\beta (V_{2,1\beta}; V_{4,1\beta}) + 2\sum_\beta (V_{2,3\beta}; V_{4,3\beta}) = 24, \tag{4.26b}$$

$$3V_{1,1\beta\gamma}^2 - V_{3,1\gamma}^2 - (V_{2,1\beta}; V_{4,1\beta}) = 0, \tag{4.26c}$$

$$2V_{3,1\gamma}^2 - V_{3,1\gamma} \cdot \sum_\beta V_{1,1\beta\gamma} = 2, \tag{4.26d}$$

$$3V_{2,1\beta}^2 + 4(V_{2,1\beta}; V_{4,1\beta}) - 3V_{2,1\beta} \cdot \sum_\gamma V_{1,1\beta\gamma} = 12, \tag{4.26e}$$

$$6V_{4,1\beta}^2 + 2(V_{2,1\beta}; V_{4,1\beta}) - 3V_{4,1\beta} \cdot \sum_\gamma V_{1,1\beta\gamma} = 12. \tag{4.26f}$$

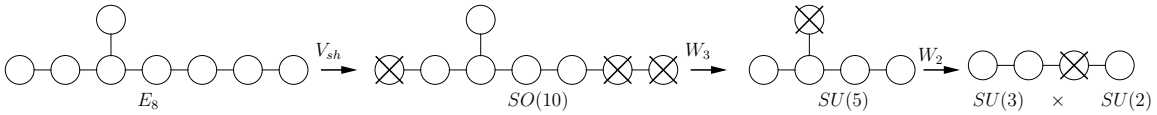

(a) Gauge group breaking to $SU(3) \times SU(2)$ in the first E_8.

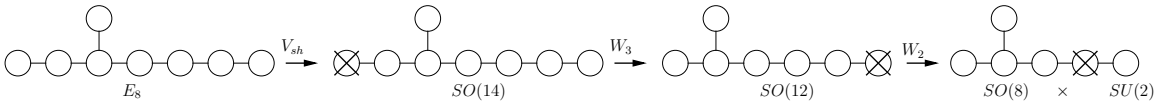

(b) Gauge group breaking to $SO(8) \times SU(2)$ in the second E_8.

Figure 4.2: It is shown how the $E_8 \times E_8$ gauge group is broken via the use of a shift vector and Wilson lines to the $SU(3) \times SU(2)$ part of the Standard Model gauge group plus an $SO(8) \times SU(2)$ gauge group in the hidden sector.

To make the notation more compact, we define

$$(v; w) := v^2 + w^2 - v \cdot w. \tag{4.27}$$

The equation resulting from integrating over R_1 is trivially fulfilled. This is due to the fact that $R_1 E_r E_{r'} = 0$ and $R_1 c_2(X) = 0$ (cf. table C.1 in the appendix). Equations (4.26a) and (4.26b) result from integrating over R_2 and R_3 respectively. Neither of them involve the bundle vectors $V_{1,1\beta\gamma}$ and they are the same as the Bianchi identities on K3, which has instanton number 24. This can be understood by noting that R_2 and R_3 have the topologies of the resolutions of K3 orbifolds $T^4/\mathbb{Z}_3$ and $T^4/\mathbb{Z}_2$ respectively. The twelve equations (4.26c) come from integrating over $E_{1,1\beta\gamma}$, while the four equations (4.26d) come from integrating over $E_{3,1\gamma}$. The equations resulting from integration over $E_{3,2\gamma}$ are trivial. Finally, the two times three equations (4.26e) and (4.26f) come from integration over $E_{2,1\beta}$ and $E_{4,1\beta}$. Integrals over $E_{2,3\beta}$ and $E_{4,3\beta}$ again yield trivial equations. So we finally arrive at the Bianchi identities. As explained before, they correspond to 24 non-linear Diophantine equations for the 32 line bundle vectors in $32 \cdot 16 = 512$ unknowns. The next step will be to solve them.

In order to get an MSSM-like model in blowup we take the data of the Mini-Landscape Benchmark model 2, which was already introduced in section 2.3. The orbifold shift vector V_{sh} given in (2.35) breaks the first E_8 to $SO(10)$, which is broken to $SU(5)$ by the order three Wilson line W_3. The order two Wilson line W_2 further reduces the gauge group to $SU(3) \times SU(2)$. In the hidden sector, V_{sh} breaks the E_8 to $SO(14)$, which is broken down to $SO(12)$ by the order three Wilson line and to $SO(8) \times SU(2)$ by the order two Wilson line, so that the gauge group is $[SU(3) \times SU(2)] \times [SO(8) \times SU(2)] \times U(1)^8$. Locally on the orbifold, there are fixed points with a larger remaining gauge group. But as the gauge background contains fields that feel all Wilson lines, the above mentioned gauge group is the largest one that remains. The procedure is illustrated in terms of Dynkin diagrams in figure 4.2.

From a phenomenological point of view it is desirable to keep the $SU(3) \times SU(2)$ gauge group living in the first E_8 in blowup, as this yields the non-Abelian part of the Standard Model gauge group. Additionally, one may not want to completely break the $SO(8) \times SU(2)$ in the second E_8, as the hidden sector gauge group must not be too small in order to allow for the right gaugino condensation scale. To preserve the Standard Model gauge group in the first E_8, one has to think about which of the $E_8 \times E_8$ vectors can be added to the line bundle

vectors. The $E_8 \times E_8$ vectors must have identical entries in components 4 and 5 as well as in components 6, 7, and 8, as this is where the $SU(2)$ and the $SU(3)$ live respectively. This already considerably reduces the number of unknowns. Initially, we do not take the gauge groups of the second E_8 into consideration, as it turns out that once we find a solution, it can be quite easily changed into a solution with better features, e.g. the preservation of a big hidden sector gauge group.

A further complication arises from the fact that the Bianchi identities contain a lot of inner products between line bundle vectors, which couples many equations; this makes it hard to reduce the Bianchi identities to sets of smaller and thus easier equations. Additionally, it is much easier to solve equations containing squares of vectors than solving equations containing inner products. Hence we aim at rewriting as many equations as possible in terms of vector squares only.

As can be seen from (4.23), for each vector in the θ^2-sector there is a vector in the θ^4-sector that has the same identification of orbifold shifts and Wilson lines up to a minus sign and addition of lattice vectors. By having a closer look at the Bianchi identities, one realizes that exactly these pairs of vectors appear in the combination defined in (4.27) . If one requires the vectors in such pairs to be exactly opposite[3], $V_{2,\alpha\beta} = -V_{4,\alpha}$, the inner product is reduced to $(V_{2,\alpha\beta}; V_{4,\alpha\beta}) = 3V_{2,\alpha\beta}^2 = 3V_{4,\alpha\beta}^2$. This allows us to replace all the inner products of the type $(\cdot\,;\cdot)$ occurring in the Bianchi identities by squares of vectors. Moreover, it further reduces the number of independent variables.

It was discussed in the last section that some line bundle vector identifications are degenerate due to the fact that there is no Wilson line in the relevant direction. This degeneracy is even enhanced in the model under investigation, as the second order two Wilson line in the third torus is not switched on. This leads to a further degeneracy of the vectors carrying an index γ, i.e. the vectors from the θ- and θ^3-sector. So for yet an additional reduction of the number of unknowns, we assume that all degenerate vectors are exactly equal, meaning $V_{1,111} = V_{1,113}$, $V_{1,112} = V_{1,114}$, $V_{3,11} = V_{3,13}$, and so on.
Finally, we require that all vectors coming from the same θ-sector have the same absolute value squared. Making these simplifications, we can cast (4.26) into the following form:

$$V_{1,1\beta\gamma}^2 = \frac{25}{18}, \quad \beta \in \{1,2,3\}\,, \ \gamma \in \{1,2,3,4\}\,, \tag{4.28a}$$

$$V_{2,\alpha\beta}^2 = V_{4,\alpha\beta}^2 = \frac{8}{9}, \quad \alpha \in \{1,3\}\,, \quad \beta \in \{1,2,3\}\,, \tag{4.28b}$$

$$V_{3,\alpha\gamma}^2 = \frac{3}{2}, \quad \alpha \in \{1,2\}\,, \quad \gamma \in \{1,2,3,4\}\,, \tag{4.28c}$$

$$V_{3,1\gamma} \cdot \sum_{\beta=1}^{3} V_{1,1\beta\gamma} = 1, \quad \gamma \in \{1,2,3,4\}\,, \tag{4.28d}$$

$$V_{2,\alpha\beta} \cdot \sum_{\gamma=1}^{4} V_{1,1\beta\gamma} = \frac{4}{9}, \quad \alpha \in \{1,3\}\,, \quad \beta \in \{1,2,3\}\,. \tag{4.28e}$$

[3] A priori they could still differ by $E_8 \times E_8$ lattice vectors.

The two remaining inner product equations (4.28d) and (4.28e) come from (4.26d) and (4.26e) respectively. Under the simplifications, (4.26f) is automatically satisfied if (4.28e) is. It is now easy to find a set of 32 line bundle vectors that satisfy the first three conditions (4.28a) - (4.28c).

However, it turns out that the assumptions made above are too restrictive, which renders it impossible to solve the whole set of equations (4.28) simultaneously. Therefore, one has to abandon some of the assumptions made before. It is, however, advantageous to keep the equations decoupled, so that we do not have to give up all the line bundle vectors we found from solving (4.28a) - (4.28c). Relaxing the condition $V_{2,1\beta} = -V_{4,1\beta}$ leads to a violation of (4.28b) and (4.28e) for $\alpha = 1$. So one has to modify at most all the vectors involved in these equations. However, when modifying the solution, one has to pay attention to maintaining the vector squares as dictated by equations (4.28a) as this guarantees that the equations are still decoupled in the sense that changing something in one equation does not influence the validity of the other equations. In our case, it was sufficient to change $V_{2,1\beta}$, $V_{4,1\beta}$, and $V_{1,1\beta 4}$.

With this procedure we can find a solution satisfying all 24 Bianchi identities. As mentioned earlier, once we find a solution, it can be modified easily. The solution presented in table 4.1 was found as described above and then altered to get a hidden sector $SU(4)$ gauge group, while the $SU(2)$ is broken to $U(1)$'s. By construction, the $SU(3) \times SU(2)$ Standard Model gauge group in the first E_8 is conserved.

It is very interesting to compare the constraints on the absolute value squares of the line bundle vectors coming from equations (4.28a) to (4.28c) with the mass-shell condition (2.24a). The values for δc are taken from (2.34). In the θ-sector, one finds from the condition in the massless case $M_L = 0$, with $p_{sh} = (p + V_g) = V_{1,1\beta\gamma}$:

$$V^2_{1,1\beta\gamma} = \frac{25}{18} - 2\tilde{N} \,, \qquad \beta \in \{1,2,3\} \,,\ \gamma \in \{1,2,3,4\} \,.$$

In the case of a vanishing oscillator number, this is exactly the condition found in (4.28a). A similar observation is made when considering the θ^3-sector. Here the massless equations read:

$$V^2_{3,\alpha\gamma} = \frac{3}{2} - 2\tilde{N} \,, \qquad \alpha \in \{1,2\} \,,$$

which is again the same condition as we obtained in (4.28c) with the oscillator number set to zero. However, for the θ^2- and θ^4-sector, things look a bit different. Here one finds

$$\begin{aligned} V^2_{2,\alpha\beta} &= \frac{14}{9} - 2\tilde{N} \,, \qquad \alpha \in \{1,3\} \,, \\ V^2_{4,\alpha\beta} &= \frac{14}{9} - 2\tilde{N} \,, \qquad \alpha \in \{1,3\} \,. \end{aligned}$$

In this sector the simplified Bianchi identities (4.28b) dictate a non-vanishing $\tilde{N}$ for the massless spectrum. The solution we are giving in table 4.1 was modified such that $V^2_{2,\alpha\beta} = V^2_{4,\alpha\beta} = \frac{14}{9}$ holds for as many of these vectors as considered possible (i.e. for all but $V_{2,11}$ and $V_{2,12}$). Note that it was also condition (4.28b) that was relaxed in order to find a solution.

This shows that it is also possible to demand $V^2_{2,\alpha\beta} = V^2_{4,\alpha\beta} = \frac{14}{9}$ instead of (4.28b). However, the absolute value of these bundle vectors is still constrained by the relation $(V_{2,\alpha\beta}; V_{4,\alpha\beta}) \stackrel{!}{=} \frac{8}{3}$, which is needed in order to solve the Bianchi identity (4.26b) coming

V_r	expression for the bundle vector V_r
$V_{1,111}, V_{1,113}$	$(-\frac{1}{6}\ 0\ 0\ -\frac{1}{2}\ -\frac{1}{2}\ -\frac{1}{2}\ -\frac{1}{2}\ -\frac{1}{2})\ (0\ \frac{1}{3}\ 0\ 0\ 0\ 0\ 0\ 0)$
$V_{1,112}, V_{1,114}$	$(-\frac{5}{12}\ \frac{1}{4}\ -\frac{3}{4}\ -\frac{1}{4}\ -\frac{1}{4}\ \frac{1}{4}\ \frac{1}{4}\ \frac{1}{4})\ (-\frac{1}{2}\ -\frac{1}{6}\ 0\ 0\ 0\ 0\ 0\ 0)$
$V_{1,121}, V_{1,123}$	$(-\frac{1}{6}\ 0\ \frac{2}{3}\ \frac{1}{6}\ \frac{1}{6}\ \frac{1}{6}\ \frac{1}{6}\ \frac{1}{6})\ (\frac{1}{3}\ -\frac{2}{3}\ -\frac{1}{3}\ -\frac{1}{3}\ 0\ 0\ 0\ 0)$
$V_{1,122}, V_{1,124}$	$(\frac{1}{12}\ -\frac{1}{4}\ \frac{5}{12}\ -\frac{1}{12}\ -\frac{1}{12}\ \frac{5}{12}\ \frac{5}{12}\ \frac{5}{12})\ (-\frac{1}{6}\ -\frac{1}{6}\ -\frac{1}{3}\ \frac{2}{3}\ 0\ 0\ 0\ 0)$
$V_{1,131}, V_{1,133}$	$(-\frac{1}{6}\ 0\ \frac{1}{3}\ -\frac{1}{6}\ -\frac{1}{6}\ -\frac{1}{6}\ -\frac{1}{6}\ -\frac{1}{6})\ (\frac{1}{6}\ -\frac{1}{6}\ -\frac{1}{6}\ -\frac{1}{6}\ \frac{1}{2}\ \frac{1}{2}\ \frac{1}{2}\ \frac{1}{2})$
$V_{1,132}, V_{1,134}$	$(\frac{1}{12}\ -\frac{1}{4}\ \frac{1}{12}\ -\frac{5}{12}\ -\frac{5}{12}\ \frac{1}{12}\ \frac{1}{12}\ \frac{1}{12})\ (\frac{1}{6}\ -\frac{1}{6}\ -\frac{2}{3}\ -\frac{2}{3}\ 0\ 0\ 0\ 0)$
$V_{2,11}$	$(-\frac{1}{3}\ 0\ -1\ 0\ 0\ 0\ 0\ 0)\ (0\ -\frac{1}{3}\ 0\ -1\ 0\ 0\ 0\ 0)$
$V_{2,12}$	$(-\frac{1}{3}\ 1\ \frac{1}{3}\ \frac{1}{3}\ \frac{1}{3}\ \frac{1}{3}\ \frac{1}{3}\ \frac{1}{3})\ (-\frac{1}{3}\ -\frac{1}{3}\ \frac{1}{3}\ \frac{1}{3}\ 0\ 0\ 0\ 0)$
$V_{2,13}$	$(-\frac{5}{6}\ \frac{1}{2}\ \frac{1}{6}\ \frac{1}{6}\ \frac{1}{6}\ \frac{1}{6}\ \frac{1}{6}\ \frac{1}{6})\ (\frac{1}{3}\ -\frac{1}{3}\ -\frac{1}{3}\ -\frac{1}{3}\ 0\ 0\ 0\ 0)$
$V_{2,31}$	$(\frac{2}{3}\ 0\ 0\ 0\ 0\ 0\ 0\ 0)\ (0\ -\frac{1}{3}\ 0\ -1\ 0\ 0\ 0\ 0)$
$V_{2,32}$	$(\frac{1}{6}\ -\frac{1}{2}\ -\frac{1}{6}\ -\frac{1}{6}\ -\frac{1}{6}\ -\frac{1}{6}\ -\frac{1}{6}\ -\frac{1}{6})\ (\frac{2}{3}\ -\frac{1}{3}\ \frac{1}{3}\ -\frac{2}{3}\ 0\ 0\ 0\ 0)$
$V_{2,33}$	$(\frac{1}{6}\ -\frac{1}{2}\ \frac{1}{6}\ \frac{1}{6}\ \frac{1}{6}\ \frac{1}{6}\ \frac{1}{6}\ \frac{1}{6})\ (\frac{1}{3}\ \frac{2}{3}\ \frac{2}{3}\ -\frac{1}{3}\ 0\ 0\ 0\ 0)$
$V_{3,11}, V_{3,13}$	$(0\ -\frac{1}{2}\ \frac{1}{2}\ 0\ 0\ 0\ 0\ 0)\ (0\ -1\ 0\ 0\ 0\ 0\ 0\ 0)$
$V_{3,12}, V_{3,14}$	$(\frac{1}{4}\ -\frac{3}{4}\ \frac{1}{4}\ -\frac{1}{4}\ -\frac{1}{4}\ \frac{1}{4}\ \frac{1}{4}\ \frac{1}{4})\ (\frac{1}{2}\ -\frac{1}{2}\ 0\ 0\ 0\ 0\ 0\ 0)$
$V_{3,21}, V_{3,23}$	$(0\ -\frac{1}{2}\ \frac{1}{2}\ 0\ 0\ 0\ 0\ 0)\ (0\ -1\ 0\ 0\ 0\ 0\ 0\ 0)$
$V_{3,22}, V_{3,24}$	$(\frac{1}{4}\ -\frac{3}{4}\ \frac{1}{4}\ -\frac{1}{4}\ -\frac{1}{4}\ \frac{1}{4}\ \frac{1}{4}\ \frac{1}{4})\ (\frac{1}{2}\ -\frac{1}{2}\ 0\ 0\ 0\ 0\ 0\ 0)$
$V_{4,11}, V_{4,31}$	$(\frac{1}{3}\ 0\ -1\ 0\ 0\ 0\ 0\ 0)\ (0\ -\frac{2}{3}\ 0\ 0\ 0\ 0\ 0\ 0)$
$V_{4,12}, V_{4,32}$	$(-\frac{1}{6}\ \frac{1}{2}\ \frac{1}{6}\ \frac{1}{6}\ \frac{1}{6}\ \frac{1}{6}\ \frac{1}{6}\ \frac{1}{6})\ (\frac{1}{3}\ -\frac{2}{3}\ \frac{2}{3}\ -\frac{1}{3}\ 0\ 0\ 0\ 0)$
$V_{4,13}$	$(-\frac{1}{6}\ \frac{1}{2}\ -\frac{1}{6}\ -\frac{1}{6}\ -\frac{1}{6}\ -\frac{1}{6}\ -\frac{1}{6}\ -\frac{1}{6})\ (-\frac{1}{3}\ -\frac{2}{3}\ \frac{1}{3}\ -\frac{2}{3}\ 0\ 0\ 0\ 0)$
$V_{4,33}$	$(\frac{5}{6}\ -\frac{1}{2}\ -\frac{1}{6}\ -\frac{1}{6}\ -\frac{1}{6}\ -\frac{1}{6}\ -\frac{1}{6}\ -\frac{1}{6})\ (-\frac{1}{3}\ \frac{1}{3}\ \frac{1}{3}\ \frac{1}{3}\ 0\ 0\ 0\ 0)$

Table 4.1: Set of 32 line bundle vectors such that they solve the Bianchi identities (4.26) obtained by using resolution (i) for all 12 $\mathbb{C}^3/\mathbb{Z}_{6\text{-II}}$ fixed points.

from R_3. Relaxing the condition $V_{2,\alpha\beta} = -V_{4,\alpha\beta}$ merely allows for adding different $E_8 \times E_8$ vectors to $V_{2,\alpha\beta}$ and $V_{4,\alpha\beta}$. Interestingly, in our solution $V_{2,11}^2 = V_{2,12}^2 = \frac{20}{9}$, which can only be satisfied for $M_L > 0$ in (2.24a), hence these vectors correspond to massive twisted states. Note that the level-matching condition (2.24c) can still be satisfied by choosing an appropriate $SO(8)$ vector q.

It is noteworthy that the solution for the Bianchi identities is by far not unique. The non-uniqueness is two-fold: On the one hand, given a combination of resolutions for the twelve fixed points (in our example resolution (i) twelve times), it is possible to find different combinations of line bundle vectors that satisfy the associated Bianchi identities. Different solutions exhibit different behavior with respect to the unbroken gauge groups and the number of scalars and vector-like exotics in the model. For example, if one adds the $E_8 \times E_8$ lattice vector $(0^3, 1^2, 0^3)(0^8)$ to $V_{1,111}$ and/or to $V_{1,113}$, the particle content of the model is changed with respect to the exotics, yet the new set of vectors still satisfies the Bianchi identities. This can be understood by noting that adding lattice vectors to the orbifold states can take one away from the original model and lead to a brother or grandchild model, cf. section 2.2.3. Furthermore, as we will see in section 5.2, the hypercharge is anomalous and therefore not a good quantum number anymore.

On the other hand, given a set of 32 line bundle vectors, there exist different combinations of local resolutions such that the resulting Bianchi identities are satisfied by this set of vectors.

θ-sector	θ^2-sector	θ^3-sector	θ^4-sector
$V_{1,111} \leftrightarrow \overline{n}_1$	$V_{2,11} \leftrightarrow$ massive	$V_{3,11} \leftrightarrow$ projected out	$V_{4,11} \leftrightarrow s^0_{26}$
$V_{1,112} \leftrightarrow s^-_2$	$V_{2,12} \leftrightarrow$ massive	$V_{3,12} \leftrightarrow s^+_{14}$	$V_{4,12} \leftrightarrow h_7$
$V_{1,113} \leftrightarrow \overline{n}_4$	$V_{2,13} \leftrightarrow \overline{n}_{15}$	$V_{3,13} \leftrightarrow$ projected out	$V_{4,13} \leftrightarrow h_{12}$
$V_{1,114} \leftrightarrow s^-_5$	$V_{2,31} \leftrightarrow h_{20}$	$V_{3,14} \leftrightarrow s^+_{18}$	$V_{4,31} \leftrightarrow s^0_{28}$
$V_{1,121} \leftrightarrow n_4$	$V_{2,32} \leftrightarrow h_{21}$	$V_{3,21} \leftrightarrow$ projected out	$V_{4,32} \leftrightarrow h_9$
$V_{1,122} \leftrightarrow x^-_1$	$V_{2,33} \leftrightarrow h_{25}$	$V_{3,22} \leftrightarrow s^+_{15}$	$V_{4,33} \leftrightarrow n_8$
$V_{1,123} \leftrightarrow n_6$		$V_{3,23} \leftrightarrow$ projected out	
$V_{1,124} \leftrightarrow x^-_2$		$V_{3,24} \leftrightarrow s^+_{19}$	
$V_{1,131} \leftrightarrow w_1$			
$V_{1,132} \leftrightarrow s^-_7$			
$V_{1,133} \leftrightarrow w_2$			
$V_{1,134} \leftrightarrow s^-_{10}$			

Table 4.2: Identification of the orbifold states with the line bundle vectors. The nomenclature of the twisted states is summarized in table 2.2 and taken from [21]. Here "massive" means that the vector corresponds to a massive orbifold state. The vectors tagged with "projected out" are present in the six-dimensional theory but are projected out in four dimensions.

In our case, one could for example use any combination of the five possible triangulations at the fixed points $E_{1,131}$ and $E_{1,133}$. Unfortunately, the meaning of this is not fully understood as it has not yet been worked out what exactly it is that determines the resolution which one can choose to describe the blowup of the orbifold.

As discussed in section 4.4, the axionic states can be identified with twisted states from the orbifold. The spectrum of the orbifold for the chosen model is given in the appendix of [21]. The identifications can be made by comparing the bundle vectors with the weights of the corresponding twisted states (or equivalently by comparing the charges and non-Abelian representations given in the table of [21]). Since the complex scalars in chiral multiplets are composed of two real scalars that are each other's charge conjugates, these identifications are made up to overall signs of the weight vectors. Table 4.2 gives a list of the line bundle vectors and the corresponding orbifold states. In the θ^2-sector, the two vectors $V_{2,11}$ and $V_{2,12}$ that acquire a mass do not have a matching orbifold state in the table of [21]. All other states from this sector can be identified with line bundle vectors. In the θ^3 case this is similar. For $V_{3,2\gamma}$, each line bundle vector can be found in the third twisted sector as well. The four vectors $V_{3,1\gamma}$ are present in the six-dimensional spectrum, but are projected out in four dimensions. The θ^3-sector defines a six-dimensional theory, as the second torus is fixed under its action and consequently the $E_{3,\alpha\gamma}$ fixed points are of complex codimension two. In the θ- and θ^4-sector, there is again an orbifold state for each line bundle vector.

The possibility of identifying orbifold states and line bundle vectors suggests a different approach to solving the Bianchi identities. Namely one starts with a set of 32 line bundle vectors that satisfy the resolution independent Bianchi identities (4.26a) and (4.26b) and scans over possible combinations of triangulations. At first sight this seems hopeless due to the vast amount of physically inequivalent models that can be obtained by combining the five different resolutions (cf. section 3.3.3). However, as stated previously, the twelve Bianchi identities obtained from integrating over $E_{1,1\beta\gamma}$ depend on the local resolution only. This makes it possible to check for each of the twelve $\mathbb{C}^3/\mathbb{Z}_{6\text{-II}}$ fixed points which of the five

resolutions are allowed. One can hope that this leaves a subset small enough to compute the Bianchi identities for all possible combinations of the subset and check whether a combination of resolutions exists such that the associated Bianchi identities are solved by the initially chosen set of line bundle vectors.

4.6 Example: Solving the Bianchi identities for the $\mathbb{Z}_2 \times \mathbb{Z}_2$ orbifold

This section deals with the Bianchi identities for our second model, the $\mathbb{Z}_2 \times \mathbb{Z}_2$ orbifold. As in the previous chapter we start by computing the relations (4.9). The equivalences in terms of the orbifold shift and Wilson lines can be worked out for the three θ-sectors using tables 2.10 - 2.12.

The identification in the θ_1-sector is

$$V_{(\theta_1, l_{\beta\gamma})} \equiv \int_{D_{2,\beta},\ D_{3,\gamma}} \frac{\mathcal{F}}{2\pi}\bigg|_{\beta\gamma} = V_{1,\beta\gamma}. \tag{4.29}$$

The identification of the orbifold shift vector and Wilson lines are

$$\begin{aligned}
V_{1,11} &\equiv V_{sh}^1 &,\quad V_{1,12} &\equiv V_{sh}^1 + W_6,\\
V_{1,13} &\equiv V_{sh}^1 + W_5 &,\quad V_{1,14} &\equiv V_{sh}^1 + W_5 + W_6,\\
V_{1,21} &\equiv V_{sh}^1 + W_4 &,\quad V_{1,22} &\equiv V_{sh}^1 + W_4 + W_6,\\
V_{1,23} &\equiv V_{sh}^1 + W_4 + W_5 &,\quad V_{1,24} &\equiv V_{sh}^1 + W_4 + W_5 + W_6,\\
V_{1,31} &\equiv V_{sh}^1 + W_3 &,\quad V_{1,32} &\equiv V_{sh}^1 + W_3 + W_6,\\
V_{1,33} &\equiv V_{sh}^1 + W_3 + W_5 &,\quad V_{1,34} &\equiv V_{sh}^1 + W_3 + W_5 + W_6,\\
V_{1,41} &\equiv V_{sh}^1 + W_3 + W_4 &,\quad V_{1,42} &\equiv V_{sh}^1 + W_3 + W_4 + W_6,\\
V_{1,43} &\equiv V_{sh}^1 + W_3 + W_4 + W_5 &,\quad V_{1,44} &\equiv V_{sh}^1 + W_3 + W_4 + W_5 + W_6.
\end{aligned} \tag{4.30}$$

The identifications in the θ_2-sector can be worked out analogously and read

$$V_{(\theta_2, l_{\alpha\gamma})} \equiv \int_{D_{1,\alpha},\ D_{3,\gamma}} \frac{\mathcal{F}}{2\pi}\bigg|_{\alpha\gamma} = V_{2,\alpha\gamma}. \tag{4.31}$$

In terms of shift vectors and Wilson lines, we find

$$\begin{aligned}
V_{2,11} &\equiv V_{sh}^2 &,\quad V_{2,12} &\equiv V_{sh}^2 + W_6,\\
V_{2,13} &\equiv V_{sh}^2 + W_5 &,\quad V_{2,14} &\equiv V_{sh}^2 + W_5 + W_6,\\
V_{2,21} &\equiv V_{sh}^2 + W_2 &,\quad V_{2,22} &\equiv V_{sh}^2 + W_2 + W_6,\\
V_{2,23} &\equiv V_{sh}^2 + W_2 + W_5 &,\quad V_{2,24} &\equiv V_{sh}^2 + W_2 + W_5 + W_6,\\
V_{2,31} &\equiv V_{sh}^2 + W_1 &,\quad V_{2,32} &\equiv V_{sh}^2 + W_1 + W_6,\\
V_{2,33} &\equiv V_{sh}^2 + W_1 + W_5 &,\quad V_{2,34} &\equiv V_{sh}^2 + W_1 + W_5 + W_6,\\
V_{2,41} &\equiv V_{sh}^2 + W_1 + W_2 &,\quad V_{2,42} &\equiv V_{sh}^2 + W_1 + W_2 + W_6,\\
V_{2,43} &\equiv V_{sh}^2 + W_1 + W_2 + W_5 &,\quad V_{2,44} &\equiv V_{sh}^2 + W_1 + W_2 + W_5 + W_6.
\end{aligned} \tag{4.32}$$

Finally, we find for the bundle vectors $V_{3,\alpha\beta}$

$$V_{(\theta_1\theta_2, l_{\alpha\beta})} \equiv \int_{D_{1,\alpha},\ D_{2,\beta}} \frac{\mathcal{F}}{2\pi}\bigg|_{\alpha\beta} = V_{3,\alpha\beta}. \tag{4.33}$$

Expressed through the shift vectors and Wilson lines, they read

$$\begin{array}{lll}
V_{3,11} \equiv V_{sh}^1 + V_{sh}^2 & , & V_{3,12} \equiv V_{sh}^1 + V_{sh}^2 + W_4, \\
V_{3,13} \equiv V_{sh}^1 + V_{sh}^2 + W_3 & , & V_{3,14} \equiv V_{sh}^1 + V_{sh}^2 + W_3 + W_4, \\
V_{3,21} \equiv V_{sh}^1 + V_{sh}^2 + W_2 & , & V_{3,22} \equiv V_{sh}^1 + V_{sh}^2 + W_2 + W_4, \\
V_{3,23} \equiv V_{sh}^1 + V_{sh}^2 + W_2 + W_3 & , & V_{3,24} \equiv V_{sh}^1 + V_{sh}^2 + W_2 + W_3 + W_4, \\
V_{3,31} \equiv V_{sh}^1 + V_{sh}^2 + W_1 & , & V_{3,32} \equiv V_{sh}^1 + V_{sh}^2 + W_1 + W_4, \\
V_{3,33} \equiv V_{sh}^1 + V_{sh}^2 + W_1 + W_3 & , & V_{3,34} \equiv V_{sh}^1 + V_{sh}^2 + W_1 + W_3 + W_4, \\
V_{3,41} \equiv V_{sh}^1 + V_{sh}^2 + W_1 + W_2 & , & V_{3,42} \equiv V_{sh}^1 + V_{sh}^2 + W_1 + W_2 + W_4, \\
V_{3,43} \equiv V_{sh}^1 + V_{sh}^2 + W_1 + W_2 + W_3 & , & V_{3,44} \equiv V_{sh}^1 + V_{sh}^2 + W_1 + W_2 + W_3 + W_4.
\end{array} \tag{4.34}$$

Having found the identification, we turn to the calculation of the Bianchi identities. This again means that we have to make a choice for the triangulation of all 64 $\mathbb{Z}_2 \times \mathbb{Z}_2$ fixed points. Unfortunately in this case the ambiguity arising from the possibility of using different triangulations is much larger than in the $\mathbb{Z}_{6-II}$ case. In the latter, we had five different triangulations for 12 fixed points, while in the former we have four different triangulations for 64 fixed points. Unlike the $\mathbb{Z}_{6-II}$ case, however, choosing the symmetric triangulation does not seem to be the best choice, as this triangulation has an intersection of all three E_r at a fixed point. This means that the Bianchi identities resulting from the integration over the E_r will be highly coupled, as no triple intersection number will be zero. In contrast, for one of the unsymmetric resolutions (*i*) to (*iii*), there are always two divisors that do not intersect. Hence, there will never be an inner product of the line bundle vectors belonging to these divisors. At first, none of the three unsymmetric resolutions can be preferred over the others. However, as the model we are investigating has not switched on one Wilson line in the first torus, it is advantageous to choose triangulation (*i*). For this triangulation, no line connects $E_{2,\alpha\gamma}$ and $E_{3,\alpha\beta}$, so the mixed scalar products that occur in the Bianchi identities are of the type $V_{1,\beta\gamma} \cdot V_{2,\alpha\gamma}$ and $V_{1,\beta\gamma} \cdot V_{3,\alpha\beta}$ but not $V_{2,\alpha\gamma} \cdot V_{3,\alpha\beta}$. The trivial Wilson line leads to a degeneracy among the vectors that carry an index α in this torus. Setting degenerate vectors equal again, many of the occurring scalar products become identical and the set of equations simplifies and reduces considerably.

The integrals over the three inherited divisors are of course triangulation-independent again. All other integrals depend in a quite involved way on a combination of triangulations at different fixed points. This has the same reason as in the $\mathbb{Z}_{6-II}$ case: all singularities are of complex codimension two, as there is always one torus fixed under the $\mathbb{Z}_2 \times \mathbb{Z}_2$ action. Thus the index corresponding to this torus is not constrained and a sum over this free index remains in the expansion of $\mathcal{F}$ and $c_2(X)$. So the result depends on the choice of triangulations at the four fixed points in the sum. Carrying out the integration for the three R_i and the 48 E_r, we obtain the following set of equations:

$$\sum_{\beta,\gamma=1}^{4} V_{1,\beta\gamma}^2 = \sum_{\alpha,\gamma=1}^{4} V_{2,\alpha\gamma}^2 = \sum_{\alpha,\gamma=1}^{4} V_{2,\alpha\gamma}^2 \quad = 24 \tag{4.35a}$$

$$\sum_{\alpha=1}^{4} (V_{2,\alpha\gamma}^2 + V_{3,\alpha\beta}^2) \quad = 12 \quad , \quad \beta, \gamma \in \{1,2,3,4\}, \tag{4.35b}$$

$$2V_{2,\alpha\gamma}^2 - V_{2,\alpha\gamma} \cdot \sum_{\beta=1}^{4} V_{1,\beta\gamma} \quad = 2 \quad , \quad \alpha, \gamma \in \{1,2,3,4\}, \tag{4.35c}$$

$$2V_{3,\alpha\beta}^2 - V_{3,\alpha\beta} \cdot \sum_{\gamma=1}^{4} V_{1,\beta\gamma} \quad = 2 \quad , \quad \alpha, \beta \in \{1,2,3,4\}. \tag{4.35d}$$

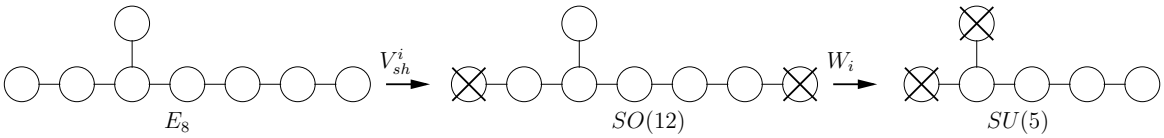

(a) Gauge group breaking to $SU(5)$ in the first E_8.

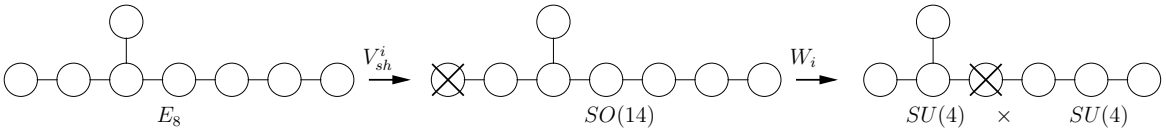

(b) Gauge group breaking to $SU(4) \times SU(4)$ in the second E_8.

Figure 4.3: It is shown how the $E_8 \times E_8$ gauge group is broken via the use of a shift vector and Wilson lines to the $SU(5)$ GUT group and an $SU(4) \times SU(4)$ gauge group in the hidden sector.

The relevant intersection numbers are given in table C.2 in the appendix. In the $\mathbb{Z}_2 \times \mathbb{Z}_2$ case no equation is trivially fulfilled. The three equations listed in (4.35a) result from integration over the three inherited divisors. They again correspond to the Bianchi identities of the K3, as their resolutions all have the topology of $T^4/\mathbb{Z}_2$. The $3 \cdot 16$ equations (4.35b) - (4.35d) come from integrating over $E_{1,\beta\gamma}$, $E_{2,\alpha\gamma}$, and $E_{3,\alpha\beta}$ respectively. In this case, we end up with 51 equations for 48 vectors with 16 unknowns, so altogether there are 768 unknowns, which is even worse than in the $\mathbb{Z}_{6-II}$ case.

In the orbifold model we investigate, the first E_8 is broken to $SU(6)$ by the orbifold shift vectors. The Wilson lines then break this to $SU(5)$. In the hidden sector, the orbifold shift vector breaks to $SO(14)$, which is then broken by the Wilson lines to $SU(4) \times SU(4)$. So the remaining gauge group is $[SU(5)] \times [SU(4) \times SU(4)] \times U(1)^5$. The breaking is schematically shown in figure 4.3.

Again, the system of equations can be simplified considerably. As we want to keep the $SU(5)$ GUT group, the added lattice vectors must have the same entries in components 4-8. The discussion in section 2.4 showed that in order to be able to consistently mod out the freely acting $\mathbb{Z}_{2,\text{free}}$, the Wilson lines in the affected direction must be equal, i.e. $W_2 = W_4 = W_6 := W$. This has consequences for the identifications (4.30) - (4.34). If there occurs a sum of two of these Wilson lines in the identification, it can be set to zero. This is due to the fact that the Wilson lines are of order two, hence $2W \equiv 0$ by adding appropriate $E_8 \times E_8$ lattice vectors, see (2.22). This reduces the number of different vectors by a factor of two. In this way, two line bundle vectors that will be mapped onto each other under the freely acting $\mathbb{Z}_{2,\text{free}}$ are chosen equal:

$$\begin{array}{llll} V_{i,11} = V_{i,22}, & V_{i,12} = V_{i,21}, & V_{i,13} = V_{i,24}, & V_{i,14} = V_{i,23} \\ V_{i,31} = V_{i,42}, & V_{i,32} = V_{i,41}, & V_{i,33} = V_{i,44}, & V_{i,34} = V_{i,43} \end{array} \quad , i \in \{1,2,3\}\,. \tag{4.36}$$

Note that, in contrast to the $\mathbb{Z}_{6-II}$ case, choosing these degenerate vectors to be equal is not optional but a consistency requirement.

There is yet another degeneracy among the line bundle vectors coming from the fact that the Wilson line W_1 is not switched on in the model. This introduces an additional degeneracy for the vectors carrying an index α. This degeneracy can be used to further reduce the number of unknowns and equations by choosing vectors which are the same under this degeneracy to

be equal as well - this is, however, optional.

Furthermore, we again assume that vectors from the same sector all have equal length. By applying all these assumptions, the underlying system of equations is simplified tremendously. Instead of 48 Diophantine equations coupled by scalar products there are only eight left. They read:

$$V_{i,\rho\sigma}^2 = \frac{3}{2}, \quad i \in \{1,2,3\}\,, \ \rho,\sigma \in \{1,2,3,4\}\,, \tag{4.37a}$$

$$(V_{1,11} + V_{1,12} + V_{1,31} + V_{1,32}) \cdot V_{2,11} = 1, \tag{4.37b}$$

$$(V_{1,11} + V_{1,12} + V_{1,31} + V_{1,32}) \cdot V_{2,12} = 1, \tag{4.37c}$$

$$(V_{1,13} + V_{1,14} + V_{1,33} + V_{1,34}) \cdot V_{2,13} = 1, \tag{4.37d}$$

$$(V_{1,13} + V_{1,14} + V_{1,33} + V_{1,34}) \cdot V_{2,14} = 1, \tag{4.37e}$$

$$(V_{1,11} + V_{1,12} + V_{1,13} + V_{1,14}) \cdot V_{3,11} = 1, \tag{4.37f}$$

$$(V_{1,11} + V_{1,12} + V_{1,13} + V_{1,14}) \cdot V_{3,12} = 1, \tag{4.37g}$$

$$(V_{1,31} + V_{1,32} + V_{1,33} + V_{1,34}) \cdot V_{3,13} = 1, \tag{4.37h}$$

$$(V_{1,31} + V_{1,32} + V_{1,33} + V_{1,34}) \cdot V_{3,14} = 1. \tag{4.37i}$$

The equations (4.37a) come from the integral over the inherited divisors (4.35a). The 16 equations (4.35b) are automatically fulfilled if (4.37a) is. The 16 equations (4.35c) coming from integrating over $E_{2,\alpha\gamma}$ reduce to the four equations (4.37b) - (4.37e). Similarly, the 16 equations (4.35c) reduce to the four equations (4.37f) - (4.37i).

It is now quite easy to find a solution to this set of equations. The K3 Bianchi identities fix the absolute value squared of all 48 vectors to 3/2. This is the same result we obtained in the $\mathbb{Z}_{6-II}$ case for the vectors $V_{3,\alpha\gamma}$. This has to be the case, as the θ^3 sector in the $\mathbb{Z}_{6-II}$ acts as $\mathbb{Z}_2$ in torus 1 and 3, leaving torus 2 invariant. So it is no suprise that we recover the same relation. Here again, (4.37a) corresponds to having states with $M_L = 0$ and no oscillator switched on when compared to the mass formula (2.24a).

The equations (4.37) can be solved using a Diophantine equation solver [4]. However, for this orbifold we can choose a different approach. Each orbifold fixed line has at least one state with absolute value squared of 3/2 which is an $SU(5)$ singlet and is not projected out in four dimensions. So one can first calculate all possible states that have these properties for all 48 fixed lines and then randomly choose a gauge background from all these states. In this way, we can produce hundreds of solutions to the Bianchi identities per second. One possible solution is given in table 4.3. In order to be compatible with the $\mathbb{Z}_{2,\text{free}}$ action, the two vectors in each table row have to be chosen equal. In the θ_2- and θ_3-sector, we made use of the additional degeneracy, hence here four vectors are chosen equal. While it is possible to find many solutions with the above procedure, we deliberately chose a solution where four states are projected out in the four-dimensional spectrum. The reason for this is discussed in chapter 7.

Table 4.4 summarizes the identification between twisted orbifold states and line bundle vectors. An overview over the spectrum is given in table 2.3. As it turns out, the states

[4] We used the methods *Reduce* and *FindInstance* of Mathematica.

V_r	expression for the bundle vector V_r
$V_{1,11}, V_{1,22}$	$(-\frac{1}{4}\ \frac{1}{4}\ \frac{1}{4}\ -\frac{1}{4}\ -\frac{1}{4}\ -\frac{1}{4}\ -\frac{1}{4}\ -\frac{1}{4})(\ 0\ 0\ 0\ 0\ 0\ 0\ -1\ 0)$
$V_{1,12}, V_{1,21}$	$(-\frac{1}{2}\ 0\ \frac{1}{2}\ 0\ 0\ 0\ 0\ 0)(-\frac{3}{4}\ \frac{1}{4}\ \frac{1}{4}\ -\frac{1}{4}\ -\frac{1}{4}\ -\frac{1}{4}\ -\frac{1}{4}\ \frac{1}{4})$
$V_{1,13}, V_{1,24}$	$(-\frac{1}{2}\ 0\ \frac{1}{2}\ 0\ 0\ 0\ 0\ 0)(\ \frac{1}{4}\ -\frac{1}{4}\ -\frac{1}{4}\ -\frac{1}{4}\ -\frac{1}{4}\ \frac{1}{4}\ -\frac{3}{4}\ \frac{1}{4})$
$V_{1,14}, V_{1,23}$	$(-\frac{1}{4}\ \frac{1}{4}\ \frac{1}{4}\ -\frac{1}{4}\ -\frac{1}{4}\ -\frac{1}{4}\ -\frac{1}{4}\ -\frac{1}{4})(\ 0\ \frac{1}{2}\ \frac{1}{2}\ 0\ 0\ -\frac{1}{2}\ \frac{1}{2}\ 0)$
$V_{1,31}, V_{1,42}$	$(-\frac{1}{4}\ \frac{1}{4}\ -\frac{3}{4}\ -\frac{1}{4}\ -\frac{1}{4}\ -\frac{1}{4}\ -\frac{1}{4}\ -\frac{1}{4})(-\frac{1}{4}\ \frac{1}{4}\ \frac{1}{4}\ \frac{1}{4}\ \frac{1}{4}\ -\frac{1}{4}\ -\frac{1}{4}\ -\frac{1}{4})$
$V_{1,32}, V_{1,41}$	$(-\frac{1}{2}\ 0\ -\frac{1}{2}\ 0\ 0\ 0\ 0\ 0)(\ 0\ -\frac{1}{2}\ \frac{1}{2}\ 0\ 0\ -\frac{1}{2}\ \frac{1}{2}\ 0)$
$V_{1,33}, V_{1,44}$	$(\ \frac{1}{2}\ -1\ -\frac{1}{2}\ 0\ 0\ 0\ 0\ 0)(\ 0\ 0\ 0\ 0\ 0\ 0\ 0\ 0)$
$V_{1,34}, V_{1,43}$	$(-\frac{1}{4}\ -\frac{3}{4}\ \frac{1}{4}\ -\frac{1}{4}\ -\frac{1}{4}\ -\frac{1}{4}\ -\frac{1}{4}\ -\frac{1}{4})(-\frac{1}{4}\ -\frac{1}{4}\ -\frac{1}{4}\ \frac{1}{4}\ \frac{1}{4}\ \frac{1}{4}\ \frac{1}{4}\ -\frac{1}{4})$
$V_{2,11}, V_{2,22}$ $V_{2,31}, V_{2,42}$	$(\ \frac{1}{4}\ -\frac{1}{4}\ \frac{1}{4}\ -\frac{1}{4}\ -\frac{1}{4}\ -\frac{1}{4}\ -\frac{1}{4}\ -\frac{1}{4})(\ 0\ 0\ 0\ 0\ 0\ 0\ -1\ 0)$
$V_{2,12}, V_{2,21}$ $V_{2,32}, V_{2,41}$	$(\ 0\ \frac{1}{2}\ -\frac{1}{2}\ 0\ 0\ 0\ 0\ 0)(-\frac{1}{4}\ -\frac{1}{4}\ -\frac{1}{4}\ \frac{1}{4}\ \frac{1}{4}\ \frac{1}{4}\ -\frac{3}{4}\ -\frac{1}{4})$
$V_{2,13}, V_{2,24}$ $V_{2,33}, V_{2,44}$	$(\ 0\ -\frac{1}{2}\ \frac{1}{2}\ 0\ 0\ 0\ 0\ 0)(\ \frac{1}{4}\ \frac{3}{4}\ -\frac{1}{4}\ -\frac{1}{4}\ -\frac{1}{4}\ \frac{1}{4}\ \frac{1}{4}\ \frac{1}{4})$
$V_{2,14}, V_{2,23}$ $V_{2,34}, V_{2,43}$	$(\ \frac{1}{4}\ -\frac{1}{4}\ \frac{1}{4}\ -\frac{1}{4}\ -\frac{1}{4}\ -\frac{1}{4}\ -\frac{1}{4}\ -\frac{1}{4})(\ 0\ \frac{1}{2}\ \frac{1}{2}\ 0\ 0\ -\frac{1}{2}\ \frac{1}{2}\ 0)$
$V_{3,11}, V_{3,22}$ $V_{3,31}, V_{3,42}$	$(\ \frac{1}{2}\ \frac{1}{2}\ 1\ 0\ 0\ 0\ 0\ 0)(\ 0\ 0\ 0\ 0\ 0\ 0\ 0\ 0)$
$V_{3,12}, V_{3,21}$ $V_{3,32}, V_{3,41}$	$(-\frac{1}{4}\ -\frac{1}{4}\ \frac{3}{4}\ -\frac{1}{4}\ -\frac{1}{4}\ -\frac{1}{4}\ -\frac{1}{4}\ -\frac{1}{4})(-\frac{1}{4}\ -\frac{1}{4}\ -\frac{1}{4}\ \frac{1}{4}\ \frac{1}{4}\ \frac{1}{4}\ \frac{1}{4}\ -\frac{1}{4})$
$V_{3,13}, V_{3,24}$ $V_{3,33}, V_{3,44}$	$(-\frac{1}{2}\ -\frac{1}{2}\ 0\ 0\ 0\ 0\ 0\ 0)(\ \frac{3}{4}\ \frac{1}{4}\ \frac{1}{4}\ \frac{1}{4}\ \frac{1}{4}\ -\frac{1}{4}\ -\frac{1}{4}\ -\frac{1}{4})$
$V_{3,14}, V_{3,23}$ $V_{3,34}, V_{3,43}$	$(-\frac{1}{4}\ -\frac{1}{4}\ -\frac{1}{4}\ -\frac{1}{4}\ -\frac{1}{4}\ -\frac{1}{4}\ -\frac{1}{4}\ -\frac{1}{4})(-\frac{1}{2}\ 0\ 0\ -\frac{1}{2}\ -\frac{1}{2}\ 0\ 0\ \frac{1}{2})$

Table 4.3: Set of 48 line bundle vectors such that they solve the Bianchi identities (4.35) obtained by using resolution (i) for all 64 $\mathbb{C}^3/\mathbb{Z}_2 \times \mathbb{Z}_2$ fixed points.

which are projected out in four dimensions are the negatives of vectors which survive the projection conditions. In the $\mathbb{Z}_2 \times \mathbb{Z}_2$ case, all orbifold states à priori come together with their negative states, which are indicated with a minus sign in front of them.

We also tried to get a solution by starting from the bundle vectors and choosing a triangulation which produces intersection numbers such that the resulting Bianchi identities are fulfilled. This is, however, much more involved as in the $\mathbb{Z}_{6-II}$ case. There, we had the twelve $\mathbb{Z}_{6-II}$ fixed points, which only depended on the choice of triangulation at one fixed point whereas in the $\mathbb{Z}_2 \times \mathbb{Z}_2$ case, every intersection number depends on the triangulation at four fixed points. When integrating over $E_{1,\beta\gamma}$, the index α is not fixed and hence we need to specify the triangulations at the fixed points $(1\beta\gamma)$, $(2\beta\gamma)$, $(3\beta\gamma)$, and $(4\beta\gamma)$. For the integrals over $E_{2,\alpha\gamma}$, β is unspecified and we need to choose the triangulations at $(\alpha 1\gamma)$, $(\alpha 2\gamma)$, $(\alpha 3\gamma)$, and $(\alpha 4\gamma)$, and for $E_{3,\alpha\beta}$ similarly with γ open. So we can calculate all $4^4 = 256$ possible equations that can arise from integrating over one particular E_r and do this for all 48 divisors, which amounts to computing $48 \cdot 256 = 12288$ integrals. For each divisor, we store all

θ_1-sector	θ_2-sector	θ_3-sector
$V_{1,11} \leftrightarrow T_1^1$	$V_{2,11} \leftrightarrow \overline{T_5^1}$	$V_{3,11} \leftrightarrow S_{31}$
$V_{1,12} \leftrightarrow \overline{T_1^2}$	$V_{2,12} \leftrightarrow -\overline{T_5^1}$	$V_{3,12} \leftrightarrow S_{35}$
$V_{1,13} \leftrightarrow T_2^1$	$V_{2,13} \leftrightarrow \overline{T_6^1}$	$V_{3,13} \leftrightarrow T_9^2$
$V_{1,14} \leftrightarrow \overline{T_2^1}$	$V_{2,14} \leftrightarrow \overline{T_6^1}$	$V_{3,14} \leftrightarrow \overline{T_9^2}$
$V_{1,21} \leftrightarrow \overline{T_3^2}$	$V_{2,21} \leftrightarrow -T_7^1$	$V_{3,21} \leftrightarrow S_{37}$
$V_{1,22} \leftrightarrow T_3^1$	$V_{2,22} \leftrightarrow \overline{T_7^1}$	$V_{3,22} \leftrightarrow S_{40}$
$V_{1,23} \leftrightarrow \overline{T_4^1}$	$V_{2,23} \leftrightarrow \overline{T_8^1}$	$V_{3,23} \leftrightarrow \overline{T_{10}^2}$
$V_{1,24} \leftrightarrow T_4^1$	$V_{2,24} \leftrightarrow T_8^1$	$V_{3,24} \leftrightarrow T_{10}^2$
$V_{1,31} \leftrightarrow S_8$	$V_{2,31} \leftrightarrow T_9^1$	$V_{3,31} \leftrightarrow S_{45}$
$V_{1,32} \leftrightarrow \overline{V_1^1}$	$V_{2,32} \leftrightarrow -\overline{T_9^1}$	$V_{3,32} \leftrightarrow S_{49}$
$V_{1,33} \leftrightarrow S_{13}$	$V_{2,33} \leftrightarrow T_{10}^1$	$V_{3,33} \leftrightarrow T_{11}^2$
$V_{1,34} \leftrightarrow S_{16}$	$V_{2,34} \leftrightarrow \overline{T_{10}^1}$	$V_{3,34} \leftrightarrow \overline{T_{11}^2}$
$V_{1,41} \leftrightarrow \overline{V_2^1}$	$V_{2,41} \leftrightarrow -T_{11}^1$	$V_{3,41} \leftrightarrow S_{51}$
$V_{1,42} \leftrightarrow S_{19}$	$V_{2,42} \leftrightarrow T_{11}^1$	$V_{3,42} \leftrightarrow S_{54}$
$V_{1,43} \leftrightarrow S_{22}$	$V_{2,43} \leftrightarrow \overline{T_{12}^1}$	$V_{3,43} \leftrightarrow \overline{T_{12}^2}$
$V_{1,44} \leftrightarrow S_{26}$	$V_{2,44} \leftrightarrow T_{12}^1$	$V_{3,44} \leftrightarrow T_{12}^2$

Table 4.4: Identification between the orbifold states and the line bundle vectors. The nomenclature of the twisted states is summarized in table 2.3. The 4 vectors in the θ_2-sector with a minus sign are present in the six-dimensional theory but are projected out in four dimensions. The negative of these vectors are present in four dimensions.

possible sets of combinations of triangulations. The complicated part now is to find a set of 64 triangulations that do not contradict any of these 48 sets. While it is extremely complicated to find such a combination, it can be relatively easy to check whether the originally chosen gauge background is a solution to the Bianchi identities for any triangulation at all. For this, one only has to check whether integrating over one E_r forces a special triangulation onto one fixed point, which is forbidden by integrals over other E_r. Let us illustrate this by giving an example. Say from integrating over $E_{1,11}$, we find that all the possible triangulation combinations use only triangulation (i) at the fixed point (111). The fixed point (111) occurs again when integrating over $E_{2,\alpha\gamma}$ in the combination $\{(111), (121), (131), (141)\}$ and when integrating over $E_{3,\alpha\beta}$ in the combination $\{(111), (112), (113), (114)\}$. If now neither of these combinations allows for triangulation (i), then the gauge background is not a solution to any Bianchi identity. Although this is much work, it is still way better than naively computing 4^{64} triangulation combinations. Using this approach, we could show that there are many gauge backgrounds that are inconsistent with the Bianchi identities. Which property exactly causes them to be inconsistent is, however, still under investigation.

Chapter 5

. . . . . .

Spectrum computation

In the last section we discussed how to derive, compute and solve the Bianchi identities. The next question to address is what the particle spectrum of the blowup model is like. The massless spectrum of the matter states can be computed elegantly by using an index theorem which links topological properties of the Calabi-Yau to the zero modes of the Dirac operator [26, 27]. After a brief summary of the necessary group theoretical background, we outline how this procedure works and then do the computation of the spectrum for our two examples. We also look at the anomalies that can arise and compute them explicitly.

5.1 Group theory, the index theorem, and anomalies

The first question to address is the branching of $E_8 \times E_8$ upon compactification, and to find out under which representation the states transform. For this let us first quickly review the most important properties of Lie algebras. A nice introduction to Lie algebras is given in [50]. Many useful details and tables can be found in [51]. The rank of a simple Lie algebra G is the maximum number of simultaneous diagonalizable generators. The total number of linearly independent generators is called the dimension of G. The maximal Abelian subalgebra of a Lie algebra is called the Cartan algebra. It contains the diagonalizable generators H_I. As simultaneously diagonalizable matrices commute, there are as many Cartan generators as the rank of the Lie algebra is. The remaining generators E_α are chosen such that they fulfill

$$\begin{aligned} [H_I, H_J] &= 0 \\ [H_I, E_\alpha] &= \alpha_I E_\alpha \end{aligned} \qquad \text{with } I, J = 1, 2, \ldots, \text{rank}(G),\ \alpha = 1, 2, \ldots, \dim(G) - \text{rank}(G). \quad (5.1)$$

The eigenvalues α_I are structure constants of the algebra. They are combined into a rank(G)-dimensional vector, the root vector. Let $|\lambda_R\rangle$ be the states of a representation R. Then the eigenvalues μ_I of $H_I |\lambda_R\rangle = \mu_I |\lambda_R\rangle$ are called weights of the representation vector, the rank(G)-dimensional vector μ made of these eigenvalues is called weight vector. In the adjoint representation, the states correspond to the generators themselves, $|\lambda_{\text{adj}}\rangle = |E_\alpha\rangle$, which means that the roots are the weights of the adjoint representation. A special choice for the basis of the rank(G)-dimensional root space are the simple roots. The importance of the simple roots is that the length and angle relations among them completely characterize any simple Lie algebra. These relations are conveniently summarized graphically in terms of

Dynkin diagrams. Analogously, one can give the Cartan matrix for the simple roots. The simple roots can also be used to find the irreducible representations. As an example, the root lattice of E_8 was given in (2.19). Its fundamental is equal to its adjoint and the root lattice is even and self-dual. It has rank 8 (hence eight Cartan generators) and dimension 248, where the first part of the direct sum in (2.19) has dimension 112, the second part has dimension $2^8 = 128$ and there are 8 Cartan elements, $112 + 128 + 8 = 248$. This completes our short review of group theory. We have now at hand all we need in order to perform the spectrum computation from a group theoretical point of view.

For the spectrum computation we start with the gaugino anomaly polynomial in ten dimensions and integrate out our six-dimensional internal space. This procedure coincides with computing the Dirac indices on the resolution X using Atiyah-Singer index theorems. The anomaly polynomial for gauginos in 10 dimensions is

$$\begin{aligned} I_{12} = \tfrac{1}{2}\tfrac{1}{(2\pi)^5}\big[-\tfrac{1}{720}\mathrm{tr}(i\mathfrak{F})^6 + \tfrac{1}{24\cdot 48}\mathrm{tr}(i\mathfrak{F})^4\mathrm{tr}\mathfrak{R}^2 - \tfrac{1}{256}\mathrm{tr}(i\mathfrak{F})^2\left(\tfrac{1}{45}\mathrm{tr}\mathfrak{R}^4 + \tfrac{1}{36}(\mathrm{tr}\mathfrak{R}^2)^2\right) \\ + \tfrac{496}{64}\left(\tfrac{1}{2\cdot 2835}\mathrm{tr}\mathfrak{R}^6 + \tfrac{1}{4\cdot 1080}\mathrm{tr}\mathfrak{R}^2\mathrm{tr}\mathfrak{R}^4 + \tfrac{1}{8\cdot 1296}(\mathrm{tr}\mathfrak{R}^2)^3\right)\big]\,. \end{aligned} \tag{5.2}$$

We then expand the ten-dimensional curvature $\mathfrak{R}$ in the six-dimensional curvature $\mathcal{R}$ and the four-dimensional curvature R, $\mathfrak{R} = \mathcal{R} + R$. The same is done for the 10-dimensional gauge field strength $\mathfrak{F}$, $\mathfrak{F} = \mathcal{F} + F$ with $\mathcal{F}$ and F living in six and four dimensions respectively. Next, we integrate out the internal space and compare the result to the anomaly polynomial in four dimensions, which, with the help of trace identities, can be written as [28]

$$\begin{aligned} I_6 = \tfrac{1}{(2\pi)^6}\int_X \Big\{\tfrac{1}{6}\left(\mathrm{tr}[\mathcal{F}'F']\right)^2 + \tfrac{1}{4}\left(\mathrm{tr}\mathcal{F}'^2 - \tfrac{1}{2}\mathrm{tr}\mathcal{R}^2\right)\mathrm{tr}F'^2 \\ - \tfrac{1}{16}\left(\mathrm{tr}\mathcal{F}'^2 - \tfrac{5}{12}\mathrm{tr}\mathcal{R}^2\right)\mathrm{TR}R^2\Big\}\mathrm{tr}[\mathcal{F}'F'] + (' \to ''). \end{aligned} \tag{5.3}$$

F' and F'' are the four-dimensional field strength in the first and the second E_8, so $F = F' + F''$. By comparing the expressions we find for the operator giving the multiplicity of the irreps of the chiral spectrum:

$$N = \int_X \left\{\frac{1}{6}\left(\frac{\mathcal{F}}{2\pi}\right)^3 - \frac{1}{24}\mathrm{tr}\left(\frac{\mathcal{R}}{2\pi}\right)\frac{\mathcal{F}}{2\pi}\right\}. \tag{5.4}$$

As the integral is resolution dependent, so is the multiplicity operator. Due to the fact that X is compact, N should only take integral values. The operator counts the number of generations by acting on the 496 gaugino states. In order to evaluate the expression (5.4) on a gaugino remember that $\mathcal{F}$ contains the line bundle vectors $V_r^I H^I$. Applying H^I to some state of the adjoint representation gives the corresponding weight times that vector: $V_r^I H^I\,|\lambda_R\rangle = (V_r^I \cdot \lambda)\,|\lambda_R\rangle$, with λ being the weight vector (which coincides with the root vector for the adjoint) of the state $|\lambda_R\rangle$. This means we get the number of generations by calculating inner products between line bundle vectors and $E_8 \times E_8$ roots and inserting them into the expression (5.4).

Now that we have all we need to compute the matter spectrum, we can check whether it is anomaly-free. Anomalies are symmetries of the Lagrangian that are present in classical field theories but broken by quantum effects. Anomalies that affect local conservation laws render a theory inconsistent. If it is impossible to conserve the symmetry for a particular

field, a mechanism is needed that cancels the anomalies summed over the contribution from all fields in the theory. As mentioned in section 4.4 there are several types of anomalies: pure non-Abelian anomalies, pure $U(1)$ anomalies, mixed $U(1)$-non-Abelian anomalies, and mixed $U(1)$-gravity anomalies. In four dimensions, they correspond to the triangular anomaly graph given in figure 4.1c with appropriate external legs. The relevant anomalies can be calculated via the expressions

$$\sum_{\mathbf{10}} N\,|\lambda\rangle - \sum_{\overline{\mathbf{5}}} N\,|\lambda\rangle \stackrel{!}{=} 0 \qquad \text{to be pure } SU(5) \text{ anomaly-free,} \tag{5.5a}$$

$$\sum_{\mathbf{3}} N\,|\lambda\rangle + \sum_{\overline{\mathbf{3}}} N\,|\lambda\rangle \stackrel{!}{=} 0 \qquad \text{to be pure } SU(3) \text{ anomaly-free,} \tag{5.5b}$$

$$\sum_{\mathbf{2}} N\,|\lambda\rangle \stackrel{!}{\equiv} 0 \bmod 2 \qquad \text{to be pure } SU(2) \text{ anomaly-free,} \tag{5.5c}$$

$$\sum_{\text{all }\lambda} T^3_{U(1)} N\,|\lambda\rangle \stackrel{!}{=} 0 \qquad \text{to be pure } U(1) \text{ anomaly-free,} \tag{5.5d}$$

$$\sum_{\mathbf{3}} T_{U(1)} N\,|\lambda\rangle \stackrel{!}{=} 0 \qquad \text{to be mixed } U(1) \times \mathrm{SU}(3)^2 \text{ anomaly-free,} \tag{5.5e}$$

$$\sum_{\mathbf{2}} T_{U(1)} N\,|\lambda\rangle \stackrel{!}{=} 0 \qquad \text{to be mixed } U(1) \times \mathrm{SU}(2)^2 \text{ anomaly-free,} \tag{5.5f}$$

$$\sum_{\text{all }\lambda} T_{U(1)} N\,|\lambda\rangle \stackrel{!}{=} 0 \qquad \text{to be mixed } U(1) \times \mathrm{grav}^2 \text{ anomaly-free.} \tag{5.5g}$$

The subscript at the sum indicates the representation from which the $|\lambda\rangle$ are to be taken. As mentioned before, the anomalies (5.5a)-(5.5c) should not occur if the Bianchi identities are fulfilled on all divisors. This can be used as a cross-check that our model is consistent. Even if the equations (5.5d)-(5.5g) are not satisfied, the anomalies can still be canceled by the four-dimensional Green-Schwarz mechanism (the second graph in figure 4.1c), so the model is not inconsistent, but the corresponding $U(1)$ will be broken.
In the two models we will investigate, we define a $U(1)_Y$ hypercharge generator by

$$t_Y = \Big(0,0,0,\frac{1}{2}^2,-\frac{1}{3}^3\Big)\Big(0,0,0^2,0^4\Big). \tag{5.6}$$

The hypercharge is embedded in the $SU(3) \times SU(2)$ of the Standard Model. The standard electric charge generator is given by $t_Q = t_I + t_Y$, where t_I gives the third component of the isospin. There is a relation between the Weinberg angle θ_W and the hypercharge [52], which in our normalization is given by

$$\sin^2\theta_W = \frac{1}{1+2||t_Y||^2}. \tag{5.7}$$

Note that (5.6) is nice from a phenomenological point of view [53], as at the GUT scale $\sin^2\theta_W \stackrel{!}{=} \frac{3}{8}$. This leads to $||t_Y||^2 \stackrel{!}{=} \frac{5}{6}$, which is indeed the case for the operator (5.6). In general, when the hypercharge is not of this form and the Weinberg angle is not $\frac{3}{8}$, gauge coupling unification is lost. Generically, the hypercharge operator has a larger norm [52], which leads to a smaller Weinberg angle in (5.7). Using RGE equations at one-loop level [54]

and assuming one Higgs in the SM and two Higgs in the MSSM, we find that the absolute value of the hypercharge can (in the best case) take values of

$$||t_Y||^2 = \frac{5}{6} \pm 0.12 = 0.83 \pm 0.12, \tag{5.8}$$

assuming SUSY to be broken at 1TeV and putting the cutoff scale at 10^{17}GeV. This roughly allows to add three entries of $\frac{1}{6}$ to the hypercharge operator. So one does not have much options when trying to modify the hypercharge operator such that it is orthogonal to all line bundle vectors.

Once a basis of $U(1)$ generators has been chosen, it can be rotated such that at most one $U(1)$ is anomalous [55]. In order to find such a rotated basis of $U(1)$'s, one starts by calculating all massless orbifold states $|\phi_i\rangle$ that are not projected out. If there are n such $U(1)$ factors, one can in general choose $n-1$ different $U(1)$ generators t_i that are orthogonal to each other and to the simple roots of the non-Abelian gauge group, and that have a vanishing charge trace, $\mathrm{Tr}Q_j \equiv \sum_i t_j |\phi_i\rangle = 0$ (cf. 5.5g). The n^{th} $U(1)$ generator is chosen such that it is orthogonal to all previously found generators. It will not be traceless and it generically mixes the hidden and observable sector. In the cases under investigation, we could choose the standard hypercharge operator (5.6) such that it is orthogonal to the anomalous $U(1)$ and hence is anomaly-free. Note that the anomaly can be canceled by the Green-Schwarz mechanism, but it induces a Fayet-Iliopoulos (FI) term ξ in the D-term of the superpotential (cf. chapter 7). So in order to have a D-flat configuration, some fields that are negatively charged under the anomalous $U(1)$ have to acquire a vev. We now carry out the spectrum computation and the anomaly analysis for the $\mathbb{Z}_{6-II}$ and the $\mathbb{Z}_2 \times \mathbb{Z}_2$ blowup and compare it to the orbifold.

5.2 Example: MSSM spectrum of the $\mathbb{Z}_{6-II}$ blowup

The spectrum of the $\mathbb{Z}_{6-II}$ orbifold model [21] was shown to be MSSM-like, with three net numbers of generations, where vector-like exotics can be decoupled and no triplet states mediating fast proton decay occur. All additional $U(1)$'s are broken in the configuration examined there. However, there are some orbifold fixed points where more than one twisted field acquires a vev and there are fixed points at which no field has a non-vanishing vev (e.g. the fixed point $(1, 112)$ in the θ-sector). So we could not simply choose this configuration, as we need at least one twisted field per fixed point to acquire a vev when we go to full blowup.

Let us compute the spectrum of the solution to the Bianchi identities given in table 4.1. This means we have to evaluate the integral in (5.4). The integral can be performed, as in case of the Bianchi identities, by expanding the gauge background $\mathcal{F}$ (equation (4.8)) and the second Chern class $c_2(X)$ (equation (4.10)) in terms of divisors and then using Poincaré duality to evaluate it in terms of intersection numbers. Using triangulation (i) and the shorthand notation $H_r := V_r^I H^I$, the multiplicity operator can be written as

$$\begin{aligned} N \;=\; & \sum_{\beta=1}^{3}\sum_{\gamma=1}^{4} H_{1,1\beta\gamma}\left[(H_{1,1\beta\gamma})^2 - (H_{2,1\beta})^2 - (H_{3,1\gamma})^2 - (H_{4,1\beta})^2 + H_{2,1\beta}H_{4,1\beta}\right] \\ & + \tfrac{1}{3}\sum_{\beta=1}^{3}\left[4\,(H_{2,1\beta})^3 + 4\,(H_{4,1\beta})^3 - H_{2,1\beta} - H_{4,1\beta} - 3\,(H_{2,1\beta})^2\,H_{4,1\beta}\right] \\ & + \tfrac{1}{3}\sum_{\gamma=1}^{4}\left[4\,(H_{3,1\gamma})^3 - H_{3,1\gamma}\right]. \end{aligned} \tag{5.9}$$

#	irrep	#	irrep
3	$(\mathbf{3},\mathbf{2})_{1/6}$	3	$(\overline{\mathbf{3}},\mathbf{1})_{-2/3}$
5	$(\overline{\mathbf{3}},\mathbf{1})_{1/3}$	2	$(\mathbf{3},\mathbf{1})_{-1/3}$
5	$(\mathbf{1},\mathbf{2})_{-1/2}$	2	$(\mathbf{1},\mathbf{2})_{1/2}$
6	$(\mathbf{1},\mathbf{1})_{1}$	1	$(\mathbf{1},\mathbf{1})_{-1}$
17	$(\mathbf{1},\mathbf{1})_{0}$		

(a) Massless spectrum of the first E_8

#	irrep	#	irrep
4	$(\mathbf{4})+(\overline{\mathbf{4}})$	3	$(\mathbf{6})$
44	$(\mathbf{1})$		

(b) Massless spectrum of the second E_8

Table 5.1: Chiral massless spectrum of the $\mathbb{Z}_{6-II}$ model. The multiplicities are calculated using (5.9). The representations under $SU(3)\times SU(2)$ of the first E_8 and $SU(4)$ of the second E_8 are given in boldface. The subscript denotes the hypercharge.

This is then evaluated for all $240+240$ $E_8\times E_8$ roots $|\lambda\rangle$ by substituting $H_r|\lambda\rangle = V_r\cdot\lambda$ into (5.9), as was explained in the last section. The root vectors $|\lambda\rangle$ are then categorized according to the representation they form under the gauge group of the Standard Model $SU(3)\times SU(2)\times U(1)_Y$ in case of the first E_8 and the gauge group of the hidden sector $SU(4)$ in case of the second E_8. The spectrum is given in tables 5.1a and 5.1b.

A few technical remarks concerning the spectrum are in order. First of all, each of the eigenvalues of N are integer-valued on all $240+240$ states, as it must be for compact manifolds. Looking at the complicated structure of N in (5.9) and at the rational entries that appear in the solution of the Bianchi identities (table 4.1), this is a highly non-trivial observation, as the sum in N contains terms like $\frac{7}{6}\cdot\frac{1}{3}^3 = \frac{7}{162}$. We take this feature as a strong check that the methods we employed in section 3.3 to calculate the intersection numbers are consistent. For the singlet states that do not carry hypercharge, we cannot distinguish between states and their charge conjugates with respect to the Standard Model gauge group, hence we simply add the absolute value of the eigenvalues of the multiplicity operator.

As a next step we calculate the anomalies (5.5). We find that there are no mixed $U(1)$-non-Abelian and no pure non-Abelian anomalies, which we take as a further consistency check, as the latter must be absent when the bundle vectors fulfill the Bianchi identities (the $\mathbf{6}$ of $SU(4)$ is self-conjugate and hence does not contribute to non-Abelian anomalies).

We conclude this section with some more physical remarks concerning the spectrum in tables 5.1a and 5.1b. We read off that there are vector-like exotics for the right-handed down-quarks, the left-handed lepton doublet, and the right-handed electron singlets. By comparing table 5.1 with table 2.2, we see that some massless vector-like exotics have paired up and have acquired a mass, as the numbers of exotics in blowup are less than in the orbifold spectrum. Disregarding the vector-like pairs, the spectrum is identical to that of the Standard Model, except for two additional right-handed electrons $(\mathbf{1},\mathbf{1})_1$. This means that the spectrum has anomalous $U(1)$'s and in particular that the hypercharge is anomalous. Evaluating the pure and mixed hypercharge anomalies (5.5d) and (5.5g) confirms this statement. Also, there is the possibility that the blowup model does not correspond to the orbifold model discussed in [21], but to a grandchild thereof. The fact that the hypercharge is anomalous can be understood on general grounds. This will be discussed in the next chapter. By explicitly

#	irrep	#	irrep
6	$(\mathbf{10})$	12	$(\overline{\mathbf{5}})$
6	$(\mathbf{5})$	70	$(\mathbf{1})$

(a) Massless spectrum of the first E_8

#	irrep	#	irrep
16	$(\mathbf{3},\mathbf{1})$	16	$(\overline{\mathbf{3}},\mathbf{1})$
32	$(\mathbf{1},\mathbf{2})$	80	$(\mathbf{1},\mathbf{1})$

(b) Massless spectrum of the second E_8

Table 5.2: Chiral massless spectrum of the $\mathbb{Z}_2 \times \mathbb{Z}_2$ model. The multiplicities are calculated using (5.10). The representations under $SU(5)$ of the first E_8 and $SU(3) \times SU(2)$ of the second E_8 are given in boldface.

computing the inner product with the hypercharge operator, it is immediately apparent that exactly those line bundle vectors, whose identification contains the Wilson line W_2, are not orthogonal to the hypercharge. This Wilson line is responsible for breaking the $SU(5)$ to the $SU(3) \times SU(2)$ part of the Standard Model gauge group.

5.3 Example: GUT spectrum of the $\mathbb{Z}_2 \times \mathbb{Z}_2$ blowup

In the $\mathbb{Z}_2 \times \mathbb{Z}_2$ case, the orbifold was constructed such that it contains six $\mathbf{10}$'s and six $\overline{\mathbf{5}}$'s. The $\mathbb{Z}_{2,\text{free}}$ element will break the $SU(5)$ to $SU(3) \times SU(2)$ and at the same time reduce the number of states by a factor of two, hence the GUT group should accommodate six Standard Model generations (cf. chapter 1). We start our discussion with calculating the multiplicity operator. Using triangulation (i) everywhere we obtain

$$\begin{aligned} N = & \sum_{\beta,\gamma=1}^{4} H_{1,\beta\gamma} - \tfrac{1}{3}\left[\sum_{\alpha,\gamma=1}^{4}(H_{2,\alpha\gamma} - 4H_{2,\alpha\gamma}^3) + \sum_{\alpha,\beta=1}^{4}(H_{3,\alpha\beta} - 4H_{3,\alpha\beta}^3)\right] \\ & - \sum_{\alpha,\beta,\gamma=1}^{4} H_{1,\beta\gamma}(H_{2,\alpha\gamma}^2 + H_{3,\alpha\gamma}^2). \end{aligned} \tag{5.10}$$

We now let this operator act again on all $E_8 \times E_8$ states grouped by the representation they form under $SU(5)$ in the first E_8 and under $SU(3) \times SU(2)$ in the second E_8. The results are given in table 5.2. Making the same consistency checks as in the example before, we find that the multiplicity is integral for all roots and that there is no $SU(5)$ anomaly (5.5a), as it must be. As the hypercharge is embedded in a canonical way in the $SU(5)$ and all 48 line bundle vectors are $SU(5)$ singlets, the hypercharge is orthogonal to all blowup modes. We see from table 5.2a that there are 6 generations of $\mathbf{10}$ and $12 - 6 = 6$ net generations of $\overline{\mathbf{5}}$. These irreps accommodate six SM generations. By comparing the spectrum from the blowup (table 5.2) with the orbifold spectrum (table 2.3), we see that three $\mathbf{5}$ and $\overline{\mathbf{5}}$ are removed from the massless blowup spectrum by pairing up and becoming massive. This concludes the spectrum analysis for the $\mathbb{Z}_2 \times \mathbb{Z}_2$ model.

Chapter 6

Anomalous hypercharge and the $\mathbb{Z}_{2,\mathbf{FREE}}$

This chapter deals with the problem of the anomalous hypercharge found in section 5.2 for the $\mathbb{Z}_{6-II}$ orbifold. It is investigated how to understand on general grounds why the hypercharge is broken and how the problem can be circumvented by modding out a freely acting $\mathbb{Z}_{2,\text{free}}$ element from the $\mathbb{Z}_2 \times \mathbb{Z}_2$ orbifold. In order to be able to consistently mod out the $\mathbb{Z}_{2,\text{free}}$, we find several consistency requirements arising from the partition function. Among them are the ones already given in section 2.2.2, but we also find a new consistency requirement for the additional Wilson line inducing the GUT breaking to the Standard Model. At the end we give a summary of the spectrum of the $\mathbb{Z}_2 \times \mathbb{Z}_2$ blowup after the $\mathbb{Z}_{2,\text{free}}$ has been modded out.

6.1 Anomalous hypercharge

In equation (5.3), the four-dimensional anomaly polynomial was given. Among other terms we find the four-dimensional gauge field strength in the term $\text{tr}(\mathcal{F}'F')$. In the observable sector, $F' = t_Y F_Y + \ldots$ contains the hypercharge $U(1)$ gauge field F_Y as well as further $SU(2) \times SU(3)$ SM and other Abelian and non-Abelian factors. In order to get a non-anomalous hypercharge in the theory, it is thus necessary for the hypercharge to be orthogonal to all Abelian bundle vectors $\mathcal{F}'$:

$$\text{tr}(\mathcal{F}' t_Y) = E_r V_r' \cdot t_Y \stackrel{!}{=} 0 \quad \forall r. \tag{6.1}$$

This requirement is not satisfied by any of the 223 Mini-Landscape models as a search over all models revealed that each of them has at least one fixed point which is charged under the hypercharge or some other SM gauge field. This is not surprising. The aim of the Mini-Landscape was to get the SM on the orbifold. Hence there must be at least one fixed point which includes a Wilson line that breaks the GUT group to the SM gauge group. This Wilson line cannot be orthogonal to the hypercharge embedded in the $SU(5)$. It is exactly this Wilson line, which must occur in at least one line bundle vector due to the identification (4.9), which generically spoils the orthogonality requirement (6.1). One could try to construct models with the hypercharge not embedded into $SU(5)$, which could allow for a GUT group breaking while still maintaining (6.1). Such models are constructed in [52]. However, in the models which are explicity given, the hypercharge often also lives in the second E_8, which

means that there are hidden sector fields charged under the hypercharge. Additionally, the hypercharge generators violate the condition (5.7), which is needed for the correct Weinberg angle at the GUT scale.

This means that if we want an MSSM in blowup with a conserved hypercharge which allows for the correct Weinberg angle, all our line bundle vectors have to be uncharged under the hypercharge, i.e. they must be $SU(5)$ singlets, yet the SM gauge groups have to emerge. The idea for achieving this is the following: we blow up a model which has an $SU(5)$ GUT spectrum with twice the numbers of generations in blowup. After we have performed the blowup, we mod out a freely acting $\mathbb{Z}_{2,\text{free}}$ element. The action must be free, as we do not want to introduce new fixed points for two reasons: firstly, we would get new curvature singularities in the already smoothened blowup manifold. Secondly, we do not want the Wilson line corresponding to $\mathbb{Z}_{2,\text{free}}$ to appear in the gauge flux. The construction closely resembles the one discussed in [56]. As each twist has fixed points (at least at 0), a free $\mathbb{Z}_{2,\text{free}}$ action on a torus can be achieved by a shift rather than a twist. In our convention, this shift goes in the e_2-, e_4-, and e_6-direction of T^6. As the orbifold fixed points lie at "half height" in the fundamental domain, the shift that is modded out has to be one half of these vectors. This means that the corresponding Wilson line is of order four. In order to break the $SU(5)$ to the $SU(2) \times SU(3)$ of the SM, the value of components 4 and 5 of this Wilson line needs to be different from the value of components 6 to 8. Hence we construct the order 4 Wilson line W as

$$W = \frac{1}{2}(W_2 + W_4 + W_6 + \Lambda_{E_8\times E_8}), \tag{6.2}$$

where $\Lambda_{E_8\times E_8}$ is used to break the GUT group to the non-Abelian SM groups.

6.2 Orbifold consistency requirements on $\mathbb{Z}_{2,\text{free}}$

In this rather technical section we investigate the necessary requirements to be imposed on the orbifold side in order to be allowed to mod out the $\mathbb{Z}_{2,\text{free}}$ element. To get these requirements, we have to look at the string partition functions. Let us denote the constructing elements of the two $\mathbb{Z}_2$ twists by g_1 and g_2 respectively. To shorten the notation, we define $g_3 = g_1 g_2$. Remember that g_i leaves the i^{th} torus invariant. Furthermore, let h denote the action of $\mathbb{Z}_{2,\text{free}}$. The torus lattice is taken in the directions 1 and $\tau_{\text{Orbi}} = i$. The other conventions we are using have already been introduced in section 2.2.3 and in the appendix in B. The boundary conditions for the bosonic and fermionic left- and right-movers are

$$\begin{aligned}
X^i(z+1) &= e^{-2\pi i(p_1\varphi_1+p_2\varphi_2)}X^i(z) - 2\pi[4(m_i+in_i)+2(a_i+ib_i)+ic],\\
X^i(z-\tau) &= e^{-2\pi i(\overline{p}_1\varphi_1+\overline{p}_2\varphi_2)}X^i(z) - 2\pi[4(\overline{m}_i+i\overline{n}_i)+2(\overline{a}_i+i\overline{b}_i)+i\overline{c}],\\
\psi^i\,(z+1) &= e^{2\pi i(p_1\varphi_1+p_2\varphi_2+\frac{s}{2})}\psi^i(z),\\
\psi^i\,(z-\tau) &= e^{2\pi i(\overline{p}_1\varphi_1+\overline{p}_2\varphi_2+\frac{\overline{s}}{2})}\psi^i(z)\\
\lambda^I_a\,(z+1) &= e^{2\pi i(\frac{s_a}{2}+p_1V_1+p_2V_2+a_iW_{2i-1}+b_iW_{2i}+cW)}\lambda^I_a(z),\\
\lambda^I_a\,(z-\tau) &= e^{2\pi i(\frac{\overline{s}_a}{2}+\overline{p}_1V_1+\overline{p}_2V_2+\overline{a}_iW_{2i-1}+\overline{b}_iW_{2i}+\overline{c}W)}\lambda^I_a(z),
\end{aligned} \tag{6.3}$$

where $p_1, \overline{p}_1, p_2, \overline{p}_2, a_i, \overline{a}_i, b_i, \overline{b}_i, c, \overline{c} \in \{0,1\}$, $m_i, \overline{m}_i, n_i, \overline{n}_i \in \mathbb{Z}$, and $i \in \{1,2,3\}$. The fermionic partition functions are given in equation (2.28). In the $\mathbb{Z}_2 \times \mathbb{Z}_2$ case, the local

orbifold shifts and twists read

$$\begin{aligned} V_g^{(a)} &:= p_1 V_1^{(a)} + p_2 V_2^{(a)} + a_i W_{2i-1}^{(a)} + b_i W_{2i}^{(a)} + c W^{(a)}, \quad a \in \{1,2\}, && \text{(6.4a)} \\ \Phi_g &:= p_1 \varphi_1 + p_2 \varphi_2. && \text{(6.4b)} \end{aligned}$$

The partition function for the bosons is more involved, as we need to distinguish three different cases depending on whether the θ_i act trivially (untwisted sector) or not (twisted sector). In the untwisted sector there is no orbifold action, $\theta_1 = \theta_2 = \mathbb{1}$. Hence all three tori are fixed and the theory has 10 smooth dimensions with a 6-dimensional torus lattice. If we consider the action of one θ_i, the i^{th} torus is fixed. Hence we have a 2-dimensional torus lattice, so the theory has 6 smooth and 4 orbifolded dimensions. Under the action of two distinct θ_i, no torus is fixed and we are left with a smooth 4-dimensional theory.
In the six- and four-dimensional case, we need $c = \overline{c} = 0$ as the boundary conditions of θ_{free} (which generates the $\mathbb{Z}_{2,\text{free}}$ translation) and θ_i do not commute. Let us define

$$\begin{aligned} Z_0 &:= \tfrac{1}{\sqrt{\tau_2}} \tfrac{1}{|\eta(\tau)|^2}, \\ Z_X\left[\begin{smallmatrix} \alpha \\ \overline{\alpha} \end{smallmatrix}\right] &:= Z_0 \sum_{m,\overline{m}} e^{-\frac{2\pi}{2\alpha' \tau_2} |(4\overline{m}+\overline{\alpha}) - (4m+\alpha)(\tau_1 + i\tau_2)|^2}. \end{aligned} \qquad (6.5)$$

Here X is a real boson and Z_0 gives the bosonic zero mode partition function without the (divergent) volume factor. The partition functions for the three sectors can then be written as

$$Z_X^{10D} = Z_0^2 \prod_{i=1}^{3} Z_X\left[\begin{smallmatrix} 2a_i \\ 2\overline{a}_i \end{smallmatrix}\right] Z_X\left[\begin{smallmatrix} 2b_i + c \\ 2\overline{b}_i + \overline{c} \end{smallmatrix}\right], \qquad (6.6a)$$

$$Z_X^{6D} = Z_0^2 Z_X\left[\begin{smallmatrix} 2a_i \\ 2\overline{a}_i \end{smallmatrix}\right] Z_X\left[\begin{smallmatrix} 2b_i \\ 2\overline{b}_i \end{smallmatrix}\right] \left(\left| \eta(\tau) \theta\left[\begin{smallmatrix} \frac{1-p_i}{2} \\ \frac{1-\overline{p}}{2} \end{smallmatrix}\right]^{-1} \right|^2 \right)^2, \qquad (6.6b)$$

$$Z_X^{4D} = Z_0^2 \prod_{i=1}^{3} \left| \eta(\tau) \theta\left[\begin{smallmatrix} \frac{1-p_i}{2} \\ \frac{1-\overline{p}_i}{2} \end{smallmatrix}\right]^{-1} \right|^2, \text{ with } p_3 := (p_1 + p_2) \bmod 2. \qquad (6.6c)$$

The complete partition function is then given by

$$Z = \sum_{\text{sectors}} Z_\psi Z_X Z_{\lambda_1} Z_{\lambda_2}, \qquad (6.7)$$

where the sum runs over the 10D, the 6D, and the 4D sector of the theory.

Let us now investigate modular invariance. Using (B.4e) and (B.5a) twice, we find

$$\begin{aligned} \theta\left[\begin{smallmatrix} \alpha \\ \overline{\alpha} \end{smallmatrix}\right](\tau+2)\, \eta^{-d}(\tau+2) &= e^{-2\pi i \alpha(\alpha+1)} e^{-2\pi i \frac{2d}{24}} \theta\left[\begin{smallmatrix} \alpha \\ \overline{\alpha} + 2\alpha + 1 \end{smallmatrix}\right](\tau)\, \eta^{-d}(\tau) \\ &= e^{-2\pi i (\alpha^2 + \frac{d}{12})} \theta\left[\begin{smallmatrix} \alpha \\ \overline{\alpha} + 2\alpha \end{smallmatrix}\right](\tau)\, \eta^{-d}(\tau). \end{aligned} \qquad (6.8)$$

This can only be modular invariant if α contains at most order 2 elements. As $\mathbb{Z}_{2,\text{free}}$ is an order 4 element, the partition function returns to itself up to phases only for $\tau \to \tau + 4$ if

$c \neq 0$. Applying (6.8) to the fermionic partition functions (2.28), we get

$$Z_{\lambda_a}(\tau+2) = e^{-2\pi i(V_g^2+\frac{8}{12})} Z_{\lambda_a}(\tau), \tag{6.9a}$$

$$Z_{\psi}(\tau+2) = e^{-2\pi i(\Phi^2+\frac{4}{12})} Z_{\psi}(\tau). \tag{6.9b}$$

Equation (6.9a) follows as our model given in (2.40) is constructed such that

$$e_8 V_1 \equiv e_8 V_2 \equiv e_8 W_i \equiv 2 e_8 W \equiv (1-s_a)/2 e_8^2 \equiv 0 \text{ mod } 1. \tag{6.10}$$

In (6.9a), we used that

$$e_4 \varphi_1 \equiv e_4 \varphi_2 \equiv (1-s)/2 e_4^2 \equiv 0 \text{ mod } 1. \tag{6.11}$$

As Z_X only depends on the absolute value of $\eta(\tau)$, the phases introduced by (B.5a) do not contribute and the bosonic partition function is modular invariant.

Now we can give the constraints on the complete partition function Z to be modular invariant. As explained above, for $\tau \to \tau + 2$, the whole partition function Z can only be invariant if $c = 0$, which corresponds to the 4D and 6D sector. Requiring that the phase is trivial, we get from substituting (6.9) into (6.7):

$$(p_1 V_1 + p_2 V_2 + a_i W_{2i-1} + b_i W_i)_a^2 \equiv (p_1 \varphi_1 + p_2 \varphi_2)^2, \tag{6.12}$$

where the equivalence is up to integers. By inserting values for p_i, a_i, and b_i, one recovers the modular invariances that have to be imposed on the orbifold theory as given in (2.23). However, in the $10D$ sector, $c \neq 0$ is possible. As in this sector $p_1 = p_2 = 0$, we find for $\tau \to \tau + 4$ the condition

$$2(a_i W_{2i-1} + b_i W_{2i} + cW)^2 \equiv 0 \text{ mod } 1. \tag{6.13}$$

This stringy result was not discussed by the authors of [12]. They construct an MSSM model by starting with an elliptically fibered Calabi-Yau manifold, from which they divide out a freely acting $\mathbb{Z}_3 \times \mathbb{Z}_3$ group. As we start in the blowup model construction from the orbifold perspective, we have to impose (6.13). Starting directly with a CY manifold in the SUGRA regime, it is not clear why one should impose this constraint. As the action is free, the Bianchi identities, which are the central consistency requirement of the CY manifold, are not modified. So it would be very interesting to investigate how the above derived orbifold consistency requirement can be understood when we start with a CY manifold and consider the blow down regime. This is, however, beyond the scope of this thesis.

6.3 MSSM Spectrum of the $(\mathbb{Z}_2 \times \mathbb{Z}_2) \times \mathbb{Z}_{2,\text{free}}$ orbifold

As explained before, the shift of $\mathbb{Z}_{2,\text{free}}$ leads to an identification of two fixed points, as given in (4.36). As the corresponding line bundle vectors are chosen equal, table 4.3 still holds, except that the two vectors in each row are now identical, which leads to a reduction of generations by a factor of two in table 5.2. Hence we get out the SM particle content with 3 net numbers of quarks and leptons, while the hypercharge is still conserved.

Chapter 7

The Donaldson-Uhlenbeck-Yau equations

In this chapter, we look at the integrated version of the hermitian Yang-Mills equations, the so-called Donaldson-Uhlenbeck-Yau (DUY) equations. They are necessary conditions for supersymmetry, which makes them feasible from a phenomenological point of view. We will see that the DUY equations are closely related to the volumes of the exceptional divisors which we used to smoothen the singular orbifold space. Here, we again make contact to the unprojected dual graphs introduced in section 3.1, which we used to visualize the dual toric graphs. We start this chapter with a short review of the details of supersymmetry that are needed in the subsequent discussion. We then discuss a method to find D-flat directions on the orbifold and compare it to the DUY equations and the line bundle language. At the end, we apply the methods to the $\mathbb{Z}_2 \times \mathbb{Z}_2$ orbifold.

7.1 Introduction

For SUSY calculations it is very convenient to introduce superspace. In superspace, the usual "bosonic" space-time coordinates x^μ are augmented with two "fermionic" Grassmann variables $(\theta^\alpha, \overline{\theta}^{\dot{\alpha}})$ which are two-component spinors. The supercharges Q also include operators in θ and $\overline{\theta}$. It is convenient to define the supercovariant derivatives, which are covariant under SUSY,

$$D_\alpha := \partial_\alpha + i(\sigma^m)_{\alpha\dot{\alpha}}\overline{\theta}^{\dot{\alpha}}\partial_m, \quad \overline{D}_{\dot{\alpha}} := -\overline{\partial}_{\dot{\alpha}} - i(\sigma^m)_{\alpha\dot{\alpha}}\theta^\alpha\partial_m, \tag{7.1}$$

where the σ^m are the Pauli matrices. We can use superspace to define superfields Ψ as functions of spacetime and the new coordinates, $\Psi = \Psi(x^\mu, \theta, \overline{\theta})$. They are taken such that they transform under SUSY variations as

$$\delta_\epsilon \Psi = (\epsilon^\alpha Q_\alpha + \overline{\epsilon}_{\dot{\alpha}}\overline{Q}^{\dot{\alpha}})\Psi. \tag{7.2}$$

It turns out that products, sums, and supercovariant derivatives of superfields are again superfields. Furthermore, for any superfield Ψ, the action $S := \int d^4x d^2\theta d^2\overline{\theta}\ \Psi$ is SUSY invariant, as the SUSY transformations are either total derivatives in the Grassmann or in the spacetime variables.
The most general superfield is not an irreducible SUSY representation. To obtain such a

representation, we impose the constraints giving chiral and vector superfields respectively.

The first constraint, which leads to chiral superfields Φ, is $\overline{D}_{\dot{\alpha}}\Phi = 0$. To study the particle content, we expand the superfield in the Grassmann coordinates. The components of a chiral superfield are

$$\Phi(y) = \phi(y) + \sqrt{2}\theta^{\alpha}\psi_{\alpha}(y) + \theta^{\alpha}\theta^{\beta}\epsilon_{\alpha\beta}\mathrm{F}(y), \tag{7.3}$$

with $y := x + i\theta\sigma\overline{\sigma}$. We find the bosonic spin zero scalar fields ϕ and F, and a fermionic spin $\frac{1}{2}$ field ψ. There seems to be a mismatch in the fermionic and bosonic degrees of freedom. However, F turns out to be an auxiliary field (i.e. a field with a purely algebraic equation of motion) and can hence be integrated out in the action. Furthermore, its SUSY variation is a total derivative.

Suppose we have n chiral superfields Φ^i, $\overline{\Phi}^{\bar{i}}$. We can build a SUSY invariant action by taking an arbitrary real function $K(\Phi, \overline{\Phi})$ of these superfields, where K is the Kähler potential. To find another possible term in the action, we define the chiral space as the superspace which satisfies the chirality constraint. Its superspace integrals will only involve $d^2\theta$ but not $d^2\overline{\theta}$. As the sum of two chiral superfields is again a chiral superfield, we can construct a further SUSY invariant action as a functional of a holomorphic function $W = W(\Phi^a)$ in the chiral superfields. The function W is called superpotential. Thus for chiral superfields the most general action is

$$S_C = \int d^4x d^2\theta d^2\overline{\theta}\ [K(\Phi^i, \overline{\Phi}^{\bar{i}})] + \int d^4x d^2\theta\ [W(\Phi) + h.c.]. \tag{7.4}$$

The second constraint, which leads to vector superfields V, is that the superfield is real. This does, however, not lead to an irreducible representation, as V can still contain chiral superfields Λ. They give rise to super gauge transformations $V \to V + \Lambda + \overline{\Lambda}$ (in the Abelian case). We can use these gauge transformations to set the lowest components in the expansion of V to zero. This partial gauge fixing is called Wess-Zumino gauge, which leads to the following component expansion of V:

$$V = -\theta\sigma_{\mu}\overline{\theta}\, A^{\mu}(x) + i\theta\,\theta\,\overline{\theta}\,\overline{\lambda}(x) - i\overline{\theta}\,\overline{\theta}\,\theta\,\lambda(x) + \frac{1}{2}\theta\,\theta\,\overline{\theta}\,\overline{\theta}\,\mathrm{D}(x). \tag{7.5}$$

Here, A^{μ} is a vector field, λ is a Weyl spinor and D is a real scalar. Like the F-field in the chiral case, the D-field also transforms into a total derivative under a SUSY transformation and it is also an auxiliary field. For the discussion of SUSY gauge theories, it is convenient to introduce the super field strength $\mathcal{W}$, which is chiral and invariant under super gauge transformations, $\mathcal{W} := -\frac{1}{4}\overline{D}^2 D_{\alpha}V$. By introducing the gauge invariant, holomorphic gauge kinetic function of the chiral multiplets $f(\Phi)$, we can give a super gauge invariant action which respects SUSY,

$$S_f = \frac{1}{4}\int d^4x d^2\theta\ f(\Phi)\mathcal{W}^{\alpha}\mathcal{W}_{\alpha} + h.c. \tag{7.6}$$

A further SUSY and super gauge invariant action is the Fayet-Iliopoulos action

$$S_{FI} = \int d^4x d^2\theta d^2\overline{\theta}\ 2\xi V = \int d^4x\ \xi\mathrm{D}. \tag{7.7}$$

As stated before, the equations of motion for the D- and F-term are purely algebraic. They are found to be

$$\mathrm{D}_a^{\text{Abelian}} = -g\sum_i Q_i^a|\phi_i|^2 + \xi, \tag{7.8a}$$

$$\mathrm{D}_a^{\text{Non-Abelian}} = -g\sum_c\sum_i \phi_i^* T_c \phi_i, \tag{7.8b}$$

$$\mathrm{F}_i = \left(\frac{\partial W(\phi_i)}{\partial \phi_i}\right)^*, \tag{7.8c}$$

where a labels the different charges in the theory, the ϕ_i are the scalar components of the supermultiplets Φ, and the T_c are the non-Abelian group generators. If one or more of these equations of motion do not hold, supersymmetry is violated.

7.2 D-flatness and the DUY equations

There is a very useful technique to construct D-flat directions on the orbifold [55, 57], which is briefly reviewed here. We start with discussing the non-anomalous Abelian D-flatness constraints. In this case the FI term ξ does not appear in (7.8a). Hence to get a flat direction in the D-term potential, the right hand side of (7.8a) has to vanish. In the presence of an anomalous $U(1)$, the vevs of the fields have to be such that they cancel the FI-term induced by the Green-Schwarz anomaly cancelation mechanism. As explained in section 5.1, we can always choose a basis of $U(1)$ generators on the orbifold such that at most one $U(1)$ is anomalous .
In order to search for D-flat directions, it is advantageous to introduce the notion of a holomorphic invariant monomial (HIM)[1]. A HIM is defined as a product of chiral multiplets

$$P := \prod_i \Phi_i^{n_i}. \tag{7.9}$$

Requiring that the HIM be $U(1)_a$ gauge invariant leads to $\sum_i n_i Q_i^{(a)} = 0$. Let us now take $|\phi_i|^2 = n_i|\psi|^2$ for some arbitrary $|\psi|$. Substituting this into (7.8a) gives

$$\mathrm{D}_a = \sum_i Q_i^{(a)} n_i |\psi|^2 = 0, \tag{7.10}$$

i.e. D-flatness is automatically fulfilled for this choice if the HIM is gauge invariant for non-anomalous $U(1)$'s. From the above equation it is apparent that the exponents of the supermultiplets in the HIM correspond to the relative size of the vevs of the fields. In the case of P being the product of two HIM's, $P = [\prod_i \Phi_i^{n_i}][\prod_j \Phi_j^{m_j}]$, the vevs can be chosen to be $|\phi_i|^2 = n_i|\psi_1|^2 + m_i|\psi_2|^2$ where both ψ_1 and ψ_2 are arbitrary. This corresponds to a multidimensional flat direction. With appropriate rescaling, the n_i can always be made integer-valued. Holomorphicity requires them to be non-negative. If one n_i is zero, the corresponding field does not appear in the HIM. If a field appears in no HIM at all, giving a vev to this field always spoils D-flatness.

[1] This invariant monomial has to be distinguished from the orbifold invariant monomials u_i introduced in chapter 3, which are invariant under the orbifold action.

As for a supersymmetric solution equation (7.8a) has to vanish for all a, it is convenient to define the charge matrix $\mathbf{Q} = (Q_i^{(a)})$ containing all $U(1)$ charges of all fields ϕ. Combining the n_i to a vector n, the configuration is automatically gauge invariant and D-flat if $\mathbf{Q}\cdot n = 0$. Hence the task of finding a gauge invariant D-flat solution is reduced to finding the kernel of the charge matrix. Having found the kernel, we have to construct non-negative integer-valued vectors n in this space. These will specify the HIMs and thus the relation among the vevs of the fields.

The only thing that changes for the anomalous $U(1)$ is that the D-flatness condition reads $\sum_i n_i Q_i^{(A)}|\psi|^2+\xi$ where ξ is the value of the FI term. This means that in this case $\sum_i n_i Q_i^{(A)}$ has to be chosen such that the sign is opposite to the one of the FI term. The discussion of the non-Abelian D-flatness constraints is analogous to the Abelian case. The HIM will be gauge invariant with respect to the non-Abelian gauge groups if $n_i\lambda_k\cdot\phi_i = 0$ for all k and i where λ_k are the simple roots of these groups.

Let us now look at the D-term conditions of the DUY equations. Without taking loop corrections into consideration, they simply read

$$\int_X J\wedge J\wedge\mathcal{F} = \int_X J\wedge J\wedge E_r V_r^I H^I = 0. \tag{7.11}$$

These are 16 equations involving the components of the line bundle vectors V_r^I. They correspond to the second part of the HYM equations, given in (2.5). The correspondence can be established by decomposing the ten-dimensional YM action to four dimensions. In the decomposition, we find the structure of $\mathcal{N}=1$ SUSY D- and F-terms [58–60]. The equation of motion derived from this action reads for an Abelian field strength

$$\mathrm{D} = i\mathcal{F}_{i\bar{i}}G^{i\bar{i}}. \tag{7.12}$$

Using (2.10), we can rephrase the DUY equations (7.11) in terms of the volumes of the exceptional divisors as $\mathrm{vol}(E_r)V_r = 0$. In the Cartan basis we can rewrite this as

$$\mathrm{vol}(E_r)Q_r^{(a)} = 0, \tag{7.13}$$

where the $Q_r^{(a)}$ are the charges of the V_r. By comparing the resulting set of equations (7.13) to the D-flatness constraints (7.10), we see that the volumes of the exceptional divisors are the exponents n_i and thus the relative size of the vevs of the orbifold fields. Note however that this does not work for the anomalous $U(1)$. In the orbifold case, we found that the n_i have to be chosen such that they cancel the FI term, while the DUY equations dictate a zero right hand side for all $U(1)$'s. The solution to this is that the DUY receive loop corrections [28, 47]. Equation (7.11) is only valid in the limit of vanishing string coupling. The one-loop corrected version of this equation reads

$$\frac{1}{2}\int_X J\wedge J\wedge\frac{\mathcal{F}}{2\pi} = \frac{e^{2\phi}}{16\pi}\int_X\frac{1}{(2\pi)^3}\left[\left(\mathrm{tr}\mathcal{F}'^2-\frac{1}{2}\mathrm{tr}\mathcal{R}^2\right)\mathcal{F}'+\left(\mathrm{tr}\mathcal{F}''^2-\frac{1}{2}\mathrm{tr}\mathcal{R}^2\right)\mathcal{F}''\right]. \tag{7.14}$$

Clearly the right hand side is generically non-zero now. Note that the integrals of (7.14) are triangulation-dependent. Remember that it was the Bianchi identity that told us which triangulation to use for the gauge background $\mathcal{F}$ we chose. This means that we have to solve

the Bianchi identities in order to discuss the DUY equations, as this fixes the triangulation. Also note that in section 4.4 we pointed out that taking the orbifold limit corresponds to taking the volume of the exceptional divisors to $-\infty$ in the algebraic measure, while the n_i have to be positive due to holomorphicity. How this can be understood is still under investigation. In the blowup case, there can be several anomalous $U(1)$'s, which are canceled by the axions found in section (4.4), while on the orbifold there is at most one anomalous $U(1)$ canceled by the universal axion. Hence in order to analyze the D-flatness in the presence of anomalous $U(1)$'s and to compare it to the orbifold, it would be interesting to extract the universal axion from equation (7.14). This is however beyond the scope of this thesis.

Interestingly, there is a remarkable connection between the volumes as derived from the unprojected dual graph procedure and the volumes as they can be calculated using (2.10). It turns out that the d_i and t_r parameterizing the position of the planes in the unprojected dual graphs are linked to the Kähler moduli as defined in (4.15) and thus to the volume of curves and divisors. Remember from the discussion in chapter 3 that changing these parameters allows to switch between the different triangulation possibilities. Therefore, the connection could help figuring out which triangulation has to be used at the orbifold fixed points during the resolution procedure. However, as this discussion is intrinsically model-dependent, we will not give a general discussion but rather illustrate this point in the example section for the $\mathbb{Z}_2 \times \mathbb{Z}_2$ orbifold at the end of this chapter[2].

7.3 F-flatness and holomorphicity

The search for F-flat directions on the orbifold is a rather complicated task which requires finding and analyzing the superpotential W. As in the D-flatness case, we can again establish a connection between the HYM equations (2.5) and the F-flatness constraint $F_i = 0$, cf. equation (7.8c). The equations of motion, taken from the decomposition [60], in this case read

$$\mathrm{F}_i = \frac{1}{2}\epsilon_{i\,j\,k}\mathcal{F}_{\bar{j}\,\bar{k}}, \quad \mathrm{F}_{\bar{i}} = \frac{1}{2}\epsilon_{\bar{i}\,\bar{j}\,\bar{k}}\mathcal{F}_{j\,k}. \tag{7.15}$$

As the exact form of the superpotential is unknown, the analysis is rather involved. In general, F-flatness can only be checked up to a certain order in the superpotential. One writes down the most generic W in each order and checks whether the vevs of the orbifold fields can be chosen such that the F-terms vanish or cancel. The cancelation analysis is, however, difficult. If there is to be a cancelation between terms of different order in W, the vevs and the coefficients of them are restricted to take certain values that allow for a cancelation. Furthermore, there are holomorphic functions which are non-zero everywhere but have zeros to every order in their power-series expansion, like the ordinary exponential function. So it might seem that there is a cancelation possible while there is not. Thus a sufficient (but not necessary) condition for F-flatness is that at each order the terms vanish independently. As blowing up the singularities corresponds to giving a vev to one twisted state per fixed point or line, each term must involve at least one orbifold state which is not used as a blowup mode and thus has a vanishing vev. Another possibility is to analyze whether the superpotential can be written as some invariant prefactor times an (arbitrary)

[2] The discussion is more involved in the $\mathbb{Z}_{6-II}$ case. It has also been checked qualitatively, but we refrain from giving it here.

holomorphic function in the chiral superfields. If the prefactor can be shown to vanish, then so does the most general superpotential.

On the blowup side, things look a lot different. The gauge flux $\mathcal{F}$ is F-flat by construction. This is true as we expanded $\mathcal{F}$ in divisors, which are $(1,1)$-forms and thus holomorphic. As our blowup model intrinsically satisfies the F-flatness constraints, it is extremely hard to make a connection to the orbifold picture in this case.

7.4 Example: DUY and moduli of the $\mathbb{Z}_2 \times \mathbb{Z}_2$ orbifold

From constructing the HIMs given by equation (7.9), we find that six singlet states do not appear in any HIM. Hence giving them a vev always spoils D-flatness. Interestingly, these six states are the only ones in the orbifold spectrum which are charged under the $U(1)$

$$t_{\text{ub}}=\left(\frac{45}{4},\frac{45}{4},-\frac{45}{4},\frac{27}{4},\frac{27}{4},\frac{27}{4},\frac{27}{4},\frac{27}{4}\right)\left(\frac{45}{4},\frac{45}{4},\frac{45}{4},-\frac{45}{4},-\frac{45}{4},-\frac{45}{4},-\frac{45}{4},\frac{45}{4}\right) \tag{7.16}$$

Hence, if we do not give a vev to them, the $U(1)$ will be unbroken, which is not desirable from a phenomenological point of view. A way out of this problem could be using orbifold states which live in six rather than in four dimensions. In this case, D-flatness has to be checked for the six-dimensional theory, while the methods introduced above apply to four dimensions.

The solution to the Bianchi identities, given in table 4.3, contains all six orbifold states (S_{16}, S_{22}, S_{35}, S_{37}, S_{49}, S_{51} in table 4.4) charged under the above $U(1)$. If we still want to preserve D-flatness and thus supersymmetry, we also have to include fields which live in six dimensions but are projected out in four dimensions. These are precisely the four fields tagged with a minus sign in table 4.4.

To see whether the solution is consistent with the DUY equations, we insert the gauge flux into equation (7.14). By explicitly constructing a solution for the volumes of the exceptional divisors occurring in the resulting set of equations, we could show that all volumes can be chosen positive. This means that the gauge flux is also consistent with the DUY equations, which guarantee that SUSY is unbroken. So we found a model in complete blowup which has a net number of three SM generations, conserves supersymmetry, and the only unbroken $U(1)$ is the hypercharge. Furthermore, the rank of the hidden sector gauge groups is in the right ballpark for SUSY breaking via gaugino condensation at lower energy scales. This finishes the construction of an MSSM-like model on the blowup manifold.

At last we want to demonstrate qualitatively that the Kähler moduli (a_i, b_r) are related to the positions d_i, t_r of the divisor planes in the unprojected dual graphs. Remember that these numbers parameterize the distance of the planes from the origin. The parameters d_i determine the length, width, and depth of the cuboid. The t_k parameterize how far the E_r planes reach into the cuboid, starting from its edges. The larger the t_k, the more is eaten away from the cube edges, cf. figure 3.2. The volume of the relevant curves in terms of the Kähler moduli are calculated using (2.10) and (4.15) with the help of the intersection numbers given in appendix C.2. Self-intersections are omitted as they are not well-defined in the strict sense of an intersection of hypersurfaces (cf. end of section 3.1). With our choice of signs in the Kähler form, it follows from considering all intersections that $a_i, b_r \geq 0$ in order to obtain non-negative volumes for all curves. The result of the qualitative analysis is that changing the value of the Kähler parameters a_i has the same effect on the volume

of the curves as changing the parameter d_i has on the unprojected dual graph. In a similar way, changing the Kähler parameters b_r affects the volumes of the curves in the same way as they are affected by a change of the t_r in the unprojected dual graph. This strongly suggests that these quantities are linked. A similar observation was made in [61]. In the following discussion, we drop for simplicity the Greek indices labeling the fixed points and start with the case of triangulation (i). Due to the symmetry of the orbifold, the discussion for the other asymmetric triangulations follows analogously. Subsequently, we discuss the symmetric triangulation (iv).

As a first check, we observe that the volumes of the curves depend linearly on the Kähler parameter (as it depends linearly on the Kähler form). This is also true for the unprojected dual graphs. There, the "volumes" of the curves, i.e. the lengths of the lines at the intersection of two planes, also depend linearly on the parameters d_i, t_k.

As a next step, we look concretely at the intersection volumes that do not depend on a_i, i.e. the first four rows in table 7.1 for triangulation (i). The relevant graph is given in figure 7.1a. The volume of the curves E_1E_2 and E_1E_3 grows linearly with growing b_2 and b_3 respectively. The same behavior is observed for the dependence of the length of the intersection lines on the parameters t_2 and t_3 in the unprojected dual graph. Note that changing t_1 does not enlarge the length of the intersection line but merely corresponds to a shift of its position. The intersection volume of E_2E_3 is zero for triangulation (i). As long as we are not leaving triangulation (i), this cannot be changed by adjusting any Kähler modulus, as these divisors are simply not connected in the toric diagram. In the unprojected dual graph picture, the intersection is zero as E_1 lies between E_2 and E_3. None of the position parameters t_k can change this and preserve triangulation (i) at the same time.

The most interesting intersection is the curve D_1E_1. Requiring that this curve be positive yields $b_1 > b_2 + b_3$. In the unprojected dual graph picture this is a necessary condition for being in triangulation (i). As soon as $t_1 = t_2 + t_3$, triangulation (i) is lost and we make the transition to another triangulation. The length of the intersection line can be made larger by either making t_1 larger or t_2 or t_3 smaller. The same behavior can be observed for the Kähler moduli b_i.

Next we look at the compact unprojected dual graphs (figure 7.1b). For the curve D_1E_2, a larger d_2 or t_2 leads to a larger intersection line of the D_1E_2-planes. This is true as a large d_2 makes the entire edge of E_2 longer, while a larger t_2 takes away space of the D_1E_1 intersection, which is confirmed by the Kähler parameters. In contrast, enlarging t_1 eats away parts of the divisors D_1 and E_2, rendering the intersection line smaller, which again agrees with the behavior of the volume with the Kähler moduli. An equivalent observation is made for D_1E_3.

For D_2E_1, the intersection can be made larger by positioning the D_1 plane higher, i.e. increasing d_1. Making t_3 larger, the E_3-plane takes away space of the divisors E_1 and D_2, which leads to a smaller intersection curve. When $r_1 = b_3$, the volume of the curve is zero. In the unprojected dual graph, the divisor D_2 is completely eaten away at $d_3 = t_1$. Note that the curves D_2E_2 and D_3E_3 do not exist in this triangulation. Their volumes are zero.

For the symmetric triangulation, the discussion is easier. Let us again start by looking at the a_i independent intersections, which are the first three lines for triangulation (iv). The relevant graph is given in figure 7.2a. The intersection curve E_iE_j is enlarged if either t_i or t_j is made larger. Making t_k $(i \neq j \neq k)$ larger, the E_k-plane takes space from the E_iE_j plane and the intersection line gets smaller. The dependence of the volumes on the b_r exhibits the same dependence. Again, if $t_k = t_i + t_j$, we reach a point where the triangulation changes to

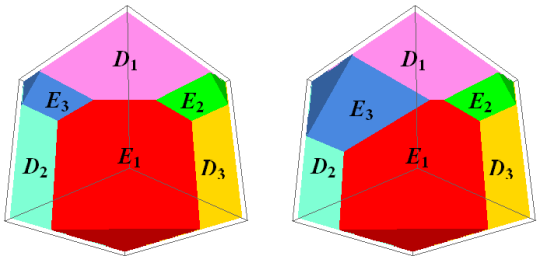

(a) Unprojected dual graphs in the non-compact case. t_3 was increased in the second picture.

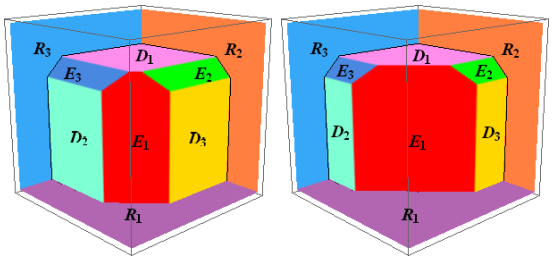

(b) Unprojected dual graphs in the compact case. t_1 was increased in the second picture.

Figure 7.1: Triangulation (i): increasing t_3 makes D_1E_1, D_2E_1 smaller and E_1E_3, D_1E_3 larger. Increasing t_1 makes D_1E_2, D_1E_3, D_2E_3, D_3E_2 smaller and D_1E_1 larger.

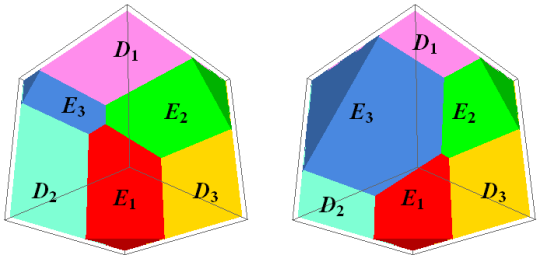

(a) Unprojected dual graphs in the non-compact case. t_3 was increased in the second picture.

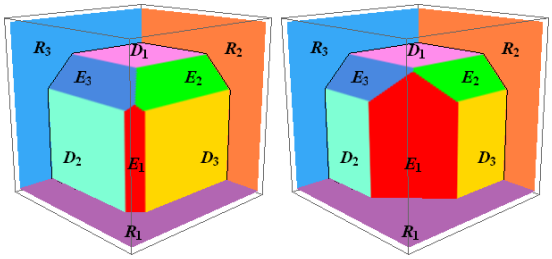

(b) Unprojected dual graphs in the non-compact case. t_1 was increased in the second picture.

Figure 7.2: Triangulation (iv): increasing t_3 makes E_1E_2, D_1E_2, D_2E_1 smaller and E_1E_3,E_2E_3 larger. Increasing t_1 makes E_2E_3, D_2E_3, D_3E_2 smaller and E_1E_2, E_1E_3 larger.

one of the asymmetric ones.

Let us now discuss D_iE_j. The curves D_iE_i do not exist in triangulation (iv) and their volumes are zero. The curve D_iE_j for $i \neq j$ can be made larger by either enlarging d_i or diminishing t_k, in full agreement with the Kähler moduli (cf. figure 7.2b).

There are three further types of intersection curves which are triangulation-independent. The intersection curve R_iE_i can be enlarged by making the E_i plane larger, which corresponds to taking a larger t_i. Note that changing d_i shifts the intersection line but does not change its size. The intersection R_iR_j can be made larger by enlarging the respective cube edge, whose length is given by d_k $(i \neq j \neq k)$. The same is true for the curve R_iD_j, as this curve lies just on the opposite side in the same R_i plane. In this case, however, part of the curve is taken away by the divisor E_i. Thus enlarging t_i reduces the curve length. All three behaviors agree with the ones predicted from the Kähler moduli as given in the lowest three lines of table 7.1.

The volume of the blowup manifold would then correspond to the volume of the cubes. The picture supports the somehow unintuitive result that the overall volume of the CY is diminished when the Kähler moduli b_r are increased. Thus blowing up the singularity of a CY reduces its volume. This qualitative result is confirmed by explicitly calculating the volume in terms of the Kähler moduli using (2.10).

Triangulation / vol$(S_1 S_2)$	(i)	(ii)
$E_{1,\beta\gamma}E_{2,\alpha\gamma}$	$b_{2,\alpha\gamma}$	$b_{1,\beta\gamma}$
$E_{1,\beta\gamma}E_{3,\alpha\beta}$	$b_{3,\alpha\beta}$	0
$E_{2,\alpha\gamma}E_{3,\alpha\beta}$	0	$b_{3,\alpha\beta}$
$D_{1,\alpha}E_{1,\beta\gamma}$	$\frac{1}{2}(b_{1,\beta\gamma} - b_{2,\alpha\gamma} - b_{3,\alpha\beta})$	0
$D_{1,\alpha}E_{2,\alpha\gamma}$	$\frac{1}{2}(a_2 + 4b_{2,\alpha\gamma} - \sum_\beta b_{1,\beta\gamma})$	$\frac{1}{2}(a_2 - \sum_\beta b_{3,\alpha\beta})$
$D_{1,\alpha}E_{3,\alpha\beta}$	$\frac{1}{2}(a_3 + 4b_{3,\alpha\beta} - \sum_\gamma b_{1,\beta\gamma})$	$\frac{1}{2}(a_3 - \sum_\gamma b_{2,\alpha\gamma})$
$D_{2,\beta}E_{1,\beta\gamma}$	$\frac{1}{2}(a_1 - \sum_\alpha b_{3,\alpha\beta})$	$\frac{1}{2}(a_1 + 4b_{1,\beta\gamma} - \sum_\alpha b_{2,\alpha\gamma})$
$D_{2,\beta}E_{2,\alpha\gamma}$	0	$\frac{1}{2}(-b_{1,\beta\gamma} + b_{2,\alpha\gamma} - b_{3,\alpha\beta})$
$D_{2,\beta}E_{3,\alpha\beta}$	$\frac{1}{2}(a_3 - \sum_\gamma b_{1,\beta\gamma})$	$\frac{1}{2}(a_3 + 4b_{3,\alpha\gamma} - \sum_\gamma b_{2,\alpha\gamma})$
$D_{3,\gamma}E_{1,\beta\gamma}$	$\frac{1}{2}(a_1 - \sum_\alpha b_{2,\alpha\gamma})$	$\frac{1}{2}(a_1 - \sum_\alpha b_{2,\alpha\gamma})$
$D_{3,\gamma}E_{2,\alpha\gamma}$	$\frac{1}{2}(a_2 - \sum_\beta b_{1,\beta\gamma})$	$\frac{1}{2}(a_2 - \sum_\beta b_{1,\beta\gamma})$
$D_{3,\gamma}E_{3,\alpha\beta}$	0	0
$R_i E_{i,\rho\sigma}$	$b_{i,\rho\sigma}$	
$R_i D_{j,\rho}$	$\frac{1}{2}(a_k - \sum_\sigma b_{i,\rho\sigma})$ $(i \neq j \neq k)$	
$R_i R_j$	a_k $(i \neq j \neq k)$	

Triangulation / vol$(S_1 S_2)$	(iii)	(iv)
$E_{1,\beta\gamma}E_{2,\alpha\gamma}$	0	$\frac{1}{2}(b_{1,\beta\gamma} + b_{2,\alpha\gamma} - b_{3,\alpha\beta})$
$E_{1,\beta\gamma}E_{3,\alpha\beta}$	$b_{1,\beta\gamma}$	$\frac{1}{2}(b_{1,\beta\gamma} - b_{2,\alpha\gamma} + b_{3,\alpha\beta})$
$E_{2,\alpha\gamma}E_{3,\alpha\beta}$	$b_{2,\alpha\gamma}$	$\frac{1}{2}(-b_{1,\beta\gamma} + b_{2,\alpha\gamma} + b_{3,\alpha\beta})$
$D_{1,\alpha}E_{1,\beta\gamma}$	0	0
$D_{1,\alpha}E_{2,\alpha\gamma}$	$\frac{1}{2}(a_2 - \sum_\beta b_{3,\alpha\beta})$	$\frac{1}{2}(a_2 - \sum_\beta b_{3,\alpha\beta})$
$D_{1,\alpha}E_{3,\alpha\beta}$	$\frac{1}{2}(a_3 - \sum_\gamma b_{2,\alpha\gamma})$	$\frac{1}{2}(a_3 - \sum_\gamma b_{2,\alpha\gamma})$
$D_{2,\beta}E_{1,\beta\gamma}$	$\frac{1}{2}(a_1 - \sum_\alpha b_{3,\alpha\beta})$	$\frac{1}{2}(a_3 - \sum_\alpha b_{3,\alpha\beta})$
$D_{2,\beta}E_{2,\alpha\gamma}$	0	0
$D_{2,\beta}E_{3,\alpha\beta}$	$\frac{1}{2}(a_3 - \sum_\gamma b_{1,\beta\gamma})$	$\frac{1}{2}(a_3 - \sum_\gamma b_{1,\beta\gamma})$
$D_{3,\gamma}E_{1,\beta\gamma}$	$\frac{1}{2}(a_1 + 4b_{1,\beta\gamma} - \sum_\alpha b_{3,\alpha\beta})$	$\frac{1}{2}(a_1 - \sum_\alpha b_{2,\alpha\gamma})$
$D_{3,\gamma}E_{2,\alpha\gamma}$	$\frac{1}{2}(a_2 + 4b_{2,\alpha\gamma} - \sum_\beta b_{3,\alpha\beta})$	$\frac{1}{2}(a_2 - \sum_\beta b_{1,\beta\gamma})$
$D_{3,\gamma}E_{3,\alpha\beta}$	$\frac{1}{2}(-b_{1,\beta\gamma} - b_{2,\alpha\gamma} + b_{3,\alpha\beta})$	0
$R_i E_{i,\rho\sigma}$	$b_{i,\rho\sigma}$	
$R_i D_{j,\rho}$	$\frac{1}{2}(a_k - \sum_\sigma b_{i,\rho\sigma})$ $(i \neq j \neq k)$	
$R_i R_j$	a_k $(i \neq j \neq k)$	

Table 7.1: Volume of curves when using the same triangulation at all $\mathbb{Z}_2 \times \mathbb{Z}_2$ orbifold fixed points.

Chapter 8

. . . . . .

Conclusion

With the dawn of the LHC it is very important to see that string theory can be used to describe and study physics beyond the Standard Model. As many physicists expect the LHC to find supersymmetry, it is important to investigate how supersymmetric extensions of the SM can be described in string theory. For the construction of MSSM-like models, heterotic string theory has proved especially useful. Exact string calculations can be carried out using conformal field theory when the compactification space is chosen to be an orbifold. However, these compactification spaces have curvature singularities. In contrast, Calabi-Yau manifolds are smooth compactification spaces. Unfortunately, their construction is quite involved, and calculations have to be carried out in the low energy regime, which is heterotic supergravity. As the metric of these spaces is unknown, calculations are very difficult and have to rely on topological invariants. For these reasons it is very desirable to have the possibility of changing between the two spaces and to know how certain properties are related. Toric geometry allows us to resolve the orbifold fixed points by assigning a topology to them. Thus we can blow up the orbifold to a CY and at the same time obtain all topological quantities that are needed. We can use them to construct MSSM-like models on the CY manifold and compare them to the underlying orbifold models. This enables us to infer relations between the two models on a more general ground and to better understand the blowup procedure. The aim of this thesis was to construct MSSM-like models by starting with an orbifold and then making the transition to a CY. In the course of this process, we found new and useful relations between the two spaces. Some of them constrain the orbifold models that can be used, while others help us to carry the orbifold analysis over to the CY manifold.

Two of the results in this thesis were derived by studying the string partition function in the orbifold picture. There, exact string calculations can be carried out using conformal field theory. In an explicit calculation, we worked out that the orbifold string partition function is not invariant under the addition of $E_8 \times E_8$ lattice vectors. It was already known that a global change (i.e. the same at all fixed points) of the orbifold shift vector and Wilson lines by lattice vectors leads to so-called brother models, which can have inequivalent spectra although the input is equivalent. By considering local $E_8 \times E_8$ shifts of the input data, we found the localized version of brother models, which we proposed to name grandchildren models. To our knowledge, there has not been made any effort to build orbifolds using this local definition scheme.

Another very interesting result was obtained by studying the modular invariance of the

bosonic and fermionic string partition function. Besides the modular invariance conditions on the orbifold shift vector and Wilson lines that were already given in the literature, we found a requirement for a Wilson line corresponding to a freely acting $\mathbb{Z}_{2,\text{free}}$ element. There are constructions where MSSM-like models are built by modding out a freely acting element directly from a CY manifold [12]. In this case, the CFT calculations are inaccessible and it is not clear why the constraint has to be imposed in this case. However, one would still expect similar constraints to arise.

We investigated the blowup procedure in chapter 3. This well-studied technique was used to smoothen the singularities of the orbifold. The outcome was a smooth CY plus important topological quantities like the intersection numbers. The first step in the blowup procedure was to look at each fixed point separately. We associated an ordinary divisor to each fixed point. In order to blow up the singularity, we had to assign a topology to it. This was done by placing exceptional divisors inside the singularities. One obtains one such divisor per twisted sector in string theory. The exceptional divisors are linked to the ordinary divisors by linear equivalence relations. The relative position of the hypersurfaces corresponding to the divisors on the CY is given by the corresponding toric diagram and its triangulation. The literature describes in detail the construction of two-dimensional graphs dual to the toric diagrams. Remembering that the toric diagram is in fact three-dimensional, we introduced a new way to draw dual graphs in three dimensions, which we called unprojected dual graphs, as the ordinary dual graphs arise from the unprojected dual graphs by a projection.

We showed how to carry out the construction of the unprojected dual graphs in the second step of the blowup procedure, where the different resolutions are glued together. The relative position of all divisors is summarized in the auxiliary polyhedra, which are compact in contrast to the toric diagrams. We extended the construction methods of the unprojected dual graph previously introduced for toric diagrams to the auxiliary polyhedra. This allowed us to find a connection between the unprojected dual graphs, the triangulation and the Kähler moduli, which we worked out qualitatively in chapter 7. Thus the unprojected dual graphs have advantages over the toric diagrams, the dual graphs, and the auxiliary polyhedra, for which we do not know of a way to infer these connections.

We also aimed at gaining a better understanding of the triangulation ambiguity in the blowup procedure as it introduces severe complications in all following discussions. A main problem is that there is a huge number ($\mathcal{O}(10^6)$ for $\mathbb{Z}_{6-II}$ and very roughly $\mathcal{O}(10^{24})$ for $\mathbb{Z}_2 \times \mathbb{Z}_2$) of triangulation possibilities leading to distinct CY manifolds. The topology of these CYs is crucial for several aspects of the blowup theory, like the Bianchi identities. As all these different models have the same orbifold model as blow down limit, scanning one orbifold for a viable model corresponds to scanning a huge number of blowup CYs. While this is advantageous for orbifold model building, it severely complicates finding a consistent model on the CY. Thus having a method which allows to determine the triangulation that has to be used significantly simplifies finding consistent CY models. In the unprojected dual graphs, we found out that the triangulation is determined by the distance parameters d_i, t_k specifying the position of the planes corresponding to the divisors. Changing these parameters results in a change of the volume of the divisors and the intersection curves of two divisors. This means that two originally non-intersecting divisors can intersect by adjusting the size of the involved divisors.

As another beneficial application of the unprojected dual graphs, we illustrated that the volume of the intersection curve of two divisors can be understood qualitatively in the unprojected dual graph picture and vice versa. The volume of the intersection curves can be

calculated in terms of the Kähler moduli a_i, b_r using the intersection numbers. After we obtained the intersection curve volumes in this way, we gave the relevant unprojected toric diagrams, which are defined by the distance parameters d_i, t_k. This allowed us to study the qualitative behavior of the volumes of the intersection curves on the Kähler moduli and on the distance parameters. We found that the volumes in both pictures exhibit the same behavior when we vary a_i in the Kähler form and d_i in the unprojected dual graph. The same observation was made for the pairs b_r and t_r. This strongly suggests that there is a connection between the Kähler moduli and the unprojected dual graph picture.

The fact that there is an anomalous $U(1)$ in the orbifold models made it necessary to analyze the Green-Schwarz anomaly cancelation procedure. From this we found the important result that the twisted orbifold states, which acquire a vev in the blowup procedure, are linked to axionic states on the CY. This explains why there can be at most one anomalous $U(1)$ on the orbifold but several anomalous $U(1)$'s on the CY: the anomalous variation of the axions can be used to cancel the multiple $U(1)$ anomalies on the CY. From this identification we deduced the astonishing result that the Kähler moduli of the exceptional divisors have to be taken to *minus infinity* in the algebraic measure in order to come back to the orbifold picture, in agreement with [32].

In chapter 4 we worked out and solved the central consistency requirement of the blown up theory, namely the Bianchi identities for the three-form field strength H. We could access the computation with the help of the intersection numbers, which allow us to carry out the relevant integrals by virtue of Poincaré duality. We argued that an Abelian gauge flux can be described by line bundle vectors and expanded it in exceptional divisors. Furthermore, we found an identification of the local orbifold shifts and the line bundle vectors up to $E_8 \times E_8$ lattice vectors.

In order to solve the Bianchi identities, we argued that they can be written as a large system of non-linear Diophantine equations. Owing to their complicated structure, we only worked out the details explicitly for the two example orbifolds. In both examples, we started with calculating the line bundle vectors in terms of the orbifold shift vector and Wilson lines. We reviewed how the $E_8 \times E_8$ is broken with the input data of the Mini-Landscape to the SM gauge groups in the observable sector. After this, we integrated the Bianchi identities over the ordinary and exceptional divisors, which form a basis of closed cycles on the CY. In the case of $\mathbb{Z}_{6-II}$, this gave us a set of 24 non-linear, coupled Diophantine equations in 512 unknowns for the 32 line bundle vectors of the gauge flux. By exploiting recurring structures in the equations, we simplified the set of equations until we were able to find a solution. We also gave an alternative approach to solving the Bianchi identities by starting with the orbifold states in the gauge flux and choosing a triangulation that is consistent with this gauge flux.

The same steps were carried out in the $\mathbb{Z}_2 \times \mathbb{Z}_2$ case. There we ended up with 51 Diophantine equations in 768 unknowns. In this case we also relied on the analysis carried out on the orbifold side. By identifying the bundle vectors with twisted orbifold states we could find a consistent solution to all Bianchi identities. The line bundle vectors were chosen such that they are compatible with an additional $\mathbb{Z}_2 \times \mathbb{Z}_2$ symmetry, which we modded out in the i-direction of all three tori simultaneously. This means that two bundle vectors which are identified under the free action were chosen equal.

The simplified version of the Bianchi identity equations was compared to the mass-shell equations in both example cases. We found that some of the simplified Bianchi identities exactly reproduce the equations for a vanishing oscillator number while others predict a

non-vanishing oscillator number. We also gave the identification of the line bundle vectors and the twisted orbifold state. Some of the blowup modes that live on the CY on a blown up complex codimension two fixed point (and thus in six dimensions) were projected out in the four-dimensional orbifold spectrum. In the $\mathbb{Z}_{6-II}$ case, two orbifold blowup modes were massive.

As a further crucial step in checking whether we find MSSM-like models on the blowup CY, we calculated the spectrum for the gauge flux found from the Bianchi identities in the previous chapter. The most important tools to analyze the spectrum are provided by group theory and the Atiyah-Singer index theorem. It should be noted that the approach we used to calculate the spectrum is more sensitive than standard index theorems, which can only count the difference between chiral and anti-chiral states. This is true because any state (even those that are not charged under the SM gauge group) is chiral with respect to some $U(1)$ factor in blowup. Additionally, the number operator giving the number of generations can be used to check the absence of several kinds of possible anomalies and as a cross-check that the blowup procedure is consistent.

Carrying out the anomaly analysis for the spectrum of the $\mathbb{Z}_{6-II}$ orbifold revealed that, while non-Abelian anomalies are absent as expected, the hypercharge is among the anomalous $U(1)$ directions and thus broken. We gave a generic argument that this is the fate of all MSSM models of the Mini-Landscape: the emergence of the anomaly could be traced back to the fact that the anomaly polynomial involves among other terms the $U(1)_Y$ generator acting on the gauge flux. Due to the relation of the line bundle vectors to the orbifold shift vectors and Wilson lines, the gauge flux always contains the Wilson line that is responsible for breaking the gauge group to the SM. The inner product of this Wilson line with the hypercharge operator is non-zero, which leads to the observed anomaly. In our construction, we used one blowup mode per fixed point. In every Mini-Landscape model, there is at least one orbifold state at each fixed point that is charged under the hypercharge or some other SM gauge group. Using these states as blowup modes yields anomalous fields. This led us to discuss how the anomalous hypercharge problem can be circumvented. To allow for the right value of the Weinberg angle and thus for gauge coupling unification, it is very convenient to embed the hypercharge generator in the $SU(5)$, which contains the $SU(3) \times SU(2)$ SM gauge groups. Choosing a different hypercharge operator generically results in a Weinberg angle which is too small.

For this reason, we considered the $\mathbb{Z}_2 \times \mathbb{Z}_2$ orbifold from which we divided out a $\mathbb{Z}_{2,\text{free}}$ action as another possibility to avoid the anomalous hypercharge . Before modding out the $\mathbb{Z}_{2,\text{free}}$, we found the same GUT spectrum as on the orbifold, which has six MSSM generations. An analysis of the anomalies showed that the spectrum is anomaly-free. With the hypercharge embedded in the $SU(5)$, in particular the $U(1)_Y$ anomaly did not occur. After modding out the $\mathbb{Z}_{2,\text{free}}$, the number of fixed points and thus the number of generations was reduced by a factor of two giving three generations and at the same time the $SU(5)$ was broken to the SM gauge group $SU(3) \times SU(2) \times U(1)_Y$. The hypercharge stayed anomaly-free as the Wilson line which is used to perform the breaking does not occur in the gauge flux in this construction. In the example section, we explicitly constructed a gauge flux which satisfies the Bianchi identities, the DUY-equations, has the $U(1)_Y$ as its only unbroken Abelian factor, and results in a net number of three SM generations.

To conclude this thesis, we want to point out further research topics inspired by our work. Firstly, it would be worthwile to gain a better understanding of the unprojected dual graphs. As we have seen, there can be a huge number of different triangulations in the blowup procedure. Although we established a qualitative connection between the Kähler moduli and the distance parameters, no quantitative analysis has been carried out. One could check whether the volume of the curves, divisors, and the CY manifold can be calculated quantitatively by pure geometrical means from the unprojected dual graphs. Augmenting this information with the D- and F-flatness constraints could help to understand how the volumes of the divisors have to be chosen and thus which triangulation has to be used in the Bianchi identities.

Another interesting point for further research is how the newly derived condition on the freely acting Wilson lines can be understood in the CY picture. On the CY, there is no known mechanism that leads to a restriction of the free action. Finding out whether there is a corresponding constraint that can be understood in the CY limit would help to better understand the connection between the two spaces.

Furthermore, it would be interesting to investigate other techniques that lead to MSSM-like CY manifolds. We examined two constructions, namely blowing up an MSSM orbifold and blowing up a GUT orbifold and dividing out a freely acting symmetry. The latter was pursued as a possible way out of the anomalous hypercharge problem. Another way could be to use only SM singlets as blowup modes. However, this requires in the case of the Mini-Landscape taking several twisted states as blowup modes at some fixed points and none at others (at those which only have states charged under the SM). We think that this is described by non-Abelian gauge bundle vectors, which are most commonly considered in heterotic CY model building. Another possibility is to go to partial blowup only and leave the divisors associated with the line bundle vectors inducing the hypercharge anomaly small. The problem is that the resulting space is neither an orbifold nor a CY manifold. So we do not know whether to apply the CFT calculation methods appropriate for the orbifold or the low energy heterotic SUGRA approximation of the CY. It would be interesting to work out tools for such intermediate models.

Finally, it would help to find other techniques besides the blowup procedure that lead to the same CY spaces via a different construction mechanism. For this it would be interesting to see whether the CYs resulting from the blowup can be written for example as complete intersection CYs.

Acknowledgments

I would like to thank my advisor and supervisor Stefan Groot Nibbelink for his immeasurable patience and for the time he invested into the supervision. Furthermore, I want to thank my second assessor Arthur Hebecker for his support. I am thankful to Patrick Vaudrevange and Michael Ratz, who constructed the $\mathbb{Z}_2 \times \mathbb{Z}_2$ orbifold model. I am also very grateful for the efficient collaboration with Johannes Held, and for valuable discussions with Michael Blaszczyk, Benjamin Galow, Sebastian Gerigk, and Sebastian Halter. My special thanks go to my girlfriend Anneli, my brother Bastian, and my parents, who supported and encouraged me during my studies.

Appendix A

. . . . . .

List of symbols

Symbol	Description
H_I	Element of the Cartan subalgebra
E_α	Non-Abelian elements
V_r	Line bundle vector
R_i	Inherited divisor
D_i	Ordinary divisor
E_r	Exceptional divisor
S_i	Any divisor R, D, E
$\mathfrak{R}$	10-dimensional curvature
$\mathcal{R}$	6-dimensional curvature
R	4-dimensional curvature
$\mathfrak{F}$	10-dimensional field strength
$\mathcal{F}$	6-dimensional field strength
F	4-dimensional field strength
TR	Trace in the fundamental of $SO(N)$
tr	Trace in the fundamental of $SU(N)$
Tr	Trace in the adjoint of E_8
c_i	i^{th} Chern class
J	Kähler $(1,1)$-form
X	Compact blowup manifold
V_{sh}	$E_8 \times E_8$ Orbifold shift vector
W_i	Wilson lines
θ^k	Orbifold twists
φ	Orbifold twist vector
Γ_T	Orbifold torus lattice
$\equiv$	Equivalence up to integers / lattice vectors
$\sim$	Equivalence of divisors
$\Lambda_{E_8\times E_8}$	$E_8 \times E_8$ root lattice

Table A.1: List of recurring symbols

Appendix B

. . . . . .

Properties of the θ and η function

In this appendix we collect properties of θ-functions and the Dedekind η-function. These functions are useful for constructing string partition functions. In the sum representation, the genus one θ-function is given by:

$$\theta\left[\begin{array}{c}\alpha\\ \beta\end{array}\right](z|\tau) = \sum_{n\in\mathbb{Z}} e^{2\pi i\tau\frac{1}{2}(n-\alpha)^2} e^{2\pi i(z-\overline{\alpha})(n-\alpha)}. \tag{B.1}$$

The function depends on the position of the field at the world-sheet torus $z \in \mathbb{C}/\Gamma_T$ and on the modular parameter τ of the torus. The parameters $\alpha, \beta \in \mathbb{R}$ are called characteristics of the θ-function. To shorten the notation we define for $\alpha, \overline{\alpha} \in \mathbb{R}^N$:

$$\theta\left[\begin{array}{c}\alpha\\ \overline{\alpha}\end{array}\right](z|\tau) := \prod_{i=1}^{N} \theta\left[\begin{array}{c}\alpha_i\\ \overline{\alpha}_i\end{array}\right](z|\tau). \tag{B.2}$$

The Dedekind η-function is defined as

$$\eta(\tau) := e^{2\pi i\tau\frac{1}{24}} \prod_{n\leq 1}(1-e^{2\pi i\tau n}), \tag{B.3}$$

where τ again is the modular parameter of the torus.
From definition (B.1), one can work out the following relations for the θ-function:

$$\theta\left[\begin{array}{c}\alpha+\Delta\alpha\\ \overline{\alpha}\end{array}\right](z|\tau) = \theta\left[\begin{array}{c}\alpha\\ \overline{\alpha}\end{array}\right](z|\tau), \Delta\alpha\in\mathbb{Z}^n \tag{B.4a}$$

$$\theta\left[\begin{array}{c}\alpha\\ \overline{\alpha}+\Delta\overline{\alpha}\end{array}\right](z|\tau) = e^{2\pi i\alpha\cdot\Delta\overline{\alpha}}\,\theta\left[\begin{array}{c}\alpha\\ \overline{\alpha}\end{array}\right](z|\tau), \Delta\overline{\alpha}\in\mathbb{Z}^n \tag{B.4b}$$

$$\theta\left[\begin{array}{c}\alpha\\ \overline{\alpha}\end{array}\right](z+1|\tau) = e^{-2\pi i\alpha}\,\theta\left[\begin{array}{c}\alpha\\ \overline{\alpha}\end{array}\right](z|\tau) \tag{B.4c}$$

$$\theta\left[\begin{array}{c}\alpha\\ \overline{\alpha}\end{array}\right](z+\tau|\tau) = e^{-2\pi i(\overline{\alpha}-z-\frac{1}{2}\tau)}\,\theta\left[\begin{array}{c}\alpha\\ \overline{\alpha}\end{array}\right](z|\tau) \tag{B.4d}$$

$$\theta\left[\begin{array}{c}\alpha\\ \overline{\alpha}\end{array}\right](z|\tau+1) = e^{-\pi i(\alpha(\alpha+1)-z-\frac{1}{2}\tau)}\,\theta\left[\begin{array}{c}\alpha\\ \overline{\alpha}+\alpha+\frac{1}{2}\end{array}\right](z|\tau) \tag{B.4e}$$

$$\theta\left[\begin{array}{c}\alpha\\ \overline{\alpha}\end{array}\right](\frac{z}{\tau}|-\frac{1}{\tau}) = \sqrt{-i\tau}e^{2\pi i(\frac{z^2}{2\tau}+\alpha\overline{\alpha})}\,\theta\left[\begin{array}{c}-\overline{\alpha}\\ \alpha\end{array}\right](z|\tau). \tag{B.4f}$$

From the definition of the η-function, we find

$$\eta(\tau+1) = e^{2\pi i\frac{1}{24}}\,\eta(\tau) \tag{B.5a}$$

$$\eta(-\frac{1}{\tau}) = \sqrt{-i\tau}\,\eta(\tau). \tag{B.5b}$$

Appendix C

. . . . . .

Intersection numbers of the $\mathbb{Z}_{6-II}$ and $\mathbb{Z}_2 \times \mathbb{Z}_2$ orbifolds

In this appendix we give the intersection numbers of the $\mathbb{Z}_{6-II}$ and the $\mathbb{Z}_2 \times \mathbb{Z}_2$ orbifold from which all quantities relevant for this thesis can be computed. Remember that, as explained in chapter 4, the calculation of the intersection numbers depend on a combination of triangulations at several fixed points. The ones given here apply only when the specified triangulation is used at all fixed points. Also remember that the R_i and E_r form a basis. Hence we only give the intersection number involving these divisors. All other intersection numbers can be deduced from the given ones using the linear equivalence relations as explained in chapter 3. Intersection numbers that are not listed are zero.

C.1 The $\mathbb{Z}_{6-II}$ orbifold

Int$(S_1S_2S_3)$ \ Triangulation	(i)	(ii)	(iii)	(iv)	(v)
$E_{1,1\beta\gamma}E_{2,1\beta}E_{3,1\gamma}$	0	0	1	0	0
$E_{1,1\beta\gamma}E_{2,1\beta}E_{4,1\beta}$	1	1	0	0	1
$E_{1,1\beta\gamma}E_{3,1\gamma}E_{4,1\beta}$	0	1	0	0	0
$E_{2,1\beta}E_{3,1\gamma}E_{4,1\beta}$	0	0	1	1	0
$E_{1,1\beta\gamma}E_{2,1\beta}^2$	-2	-2	-1	0	-2
$E_{1,1\beta\gamma}E_{3,1\gamma}^2$	-2	-1	0	1	0
$E_{1,1\beta\gamma}E_{4,1\beta}^2$	-2	-1	0	0	0
$E_{2,1\beta}E_{1,1\beta\gamma}^2$	0	0	-1	0	0
$E_{2,1\beta}E_{3,1\gamma}^2$	0	0	-1	0	0
$E_{2,1\beta}E_{4,1\beta}^2$	0	0	-4	-4	0
$E_{3,1\gamma}E_{1,1\beta\gamma}^2$	0	-1	-2	-3	0
$E_{3,1\gamma}E_{2,1\beta}^2$	0	0	-1	-2	0
$E_{3,1\gamma}E_{4,1\beta}^2$	0	-1	-2	-2	0
$E_{4,1\beta}E_{1,1\beta\gamma}^2$	0	-1	0	0	-2
$E_{4,1\beta}E_{2,1\beta}^2$	-2	-2	2	2	-2
$E_{4,1\beta}E_{3,1\gamma}^2$	0	-1	0	0	0

$E^3_{1,1\beta\gamma}$	6	7	8	9	8
$E^3_{2,1\beta}$	8	8	4	8	8
$E^3_{3,1\gamma}$	8	5	2	-1	8
$E^3_{4,1\beta}$	8	4	8	8	0
$R_1R_2R_3$	6				
$R_2E^2_{3,1\gamma}$	-2				
$R_3E^2_{2,1\beta}$	-2				
$R_2E^2_{3,2\gamma}$	-6				
$R_3E_{2,1\beta}E_{4,1\beta}$	1				
$R_3E^2_{2,3\beta}$	-4				
$R_3E_{2,3\beta}E_{4,3\beta}$	2				
$R_3E^2_{4,1\beta}$	-2				
$R_3E^2_{4,3\beta}$	-4				

Table C.1: The upper part gives the intersection numbers when using the same triangulation at all 12 $\mathbb{Z}_6$ fixed points. The lower part gives the triangulation-independent intersection numbers.

C.2 The $\mathbb{Z}_2 \times \mathbb{Z}_2$ orbifold

Int$(S_1S_2S_3)$ \ Triangulation	(i)	(ii)	(iii)	(iv)
$E_{1,\beta\gamma}E_{2,\alpha\gamma}E_{3,\alpha\beta}$	0	0	0	1
$E_{1,\beta\gamma}E^2_{2,\alpha\gamma}$	-2	0	0	-1
$E_{1,\beta\gamma}E^2_{3,\alpha\beta}$	-2	0	0	-1
$E_{2,\alpha\gamma}E^2_{1,\beta\gamma}$	0	-2	0	-1
$E_{2,\alpha\gamma}E^2_{3,\alpha\beta}$	0	-2	0	-1
$E_{3,\alpha\beta}E^2_{1,\beta\gamma}$	0	0	-2	-1
$E_{3,\alpha\beta}E^2_{2,\alpha\gamma}$	0	0	-2	-1
$E^3_{1,\beta\gamma}$	0	8	8	4
$E^3_{2,\alpha\gamma}$	8	0	8	4
$E^3_{3,\alpha\beta}$	8	8	0	4
$R_1R_2R_3$	2			
$R_1E^2_{1,\beta\gamma}$	-2			
$R_2E^2_{2,\alpha\gamma}$	-2			
$R_3E^2_{3,\alpha\beta}$	-2			

Table C.2: The upper part gives the intersection numbers when using the same triangulation at all 64 fixed points. The lower part gives the triangulation-independent intersection numbers.

Bibliography

[1] H. Georgi and S. L. Glashow, "Unity of All Elementary Particle Forces", *Phys. Rev. Lett.* **32** (1974) 438–441.

[2] H. Fritzsch and P. Minkowski, "Unified Interactions of Leptons and Hadrons", *Ann. Phys.* **93** (1975) 193–266.

[3] F. Gursey, P. Ramond, and P. Sikivie, "A Universal Gauge Theory Model Based on E6", *Phys. Lett.* **B60** (1976) 177.

[4] M. M. Nojiri *et al.*, "Physics Beyond the Standard Model: Supersymmetry", arXiv:0802.3672 [hep-ph].

[5] J. M. Maldacena, "The large N limit of superconformal field theories and supergravity", *Adv. Theor. Math. Phys.* **2** (1998) 231–252, arXiv:hep-th/9711200.

[6] M. Axenides, E. Floratos, and C. Kokorelis, "SU(5) unified theories from intersecting branes", *JHEP* **10** (2003) 006, arXiv:hep-th/0307255.

[7] C.-M. Chen, V. E. Mayes, and D. V. Nanopoulos, "MSSM via Pati-Salam from Intersecting Branes on $T^6/(\mathbf{Z_2} \times \mathbf{Z_2'})$", *Phys. Lett.* **B648** (2007) 301–311, arXiv:hep-th/0612087.

[8] F. Gmeiner, R. Blumenhagen, G. Honecker, D. Lust, and T. Weigand, "One in a billion: MSSM-like D-brane statistics", *JHEP* **01** (2006) 004, arXiv:hep-th/0510170.

[9] F. Gmeiner and G. Honecker, "Millions of Standard Models on Z6-prime?", *JHEP* **07** (2008) 052, arXiv:0806.3039 [hep-th].

[10] L. Randall and R. Sundrum, "An alternative to compactification", *Phys. Rev. Lett.* **83** (1999) 4690–4693, arXiv:hep-th/9906064.

[11] V. Bouchard and R. Donagi, "An SU(5) heterotic standard model", *Phys. Lett.* **B633** (2006) 783–791, arXiv:hep-th/0512149.

[12] V. Braun, Y.-H. He, B. A. Ovrut, and T. Pantev, "The exact MSSM spectrum from string theory", *JHEP* **05** (2006) 043, arXiv:hep-th/0512177.

[13] L. J. Dixon, J. A. Harvey, C. Vafa, and E. Witten, "Strings on Orbifolds", *Nucl. Phys.* **B261** (1985) 678–686.

[14] L. J. Dixon, J. A. Harvey, C. Vafa, and E. Witten, "Strings on Orbifolds. 2", *Nucl. Phys.* **B274** (1986) 285–314.

[15] L. E. Ibanez, H. P. Nilles, and F. Quevedo, "Orbifolds and Wilson Lines", *Phys. Lett.* **B187** (1987) 25–32.

[16] L. E. Ibanez, J. Mas, H.-P. Nilles, and F. Quevedo, "Heterotic Strings in Symmetric and Asymmetric Orbifold Backgrounds", *Nucl. Phys.* **B301** (1988) 157.

[17] L. E. Ibanez, J. E. Kim, H. P. Nilles, and F. Quevedo, "Orbifold Compactifications with Three Families of SU(3) x SU(2) x $U(1)^n$", *Phys. Lett.* **B191** (1987) 282–286.

[18] Y. Katsuki *et al.*, "Z(N) ORBIFOLD MODELS", *Nucl. Phys.* **B341** (1990) 611–640.

[19] T. Kobayashi and N. Ohtsubo, "Geometrical aspects of Z(N) orbifold phenomenology", *Int. J. Mod. Phys.* **A9** (1994) 87–126.

[20] O. Lebedev *et al.*, "A mini-landscape of exact MSSM spectra in heterotic orbifolds", *Phys. Lett.* **B645** (2007) 88–94, arXiv:hep-th/0611095.

[21] O. Lebedev *et al.*, "The Heterotic Road to the MSSM with R parity", *Phys. Rev.* **D77** (2008) 046013, arXiv:0708.2691 [hep-th].

[22] O. Lebedev, H. P. Nilles, S. Ramos-Sanchez, M. Ratz, and P. K. S. Vaudrevange, "Heterotic mini-landscape (II): completing the search for MSSM vacua in a Z6 orbifold", *Phys. Lett.* **B668** (2008) 331–335, arXiv:0807.4384 [hep-th].

[23] D. Lust, S. Reffert, E. Scheidegger, and S. Stieberger, "Resolved toroidal orbifolds and their orientifolds", *Adv. Theor. Math. Phys.* **12** (2008) 67–183, arXiv:hep-th/0609014.

[24] S. Reffert, "Toroidal orbifolds: Resolutions, orientifolds and applications in string phenomenology", arXiv:hep-th/0609040.

[25] S. Groot Nibbelink, "Blowups of Heterotic Orbifolds using Toric Geometry", arXiv:0708.1875 [hep-th].

[26] S. Groot Nibbelink, M. Trapletti, and M. Walter, "Resolutions of C^n/Z_n Orbifolds, their U(1) Bundles, and Applications to String Model Building", *JHEP* **03** (2007) 035, arXiv:hep-th/0701227.

[27] S. Groot Nibbelink, T.-W. Ha, and M. Trapletti, "Toric Resolutions of Heterotic Orbifolds", *Phys. Rev.* **D77** (2008) 026002, arXiv:0707.1597 [hep-th].

[28] S. Groot Nibbelink, J. Held, F. Ruehle, M. Trapletti, and P. K. S. Vaudrevange, "Heterotic Z6-II MSSM Orbifolds in Blowup", *JHEP* **03** (2009) 005, arXiv:0901.3059 [hep-th].

[29] A. Adem, J. Leida, and Y. Ruan, *Orbifolds and stringy topology.* Cambridge tracts in mathematics ; 171. Cambridge University Press, 2007.

[30] P. Candelas, G. T. Horowitz, A. Strominger, and E. Witten, "Vacuum Configurations for Superstrings", *Nucl. Phys.* **B258** (1985) 46–74.

[31] F. Ploger, S. Ramos-Sanchez, M. Ratz, and P. K. S. Vaudrevange, "Mirage Torsion", *JHEP* **04** (2007) 063, arXiv:hep-th/0702176.

[32] P. S. Aspinwall, B. R. Greene, and D. R. Morrison, "Measuring small distances in N=2 sigma models", *Nucl. Phys.* **B420** (1994) 184–242, arXiv:hep-th/9311042.

[33] J. Polchinski, *String Theory*, vol. 2. Cambridge University Press, 1998.

[34] K. Becker, M. Becker, J.-X. Fu, L.-S. Tseng, and S.-T. Yau, "Anomaly cancellation and smooth non-Kaehler solutions in heterotic string theory", *Nucl. Phys.* **B751** (2006) 108–128, arXiv:hep-th/0604137.

[35] W. Buchmuller, K. Hamaguchi, O. Lebedev, and M. Ratz, "Supersymmetric standard model from the heterotic string", *Phys. Rev. Lett.* **96** (2006) 121602, arXiv:hep-ph/0511035.

[36] W. Buchmuller, K. Hamaguchi, O. Lebedev, and M. Ratz, "Supersymmetric standard model from the heterotic string. II", *Nucl. Phys.* **B785** (2007) 149–209, arXiv:hep-th/0606187.

[37] J. Held, "Resolving the Singularities of Compact Heterotic Orbifolds", Master's thesis, Ruprecht-Karls Universität Heidelberg, Germany, 2009. available at the Institutsbiliothek Theoretische Physik Heidelberg.

[38] M. Nakahara, *Geometry, topology and physics.* Taylor & Francis, New York [u.a.], 2003.

[39] P. A. Griffiths and J. Harris, *Principles of algebraic geometry.* Wiley, New York [u.a.], 1994.

[40] W. Fulton, *Introduction to toric varieties.* Annals of mathematics studies ; 131. Princeton Univ. Pr., 1997.

[41] J. Erler and A. Klemm, "Comment on the generation number in orbifold compactifications", *Commun. Math. Phys.* **153** (1993) 579–604, arXiv:hep-th/9207111.

[42] R. Donagi and A. E. Faraggi, "On the number of chiral generations in Z(2) x Z(2) orbifolds", *Nucl. Phys.* **B694** (2004) 187–205, arXiv:hep-th/0403272.

[43] A. E. Faraggi, S. Forste, and C. Timirgaziu, "Z(2) x Z(2) heterotic orbifold models of non factorisable six dimensional toroidal manifolds", *JHEP* **08** (2006) 057, arXiv:hep-th/0605117.

[44] J. Polchinski, *String Theory*, vol. 1. Cambridge University Press, 1998.

[45] M. B. Green, J. H. Schwarz, and E. Witten, *Superstring Theory*, vol. 1. Cambridge University Press, 2002.

[46] K. Uhlenbeck and S. Yau, "On the existence of Hermitian-Yang-Mills connections in stable vector bundles", *Commun. Pure Appl. Math.* **39** (1986) 257–293.

[47] R. Blumenhagen, G. Honecker, and T. Weigand, "Loop-corrected compactifications of the heterotic string with line bundles", *JHEP* **06** (2005) 020, arXiv:hep-th/0504232.

[48] L. E. Ibanez, H. P. Nilles, and F. Quevedo, "Reducing the Rank of the Gauge Group in Orbifold Compactifications of the Heterotic String", *Phys. Lett.* **B192** (1987) 332.

[49] E. Witten, "Some Properties of O(32) Superstrings", *Phys. Lett.* **B149** (1984) 351–356.

[50] H. Georgi, *Lie algebras in particle physics [from isospin to unified theories]*. Frontiers in physics ; 54. Westview Press, 1999.

[51] R. Slansky, "Group Theory for Unified Model Building", *Phys. Rept.* **79** (1981) 1–128.

[52] S. Raby and A. Wingerter, "Can String Theory Predict the Weinberg Angle?", *Phys. Rev.* **D76** (2007) 086006, arXiv:0706.0217 [hep-th].

[53] G. G. Ross, *Grand unified theories*. Frontiers in physics ; 60. Benjamin/Cummings Publ. Co., 1984.

[54] D. I. Kazakov, "Beyond the standard model (in search of supersymmetry)", arXiv:hep-ph/0012288.

[55] G. Cleaver, M. Cvetic, J. R. Espinosa, L. L. Everett, and P. Langacker, "Classification of flat directions in perturbative heterotic superstring vacua with anomalous U(1)", *Nucl. Phys.* **B525** (1998) 3–26, arXiv:hep-th/9711178.

[56] R. Donagi and K. Wendland, "On orbifolds and free fermion constructions", arXiv:0809.0330 [hep-th].

[57] F. Buccella, J. P. Derendinger, S. Ferrara, and C. A. Savoy, "Patterns of Symmetry Breaking in Supersymmetric Gauge Theories", *Phys. Lett.* **B115** (1982) 375.

[58] N. Marcus, A. Sagnotti, and W. Siegel, "Ten-dimensional supersymmetric Yang-Mills Theory in terms of four-dimensional superfields", *Nucl. Phys.* **B224** (1983) 159.

[59] N. Arkani-Hamed, T. Gregoire, and J. G. Wacker, "Higher dimensional supersymmetry in 4D superspace", *JHEP* **03** (2002) 055, arXiv:hep-th/0101233.

[60] S. Groot Nibbelink, H. P. Nilles, M. Olechowski, and M. G. A. Walter, "Localized tadpoles of anomalous heterotic U(1)'s", *Nucl. Phys.* **B665** (2003) 236–272, arXiv:hep-th/0303101.

[61] E. Witten, "Phases of N = 2 theories in two dimensions", *Nucl. Phys.* **B403** (1993) 159–222, arXiv:hep-th/9301042.